A DYNAMIC TEST MODEL FOR POWER SYSTEM STABILITY AND CONTROL STUDIES

by

GRAHAM ELLIOTT DAWSON

B.A. Sc., University of British Columbia, 1963

M.A. Sc., University of British Columbia, 1966

A THESIS SUBMITTED IN PARTIAL FULFILMENT

OF THE REQUIREMENTS FOR THE DEGREE OF

DOCTOR OF PHILOSOPHY

in the Department of

Electrical Engineering

We accept this thesis as conforming to the

required standard

Research Supervisor . . . . . .

Members of the Committee . . . . . .

. . . . . .

Acting Head of the Department . . . . . .

Members of the Department

of Electrical Engineering

THE UNIVERSITY OF BRITISH COLUMBIA

December, 1969

In presenting this thesis in partial fulfilment of the requirements for an advanced degree at the University of British Columbia, I agree that the Library shall make it freely available for reference and study. I further agree tha permission for extensive copying of this thesis for scholarly purposes may be granted by the Head of my Department or by his representatives. It is understood that copying or publication of this thesis for financial gain shall not be allowed without my written permission.

Department of Electrical Engineering

The University of British Columbia
Vancouver 8, Canada

Date December 19, 1969

ABSTRACT

A new model for power system transient stability tests has been developed. It includes a dc motor simulated prime mover with a governor control synthesized by dc booster generator field control, a solid state voltage regulator and exciter, a synchronous machine with a large field time constant realized by negative resistance in the field circuit, a transmission system with time setting SCR controlled fault and clear sequence switchings, an accurate torque angle deviation transducer (Chapter 2), and analogs to realize conventional stabilization and nonlinear optimal control (Chapter 5).

Three state variable mathematical models of the test model with various degrees of detail are derived in Chapter 3. Comparisons of results of digital computation and real model tests of a typical power system disturbed by a short circuit are given also in Chapter 3. A parameter sensitivity study is carried out in Chapter 4. Comparisons of digital computation of transient stability with a nonlinear optimal control derived in this thesis and power and speed stabilization derived by another colleague of the power group at U.B.C., with the transient stability tests on the test model are given in Chapter 5.

TABLE OF CONTENTS

Page

LIST OF TABLES

LIST OF ILLUSTRATIONS

LIST OF ILLUSTRATIONS (Cont.)

ACKNOWLEDGEMENT

I wish to thank Dr. Y. N. Yu, supervisor of this project, for his guidance, interest and encouragement during the course of the research work and writing of this thesis.

The development of the solid state voltage regulator and exciter by Mr. J. Bond and the governor-prime mover system by Mr. R. Siddall is acknowledged and their efforts greatly appreciated.

Thanks are due to my colleagues for helpful discussions and suggestions, particularly with Mr. N. Thompson concerning optimal control theory and with Mr. C. Siggers concerning power system stabilizing signals.

Mr. B. Blackhall's interest and efforts in the construction and subsequent testing of the test model were most helpful.

Support from the British Columbia Telephone Company and the National Research Council of Canada through a Studentship award for 1967-1969 and grant A3626 is gratefully acknowledged.

Thanks are also due to Mrs. W. Greig for typing this thesis and Mr. A. McKenzie for draughting the figures.

I am grateful to my wife Beverley for her patient understanding and encouragement throughout my graduate program.

NOMENCLATURE

General

H	Hamiltonian
J	cost functional
J_a	augmented cost functional
p	d/dt, time derivative operator
q_r	relative value of parameter
q	parameter
q_o	intial value of parameter
x_{i,q_r}	sensitivity coefficient for state variable i with respect to parameter q_r
Δ	prefix denoting a linearized variable
λ	costate variable

DC Machines

Parameters

L_{aF}	a coefficient; $\omega_m L_{aF}$ being the speed voltage coefficient for the dc motor
R	dc motor-booster armature resistance including R_{Bm}
R_{Bm}	load setting resistance in the dc motor-booster armature circuit
R_{fB}	booster field resistance
T_{fB}	booster field time constant

Variables

i_A	dc motor-booster armature current
I_F	dc motor field current
T_L	load torque
v_{fB}	booster field voltage
v_B	booster armature voltage
v_m	dc motor armature voltage

v_{tdc} dc motor-booster armature terminal voltage

ω_g mechanical angular speed of booster generator

ω_m mechanical angular speed of dc motor

ω_{mb} mechanical angular base speed of dc motor, 188.5 rad/sec

Hydraulic Turbine and Governor

Parameters

$G(p)$ governor transfer function

$H(p)$ hydraulic operator transfer function

H inertia constant

T_A actuator servomotor time constant

T_R dashpot relaxation time

T_G gate servomotor time constant

T_W water starting time

T_m mechanical starting time of the unit

α_R coefficient of net regulation

σ permanent speed droop

δ temporary speed droop

Variables

a actuator servomotor position

a_f actuator feedback position

g gate servomotor position

n per unit relative angular speed change

t turbine torque output

Prime-Mover Governor Model

Parameters

J moment of inertia of test model

f $K_1\omega_m + K_2$: friction

K_3 $\frac{L_{aF}I_F\omega_g L_{af}}{R\,R_{fB}}$: model coefficient

K_4 $K_1 + \frac{\left(L_{aF} I_F\right)^2}{R}$; coefficient for the dc motor torque cancellation

R_{Bm} load setting resistance in dc motor-booster armature circuit

α $\frac{J}{2H}$; simulation coefficient

Regulator-Exciter

Parameters

a_1, a_2 constants used to obtain characteristics of the field voltage limiter

K_A regulator gain

T_{RE} regulator time constant

T_E exciter time constant

Variables

v_R regulator voltage

v_{ref} regulator-exciter reference voltage

Synchronous Machine

Parameters

D damping coefficient

r_a armature resistance

R_f field resistance

R'_f transformed field resistance

'slope'-ratio of synchronous machine steady state armature short circuit current and field current

T_{D1} d-axis damper leakage time constant

T'_d d-axis transient short circuit time constant

T'_{do} d-axis transient open circuit time constant

T''_d, T''_q d- and q-axis subtransient short circuit time constant

T''_{do}, T''_{qo} d- and q-axis subtransient open circuit time constant

x_{ad} mutual reactance between stator and rotor in d-axis

x_d, x_q d- and q-axis synchronous reactances

x'_d d-axis transient reactance

x''_d, x''_q d- and q-axis subtransient reactances

Variables

i_d, i_q d- and q-axis current

i_{fd} field current

P real power output of the machine

Q reactive power output of the machine

T_e energy conversion torque

T_i mechanical torque output to the rotor

v_d, v_q d- and q-axis voltages

v_t armature terminal voltage

v_{fd} field voltage

v_F $\frac{x_{ad}}{R_f} v_{fd}$; a voltage proportional to field voltage

v_{FR} voltage proportional to field current

v_{DR} voltage proportional to d-axis damper winding current

v'_{QR} voltage proportional to q-axis damper winding current

ψ_d, ψ_q d- and q-axis flux linkages

ψ_{fd} field flux linkage

ψ_F $\frac{x_{ad}}{R_f} \psi_{fd}$; flux proportional to field flux linkage

ψ_D, ψ_Q d- and q-axis damper winding flux linkages

ω_e electrical angular speed

ω_{eo} base electrical angular speed, 377 rad/sec

δ torque angle

Transmission System

Parameters

B	shunt susceptance
G	shunt conductance
r	series resistance
x	series reactance

Variables

V_o	infinite bus voltage

1. INTRODUCTION

Modern power systems have become so complex in structure and so large in size that on-line tests of some control schemes to improve the steady state and transient stability are entirely prohibitive. This is because the experiments are not only costly but also possibly destructive in nature. Therefore, it is desirable to perform tests on small test models which have similar characteristics to the actual system.

The development of the test models for large power systems is not new. Robert[1.1] in 1950 constructed a micromachine and microreseaux system. He investigated the electromagnetic and mechanical similarities of the model and real system. The same per unit reactances, equal time constants, similar inertia constants, and torque speed characteristics are used in the modeling. A rotary machine was used to obtain a negative resistance to increase the field time constant.

Venikov[1.2] designed another micromachine in 1952. A commutator machine was used to realize the negative resistance for the field time constant. Three rotors with different saliency, x_d = 0.85, 0.55, 0.40 were used. Flywheel effect was applied to vary the inertia of the micromachine.

Adkins'[1.3] micromachine was reported in 1960 and was used to investigate short circuits, synchronizing and damping torques, swing curves, asynchronous operation and resynchronization. The negative resistance of the field circuit was

realized by electronic circuits. The microturbine was realized by a separately excited dc machine with thyratron control.

More tests are reported recently in Canada by Roy[1.4] using a micromachine and microreseaux and in the U.S.A. by Dougherty[1.5] with a thyristor controlled dc motor as the prime mover for dc transmission tests.

A new model for power system dynamic studies has been developed at U.B.C. Preliminary work has been done by J. Bond on the design of a solid state voltage regulator and exciter and by R. Siddall on the simulation of a governor-prime mover. Further development work has been completed by this thesis including additional features and important tests of the complete system. The model has the following features.

1) It is versatile in that most power systems with conventional controllers can be simulated on the model on a per unit basis.

2) It has solid state components and analog simulated regulator and exciter with both linear and forced excitation characteristics.

3) It has an analog simulated governor-hydraulic operator in conjunction with a dc motor simulated prime mover.

4) It has a synchronous machine and exciter with a negative resistance in the field circuit. The negative resistance is realized by electronic circuits.

5) It has an ac transmission line which at the moment is designed for a special project.

6) It has electronic controlled switching to realize fault, fault cleared and successful or unsuccessful line reclosure at preset times.

7) It has an accurate torque angle deviation transducer utilizing the zero crossings of the terminal voltage and reference voltage waves.

8) It has a stabilizing signal generator.

The thesis also includes the following features.

1) Derivation of state variable equations for the test model with different degrees of details, Chapter 3.

2) Comprehensive comparison of digital computation and model test results of a transient short circuit on the system, Chapter 3.

3) Parameter sensitivity study, Chapter 4.

4) Comprehensive comparison of digital computation and model tests of a "bang-bang" type nonlinear optimal control of the system.

It is hoped the test model developed will be useful to the transient stability study of practical power systems.

2. REALIZATION OF THE DYNAMIC TEST MODEL

2.1 Modeling Procedure

A typical one machine-infinite bus system, Fig. 2.1, is chosen to be modeled for power system dynamics studies. The methods and procedure of modeling are kept general so that they can be extended to any multimachine power system.

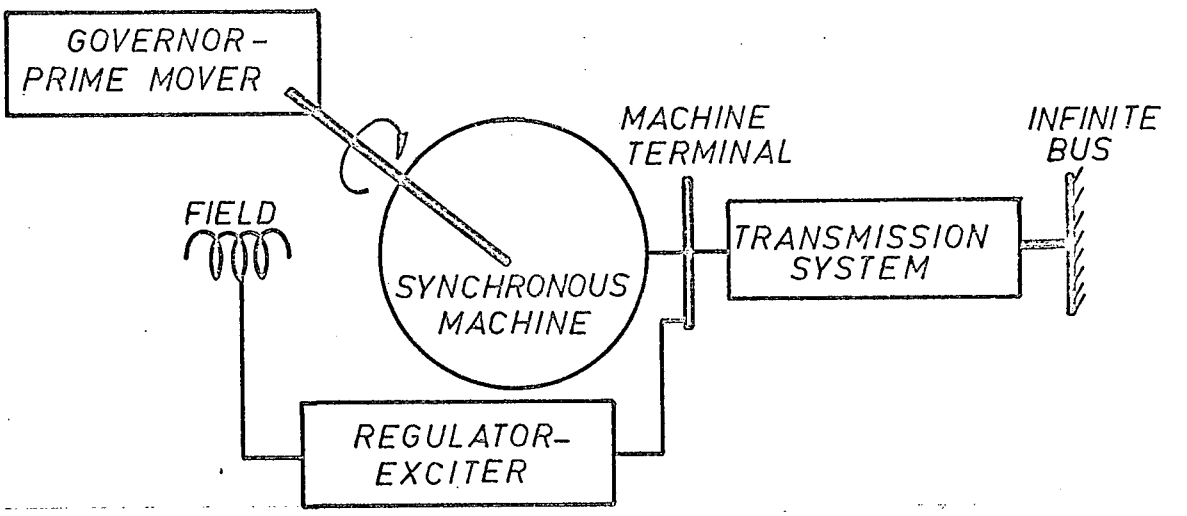

Fig. 2.1. Power System to be Modeled

The first step of modeling is to obtain a detailed mathematical description of a typical power system. For example, the synchronous machine is described by seventh order state equations, fifth order for the electrical and second order for the mechanical, but will be approximated by lower order models after checking with the test results.

The second step is to decide what ranges of parameter values of the synchronous machine, the controllers, and the transmission line of actual power systems are to be simulated.

The third step is to find the means, circuits and machines to realize the mathematical model. For example, how is the governor-prime mover system to be simulated by conventional d-c machines with solid state electronic circuits.

The fourth step is the circuit design and construction details. Evidently, it is important to carry through the tests of all the components, subsystems and the complete model. One of the basic problems is how to determine the model parameters with accuracy.

The last step is to select a base impedance and a base voltage of the test model for a particular system under investigation.

2.2 A Typical Power System

The typical power system to be modeled by the dynamic test model is shown schematically in Fig. 2.1. The four main components are the governor-prime mover which supplies power to and maintains a synchronous speed of the system, the synchronous machine for the electromechanical energy conversion, the regulator-exciter for the machine terminal voltage control, and the transmission system which connects the machine terminal to the infinite bus. For the modeling of a one machine-infinite bus system, the infinite bus is assumed to be a machine of infinite inertia and zero internal impedance.

2.3 Setting Up a Typical Power System on the Test Model

2.3.1 Determining Base Impedance, Power and Voltage

The main objective of the modeling is to achieve the same per unit value of parameters of the actual system on the dynamic test model. In other words, to make the test model per unit impedance equal to the system per unit impedance.

$$Z_{m,pu} = Z_{pu} \qquad \text{per unit} \qquad (2.1)$$

where

$$Z_{m,pu} \triangleq \frac{Z_m}{Z_{mb}} \qquad \text{per unit}$$

and $Z_{m,pu}$ = per unit impedance value of test model,

Z_{pu} = per unit impedance value of actual system,

Z_m = an impedance of the model,

Z_{mb} = model base ohms.

Equation (2.1) applies to all system components such as generators, transformers, transmission lines and loads. Therefore, the model base ohm (Z_{mb}) must be selected such that

$$Z_{mb} = \frac{Z_m}{Z_{pu}} \qquad \text{ohm} \qquad (2.2)$$

This condition must be met in order to obtain a good comparison on the per unit basis between the main parameters of the actual system and that of the test model. On the other hand, to realize a non-existing impedance (Z_m) on the model, one may apply the well known formula

$$Z_m = Z_{mb}Z_{pu} = Z\left(\frac{kV_{mb}}{kV_b}\right)^2 \left(\frac{MVA_b}{MVA_{mb}}\right) \qquad \text{ohm} \qquad (2.3)$$

Next, the base power of the test model is established from a comparison on the per unit basis of the accelerating torque equation of the test model and that of the actual system. As will be revealed in Section 2.4.1, a simulation parameter α is related to the inertia constant H(sec) of the actual power system and the moment of inertia J (joule-sec^2/rad^2) of the dynamic test model by the equation

$$\alpha = \frac{J}{2H} \qquad \text{joule-sec/rad}^2 \qquad (2.4)$$

and the base torque of the model is given by

$$T_{mb} = \alpha \omega_{mb} \qquad \text{joule/rad} \qquad (2.5)$$

where ω_{mb} (188.5 rad/sec) is the model base mechanical speed. Since the base power is given by

$$P_{mb} = \omega_{mb} T_{mb} \qquad \text{watt} \qquad (2.6)$$

substitution of (2.4) and (2.5) into (2.6) gives

$$P_{mb} = \frac{J\omega_{mb}^2}{2H} \qquad \text{watt} \qquad (2.7)$$

Equation (2.7) is the condition to be met for setting the base power of the model. Finally, the model base voltage is given by

$$V_{mb}^2 = Z_{mb} P_{mb} \qquad \text{volt}^2 \qquad (2.8)$$

and equation (2.7) and (2.8) must be satisfied simultaneously. Of course, the model voltage and power bases must be within

the rating of the model generator. It is desirable to establish a base voltage less than the model voltage rating for two reasons; first the machine saturation effects can be neglected and second, the sustained fault currents in the study will not damage the generator.

2.3.2 Numerical Values of System and Model Generator Parameters

Numerical values of generator parameters of an actual power system and those of the model are listed in Table 2.1 side by side on the per unit basis for comparison. The para-

Parameter	Model System		Actual System
	Measured		
Synchronous Machine Parameters			
r_a	.664 Ω	.042 pu	.00247 pu
x_d	16.2 Ω	1.025 pu	.973 pu
x_q	9.71 Ω	.614 pu	.55 pu
x'_d	2.74 Ω	.173 pu	.190 pu
T'_{do}	.247 sec	Adjustable*	5.00 sec
Base Impedance	---	15.8	.797
Mechanical Parameters			
Inertia	$J = .165$ joule-sec^2/rad^2	H = 4.63 sec	H = 4.63 sec
f	$2.67 \times 10^{-3}\omega_m + 1.585$ joule-sec/rad^2	--	--

*Section 2.4.2

Table 2.1 Model and Actual System Generator Parameter Values

metric values of the model in MKS units are determined directly from tests. The base kV of the system generator is 13.9 and the base MVA is 242.

To arrive at the per unit values of the model generator for a good simulation of the system, emphasis must be placed on the most 'important' parameters such as x_d', x_d, x_q, H etc. The generator has so many parameters that all of them cannot be simulated closely simultaneously because of so many constraints involved. For the particular per unit set up of Table 2.1 an exact value of H is retained.

2.3.3 Numerical Values of Model Base Quantities

From (2.7) and data of Table 2.1 the model power base equals

$$P_{mb} = \frac{J\omega_{mb}^2}{2H} = \frac{(.165)(188.5)^2}{(2)(4.63)} = 633 \text{ watts} \qquad (2.9)$$

Next if one would like to have an equal per unit value of x_d' in both systems, one shall have from (2.1)

$$z_{m,pu} = \frac{x_d'}{z_{pu}} = \frac{2.74}{.190} = 14.4 \quad \text{ohm} \qquad (2.10)$$

However, in order to get x_d', x_d and x_q simulated closely simultaneously, the base ohm is chosen as 15.8 ohms.

The remaining base values are

$$v_{mb} = 100 \text{ v} \quad \text{line to line volt} \qquad (2.11)$$

and

$$I_{mb} = 3.65 \text{ A} \quad \text{amp} \qquad (2.12)$$

The nominal ratings of the dynamic test model generator are

$P = 1600$ watts

$V = 208$ volts

$I = 5.5$ amps

2.3.4 Measurement of Model Generator Parameters

The synchronous machine reactances and time constants are determined by the standard procedures of the IEEE Test Code No. 115.[2.1] For example, the value of the direct-axis transient reactance x'_d is obtained from the armature current envelope of a three-phase sudden short circuit, and the direct-axis open-circuit transient time constant T'_{do} is obtained from the armature voltage envelope when the field winding with excitation is short circuited. The value of the direct-axis synchronous reactance found by the slip test compared favourably with the value obtained from the steady state open circuit and short circuit tests in the linear region.

The moment of inertia J of the d-c motor-synchronous machine set is determined from a retardation test and the friction f is obtained from a steady state test utilizing the energy conversion torque of the d-c motor.[2.2]

The parameter values thus obtained are presented in Table 2.1.

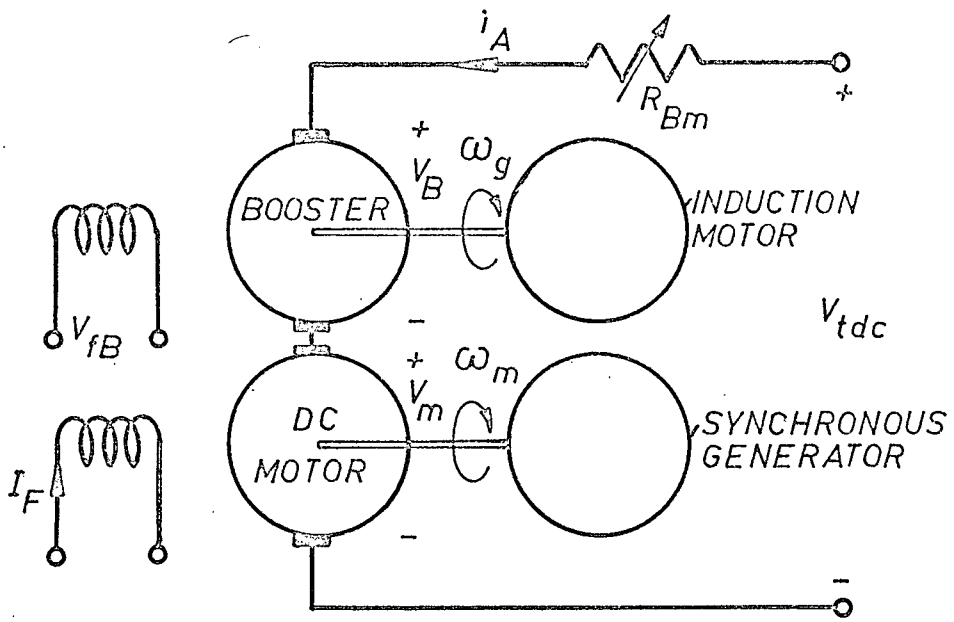

Fig. 2.2. DC Motor-Booster Unit

2.4. Development of the Dynamic Test Model for Power System Simulation

2.4.1 Governor-Prime Mover[2.3]

A d-c motor in series with a booster, Fig. 2.2, is used to simulate the prime mover. The d-c motor is given a constant excitation I_f and the initial armature current i_A and energy conversion torque are set by a load setting resistor R_{Bm}. To obtain an incremental torque as a function of speed deviation of the d-c motor synchronous machine set, the booster receives an excitation which will cause the model to respond similarly to a power system with governor control.

Neglecting the time variational but not the speed voltage effect of the d-c motor-booster armature circuit, the armature current becomes

$$i_A = \frac{1}{R}\left(v_{tdc} - \omega_m L_{aF} I_F - \frac{\omega_g L_{af}}{R_{fB}} \frac{v_{fB}}{1 + T_{fB}P}\right) \text{ amp} \quad (2.13)$$

The second term in the bracket is due to constant excitation and the third term is the speed voltage of the booster. The voltage v_{tdc} is the total d-c voltage applied to the d-c motor-booster armature circuit. The resistance R includes two armature resistances and the load setting resistor R_{Bm}.

The accelerating torque of the d-c motor is

$$\frac{Jd\omega_m}{dt} = L_{aF} I_F i_A - (K_1\omega_m + K_2) - T_L \qquad \text{joule/rad} \quad (2.14)$$

The first term of the right hand side of the equation is the energy conversion torque, the second term the friction torque experimentally determined, and the last term the load torque. For a load deviation, (2.14) becomes

$$\frac{Jd\Delta\omega_m}{dt} = L_{aF} I_F \Delta i_A - K_1\Delta\omega_m - \Delta T_L \qquad \text{joule/rad} \quad (2.15)$$

which corresponds to

$$\frac{Jd\Delta\omega_m}{dt} = G(p)H(p)(-\Delta\omega_m) - \Delta T_L \quad (2.16)$$

Substituting (2.13) into (2.14) and (2.15) and comparing the results with (2.16) yields

$$\Delta v_{fB} = -\frac{1+T_{fB}P}{K_3} (\alpha G(p)H(p) - K_4) (-\Delta\omega_m) \qquad \text{volt} \quad (2.17)$$

where $K_3 = \dfrac{L_{aF} I_F \omega_g L_{af}}{R R_{fB}}$ $\qquad \dfrac{\text{amp-sec}}{\text{rad}}$

and $$K_4 = K_1 + \frac{(L_{aF} I_F)^2}{R} \qquad \frac{\text{watt sec}^2}{\text{rad}}$$

It becomes evident that if the voltage ΔV_{fB} can be realized according to (2.17), then the d-c motor will have exactly the same torque-speed characteristics as that of a large prime mover with a governor.

Dividing through (2.16) by $\alpha\omega_{mb}$ gives

$$\frac{J}{\alpha}\frac{dn}{dt} = G(p)\,H(p)\,(-n) - \frac{\Delta T_L}{\alpha\omega_{mb}} \qquad \text{per unit} \qquad (2.18)$$

which compares with Hovey's[2.4] equation

$$T_m \frac{dn}{dt} = G(p)\,H(p)\,(-n) - \Delta M \qquad \text{per unit} \qquad (2.19)$$

Hence $$\alpha = \frac{J}{T_m} \quad , \quad T_m \triangleq 2H \qquad \text{sec} \qquad (2.20)$$

and $$T_{mb} = \alpha\omega_{mb} \qquad \text{joule/rad} \qquad (2.21)$$

For the particular model prime mover developed at U.B.C., the parameters are

$L_{aF}I_F = 0.85$ volt-sec/rad $\quad \omega_g L_{af} = 73$ ohm $\quad R_{fB} = 51.6$ ohm

$T_{fB} = 0.5$ sec $\quad K_1 = 2.67 \times 10^{-3}$ joule/sec $\quad K_2 = 1.585$ joule/rad

The total resistance R of the armature circuit including the load setting resistance R_{Bm} at no load is

$$R = 28.1 \text{ ohm} \quad ; \quad V_{tdc} = 229 \text{ V}$$

The K_3 and K_4 constants are

$$\frac{1}{K_3} = 23.29 \quad \frac{\text{rad}}{\text{amp-sec}} \qquad K_4 = 0.0258 \quad \frac{\text{watt sec}^2}{\text{rad}}$$

The mechanical parameters are presented in Section 2.3.2. The general layout of the model governor-prime mover system is shown in Fig. 2.3.

The governor-hydraulic transfer function G(p) H(p) is set up on an analog specially built for this purpose. The model is capable of representing different governor-prime mover configurations. For the governor-hydraulic transfer function shown in Fig. 2.4, the parametric values are

$T_A = 0.02$ sec $\qquad \sigma = 0.06 \qquad \delta = 0.5$

$T_R = 5.00$ sec $\qquad T_G = 0.5$ sec $\qquad T_W = 1.6$ sec

The booster field compensator circuit $(1 + T_{fB}p)$ is also built with analog components. The circuit is given in Fig. 2.5. A current amplifier is included to match the current level between the operational amplifier and the booster field. No difficulties are experienced with the differentiation since the input signal frequency is less than 1 Hz. A small value of capacitance (C = 100pf) is used to stabilize the circuit.

2.4.2 Regulator-Exciter[2.5]

The layout of the model voltage regulator-exciter system is shown in Fig. 2.6. For the studies in this thesis, the transfer function RE(p), Fig. 2.7, of the regulator-

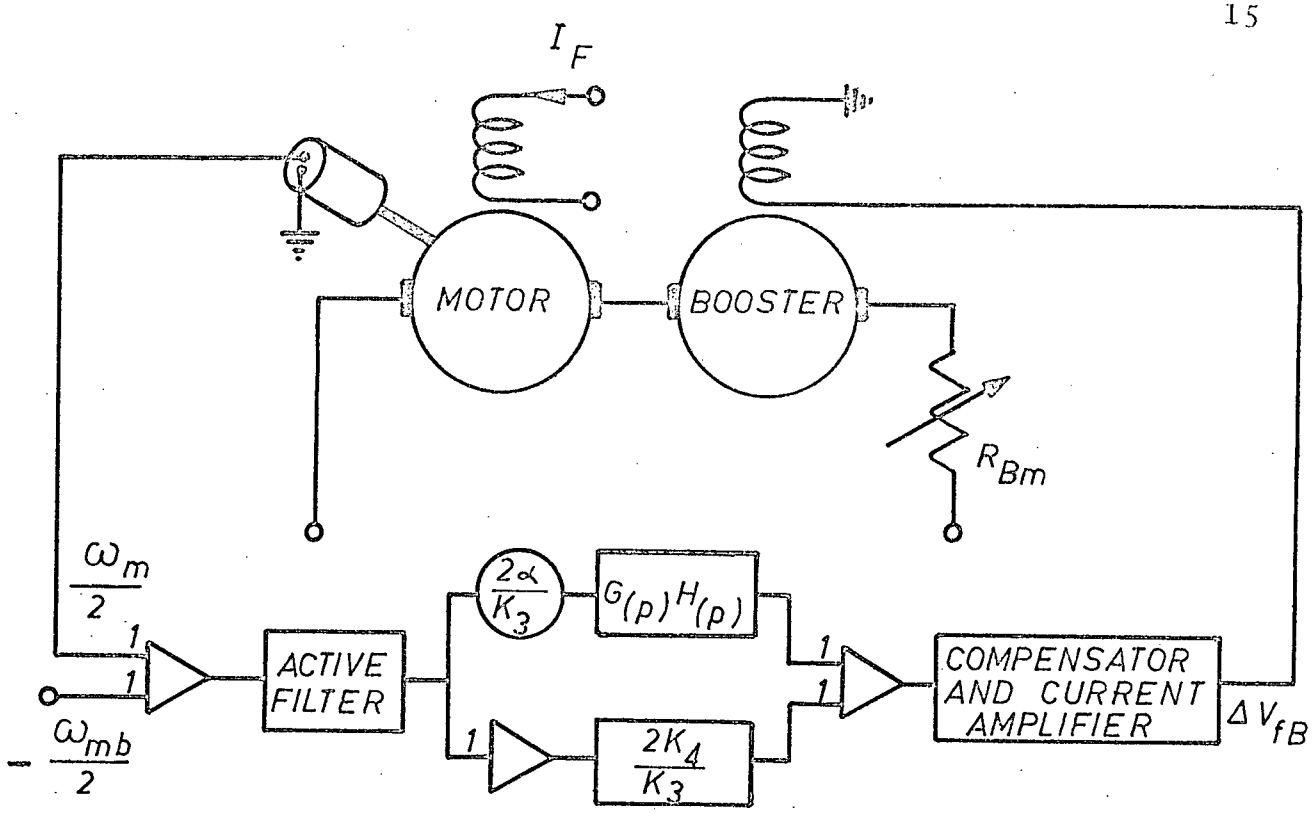

Fig. 2.3. Model Governor-Prime Mover System

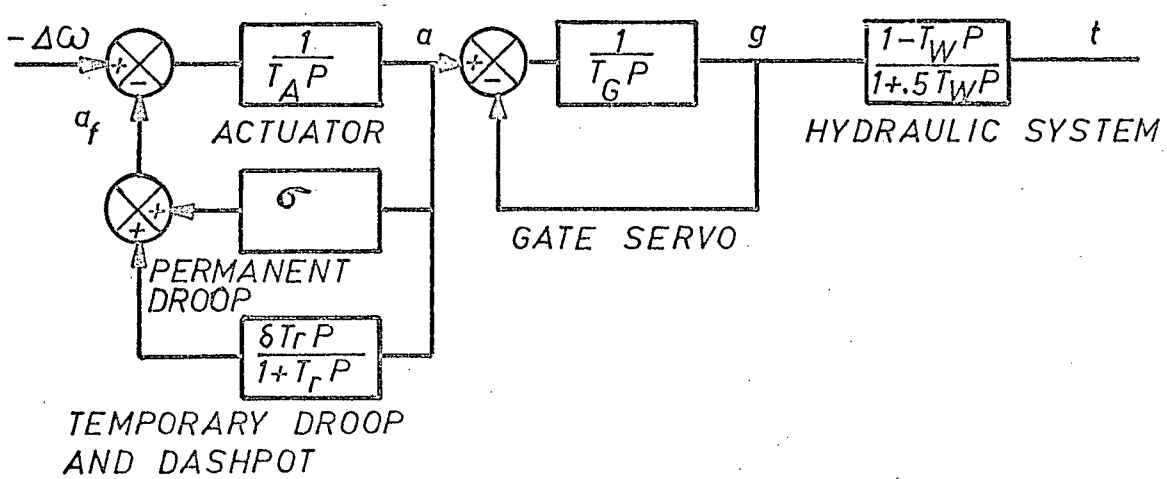

Fig. 2.4. Governor-Hydraulic System Transfer Function

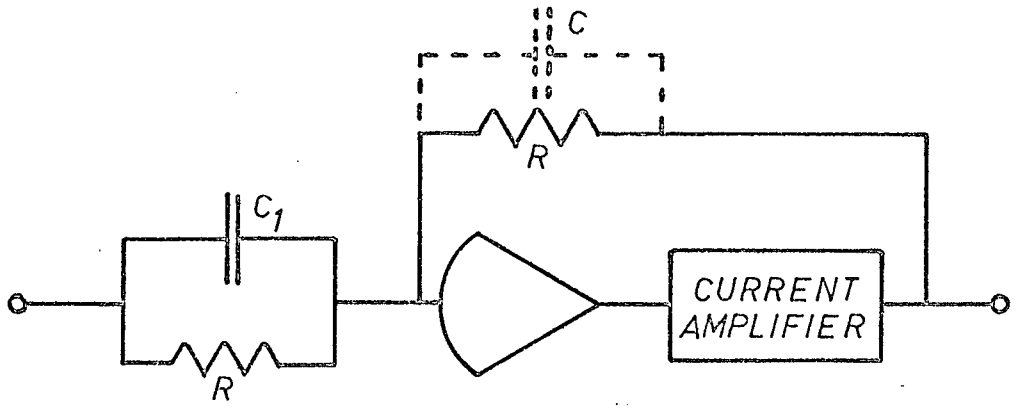

Fig. 2.5. Booster Field Compensation and Current Amplifier Circuit

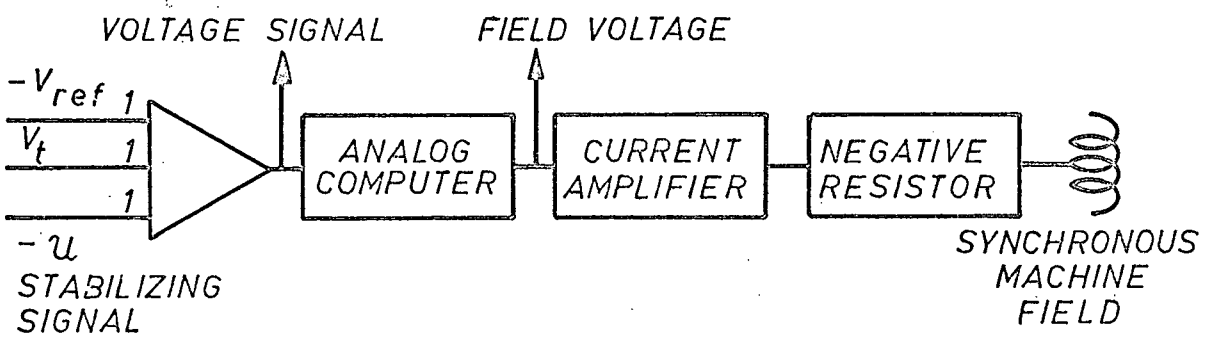

Fig. 2.6. Model Regulator-Exciter System

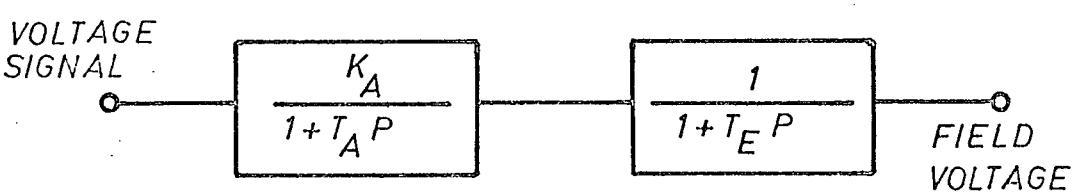

Fig. 2.7. Regulator-Exciter Transfer Function

exciter is patched onto a specially built analog computer. The parameter values of an example are

$$K_A = 0 \sim 100 \qquad T_A = 0.05 \text{ sec} \qquad T_E = 0.035 \text{ sec}$$

The voltage signal from the analog computer is then amplified to match the voltage and current levels of the synchronous machine field.

The model synchronous machine has a relatively large resistance in the field circuit. The resistance value is reduced by a negative resistor[2.4] to obtain the desired open circuit field time constant (T'_{do}). The negative resistor is realized by a scheme shown in Fig. 2.8. The idea is to obtain

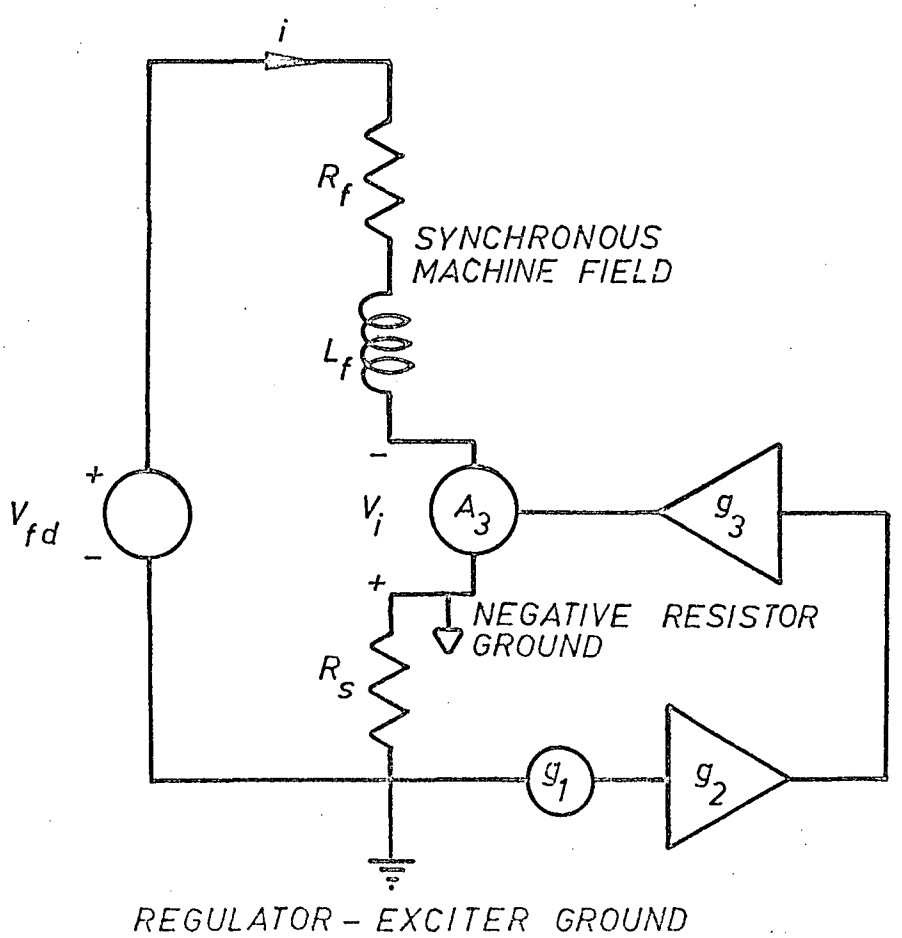

Fig. 2.8. Scheme to Realize Negative Resistance

a voltage v_i which is proportional to current

$$v_i = g_1 \, g_2 \, g_3 \, R_s i = gi \qquad \text{volt} \qquad (2.22)$$

so connected that

$$v_{fd} + v_i = (R_f + R_s + L_f p)i \qquad \text{volt} \qquad (2.23)$$

Thus one has

$$v_{fd} = (R_f + R_s - g)i + L_f \, pi \qquad \text{volt} \qquad (2.24)$$

For example, to obtain an open field time constant of 5 sec the original resistance, R_f = 69.6 ohms, of the model is reduced to 3.44 ohms.

2.4.3 Transmission Line and Circuit Breakers

A transmission line model is built to simulate a 576 mile double-circuit three-phase three-section high voltage transmission line. The distributed parameters of the high voltage transmission line are

$$z = 0.041 + j0.5309 \qquad \text{ohm/mile}$$

$$y = j7.88 \times 10^{-6} \qquad \text{mho/mile}$$

Each section of each phase of each circuit of the line is simulated by a π section with lumped parameters. The model section gives the same per unit voltage and per unit current at the ends as that of the real line with distributed parameters. This includes the effect of the shunt reactors (135 MVAR at 525 kV) of the real line at each end of the section. One circuit of one phase of the lumped parameter equivalent of

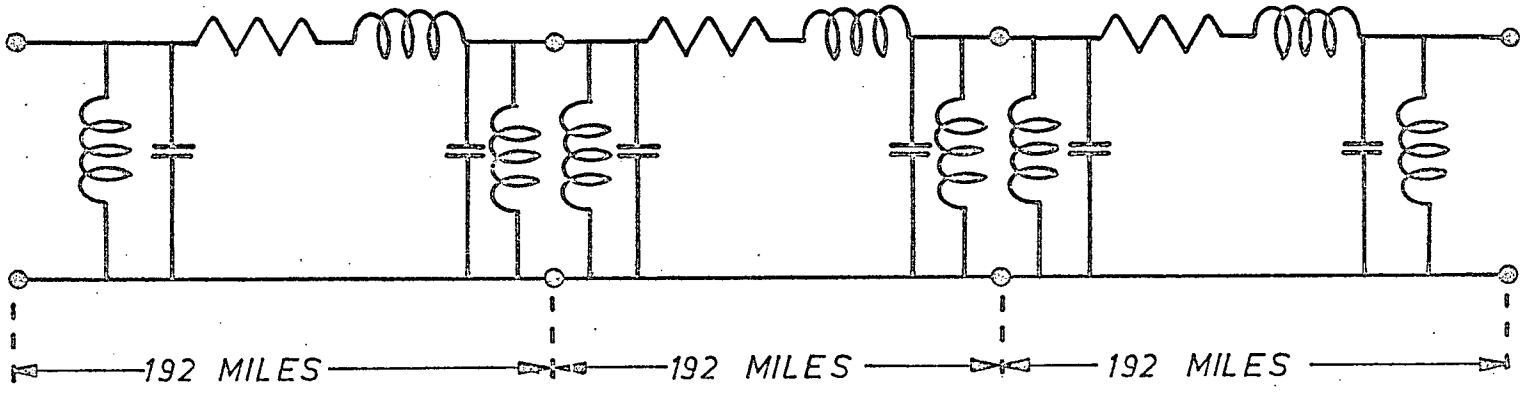

Fig. 2.9. One Phase Lumped Parameter Equivalent of a Single Circuit

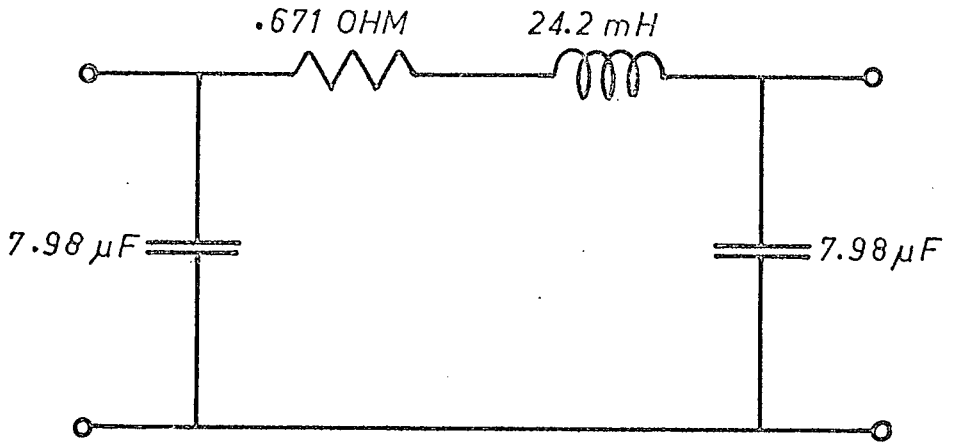

Fig. 2.10. Model π Unit of Transmission Line

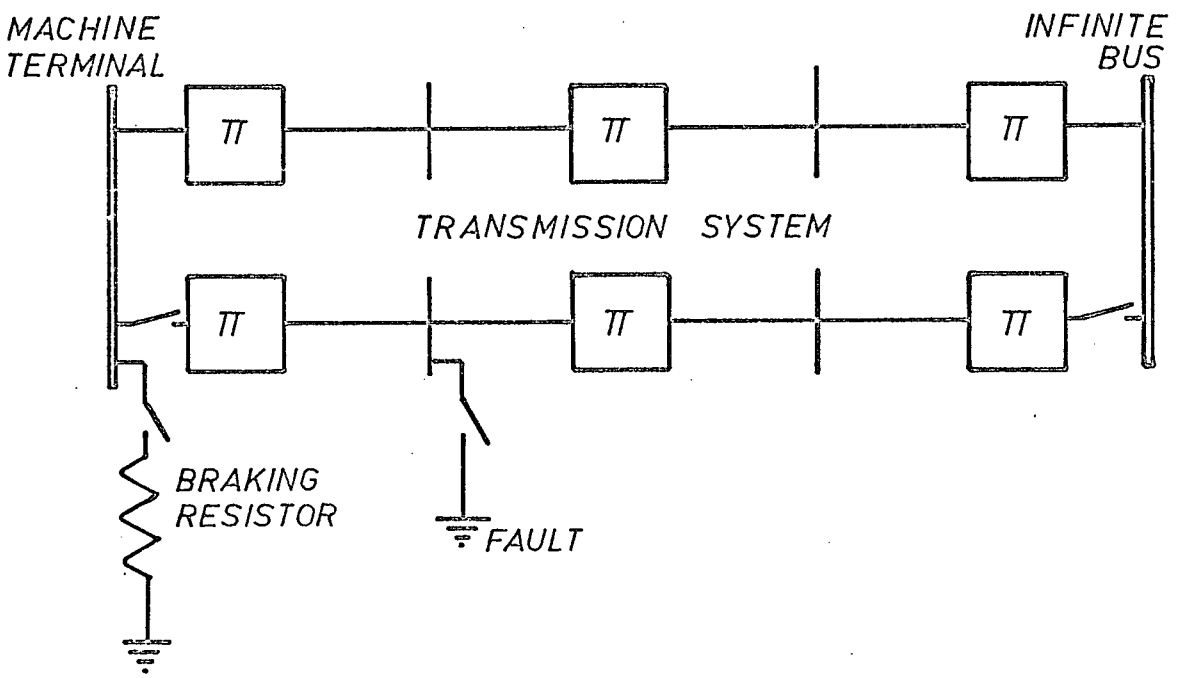

Fig. 2.11. One Phase of the Model Transmission Line

the transmission system and shunt reactors is shown in Fig. 2.9. The parametric values of the equivalent model π unit are given in Fig. 2.10. There are altogether 18 such units. They are built with resistors, iron core reactances and capacitors which are commercially available.

A three-phase braking resistor is connected to the machine terminal for special studies. Three-phase relays are used as circuit breakers for line fault, clearing and braking resistance switching. One phase of the model transmission system is shown in Fig. 2.11.

2.5. Auxiliary Measuring and Control Devices

2.5.1 Time Sequence Control

The time and switching sequence control of the transmission line and braking resistor circuit breakers, and the fault simulation is achieved with integrated circuit logic elements. The control is schematically shown in Fig. 2.12.

The crystal clock produces square waves at 16 kHz. The push button sets the flip-flop which allows the square waves to pass through the 2 input NOR gate to the frequency divider which has an output frequency of 1kHz. The 0 and 1 outputs of the 12 bit counter are connected to units containing 12 single-pole double-throw time selection switches which in turn are connected to 12 input NOR gates which output a pulse when all the inputs are 0. Two units are necessary, one pulse to turn on and a second pulse to turn off the SCR switch, for the fault simulation and braking circuit breaker operation where a CLOSE-OPEN relay action is

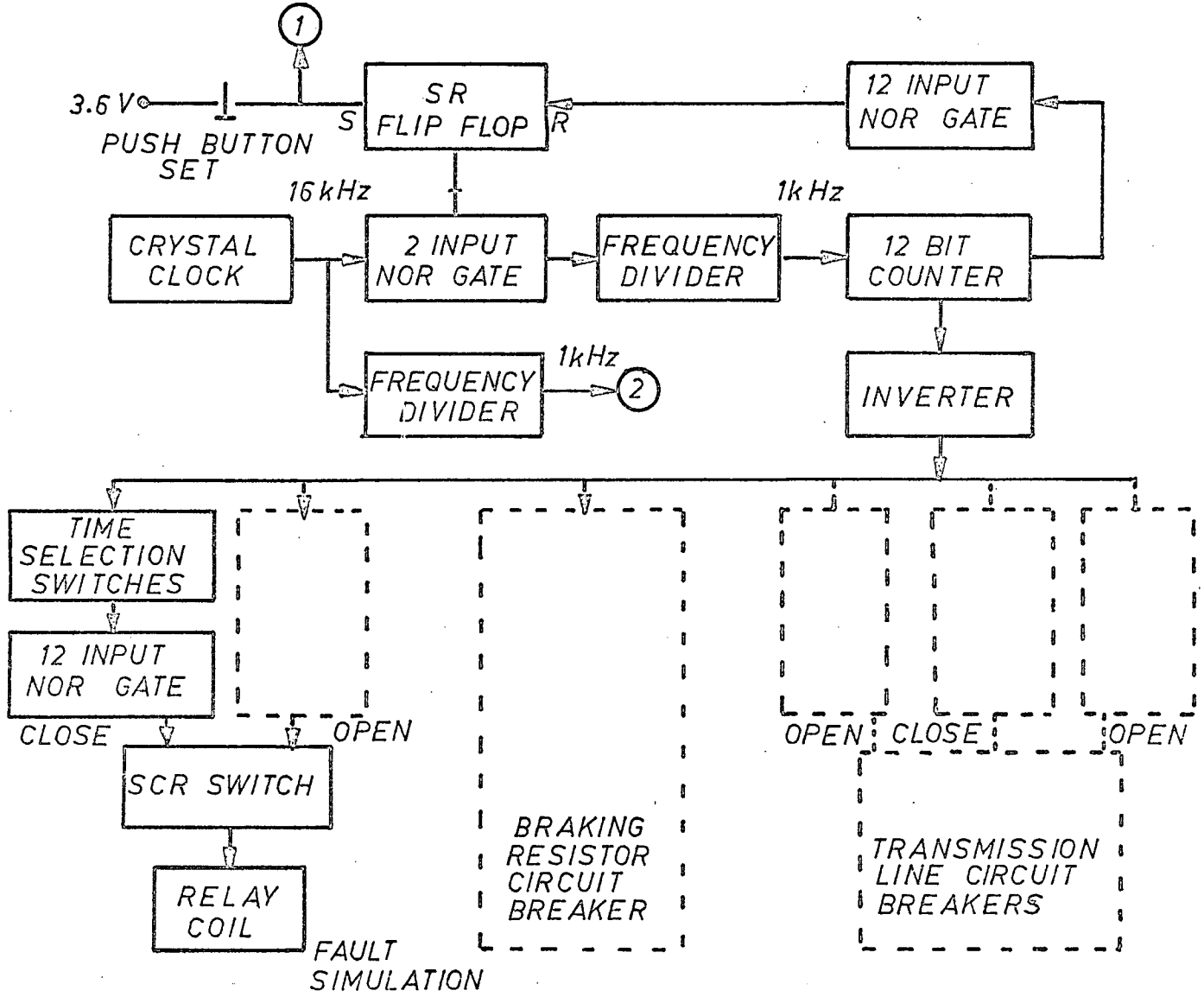

Fig. 2.12. Circuit Breaker and Fault Time-Sequence Control

desired. For the transmission line circuit breaker simulation an additional unit is incorporated for an OPEN-CLOSE-OPEN relay action to represent an unsuccessful reclosure. The time-sequence control is terminated with a feedback pulse to the set-reset flip-flop 4.096 seconds after initiating the action with the push button. This time interval allows for normal and abnormal time-sequence operation of the fault simulation, transmission line circuit breakers, and braking resistor circuit breakers.

2.5.2 Torque Angle Deviation Measurement

For power system dynamic studies, it is evidently very important to have an accurate torque angle deviation signal which can be constantly monitored and used for control purposes. To this end, a continuous voltage signal proportional to torque angle deviation is obtained by the scheme shown in Fig. 2.13. Two a-c voltage signals, one from the infinite bus and one from an a-c tachometer coupled to the generator shaft, are fed into separate comparators. The output square wave signals are connected to monostables. This eliminates intermittent switching caused by ringing at the comparator outputs. The time delay between the pulses from the monostables is proportional to the phase shift of the two signals. The a-c tachometer monostable pulse sets the set-reset flip flop to allow pulses from clock 1 through the NOR gate to the 9 bit counter 1. The frequency of clock 1 is 30.72 kHz so that 512 pulses will be counted if the phase shift is 360 degrees at

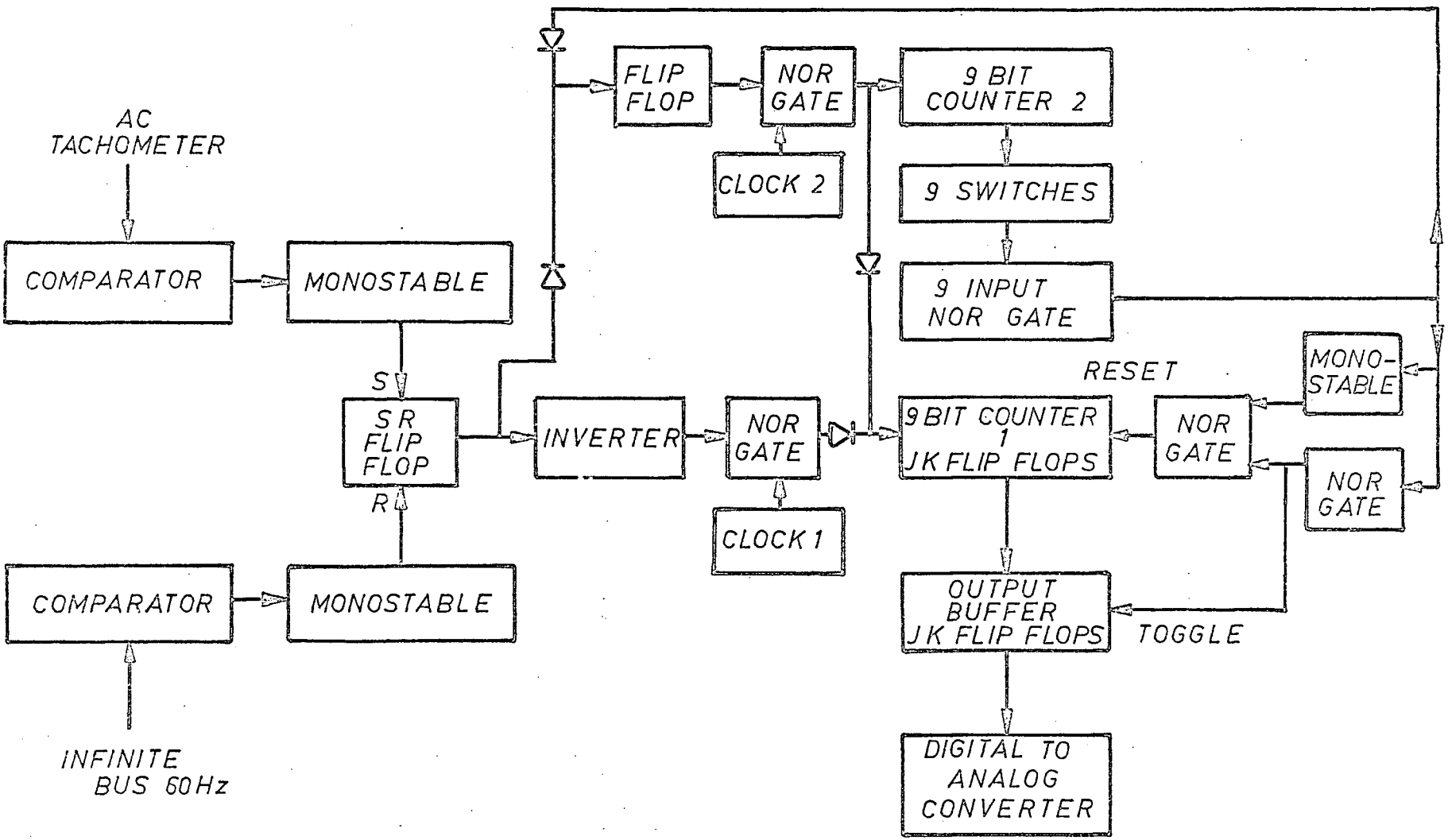

Fig. 2.13. Torque Angle Deviation Measuring Device

60 Hz. The infinite bus monostable pulse lowers the output level of the set-reset flip-flop to stop pulses from clock 1. At the same time, the falling edge of the set-reset flip-flop toggles a flip-flop to allow pulses from clock 2 into both 9-bit counter 1 and 2. This scheme allows the steady state output analog signal to be reduced to zero by setting the 9 double-throw single-pole switches. The complement of the binary value set is added to counter 1 at approximately 2.5 x 10^6 bits per second by clock 2. The end of the addition is detected by an output pulse from a 9-input NOR gate which initiates the following events; first the flip-flop is toggled to shut off the pulses from clock 2, second a pulse from the NOR gate toggles the output buffer to receive the contents of counter 1, and third a monostable is triggered. The monostable provides a delayed pulse so the contents of counter 1, before being reset, can be transfered to the output buffer. The output buffer is converted to a continuous voltage signal by a digital to analog converter with a range 0 to -10 volts. The sampling rate is 60 times a second.

2.5.3 Forced Excitation Control

Provision is made for the forced excitation control to provide a stabilizing signal for the power system during and after a system disturbance; Chapter 5. The stabilizing signal is an open-loop bang-bang voltage signal summed with the terminal and reference voltage to provide a total voltage error signal, Fig. 2.6. The block diagram of Fig. 2.14 shows a

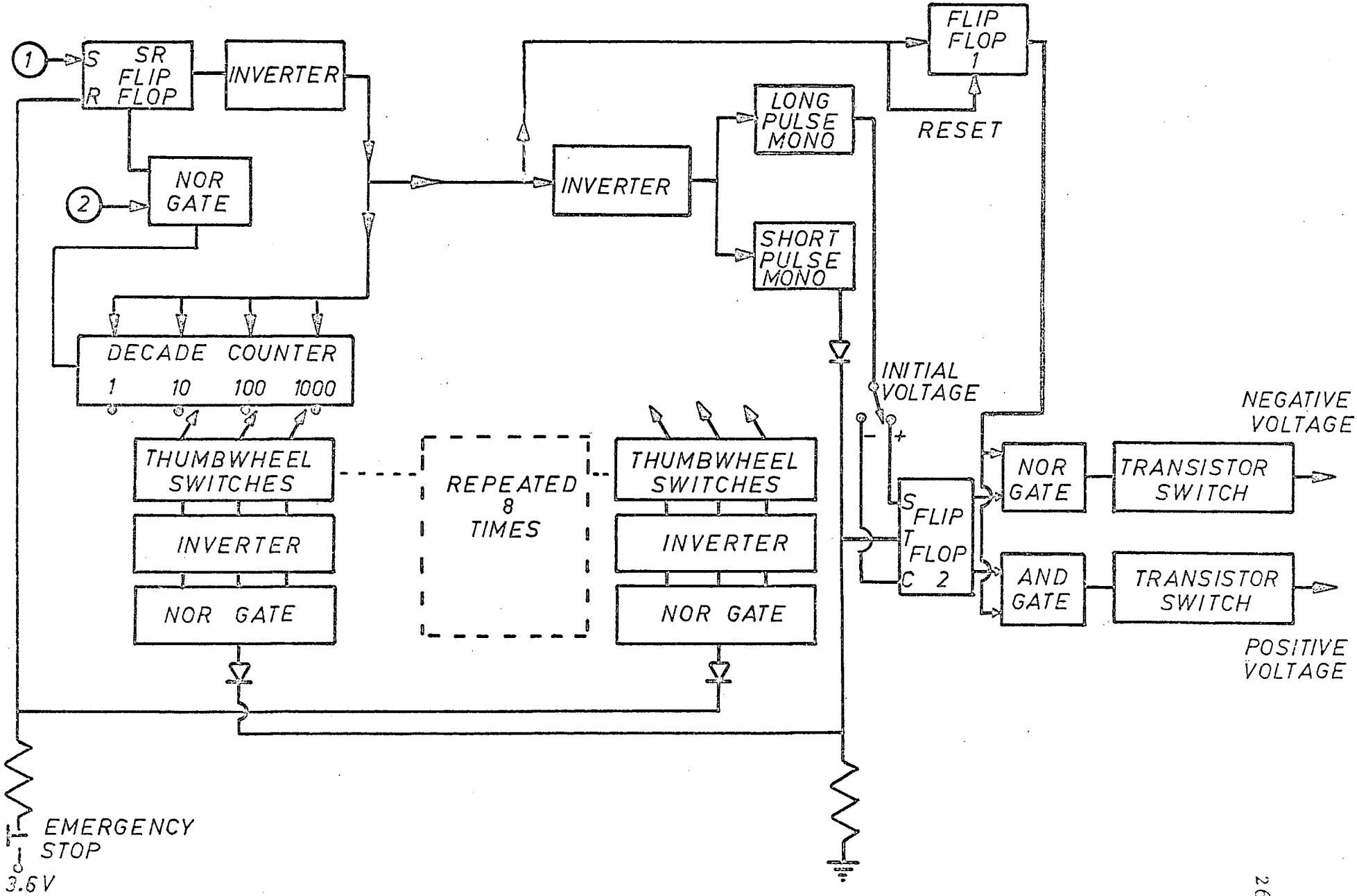

Fig. 2.14. Forced Excitation Time-Switching Control

scheme to realize the switching times and the number of switchings of the stabilizing signal.

The events of the forced excitation control are started at the instant of fault by a signal from push button set of the time-sequence control, Fig. 2.12. This signal resets a set-reset flip-flop allowing 1kHz square waves from the frequency divider, Fig. 2.12, to be counted by the decade counter. Ten units consisting of thumbwheel switches, inverters and NOR gates set the times of switching. At the instant the events are initiated, the complementary level from the set-reset flip-flop is fed into an inverter whose output performs two functions. First, two monostables are triggered through an inverter. One monostable with a long pulse establishes the initial polarity of the forced excitation and the second shorter pulse toggles the initial condition into flip-flop 2. Second, flip-flop 1 is toggled which allows the NOR gates for negative and positive voltages to be enabled. The time setting units toggle flip-flop 2 to produce a bang-bang type of forced excitation voltage signal. The last timing unit output feeds back to the set-reset flip-flop to stop the timing sequence. At the same time, the high level output of flip-flop 1 clamps the negative and positive voltages to a zero value.

3. STATE EQUATION MODELS OF THE DYNAMIC MODEL AND TEST RESULTS

One of the most important decisions to be made in power system dynamics studies is how much of the detail of the synchronous machine should be described by equations. The results of a mathematical model is a compromise between computation time and accuracy and is to be decided from direct comparison of computation and test, not by arbitrary choice. It is the objective of this chapter to investigate and to compare the computation results of synchronous machine models of different degrees of details with those from machine tests.

Another important point in modeling is that the machine must be described by equations with measureable parameters. There is much more freedom in the mathematical manipulation of equations than the methods available in obtaining reliable parameter values directly from tests. For example, the synchronous machine reactances can be determined with much better accuracy than the leakage reactances.

A third point in modeling is that since most optimal control theory, computation and nonlinear stability analysis techniques are developed from system equations in the state variable form, it is desirable to model the system equations as such to allow the application of the theory and obtain the solution by known computational methods.

In this chapter a one machine-infinite bus system model schematically shown in Fig. 3.1 will be developed. The state equation representation of the regulator-exciter is

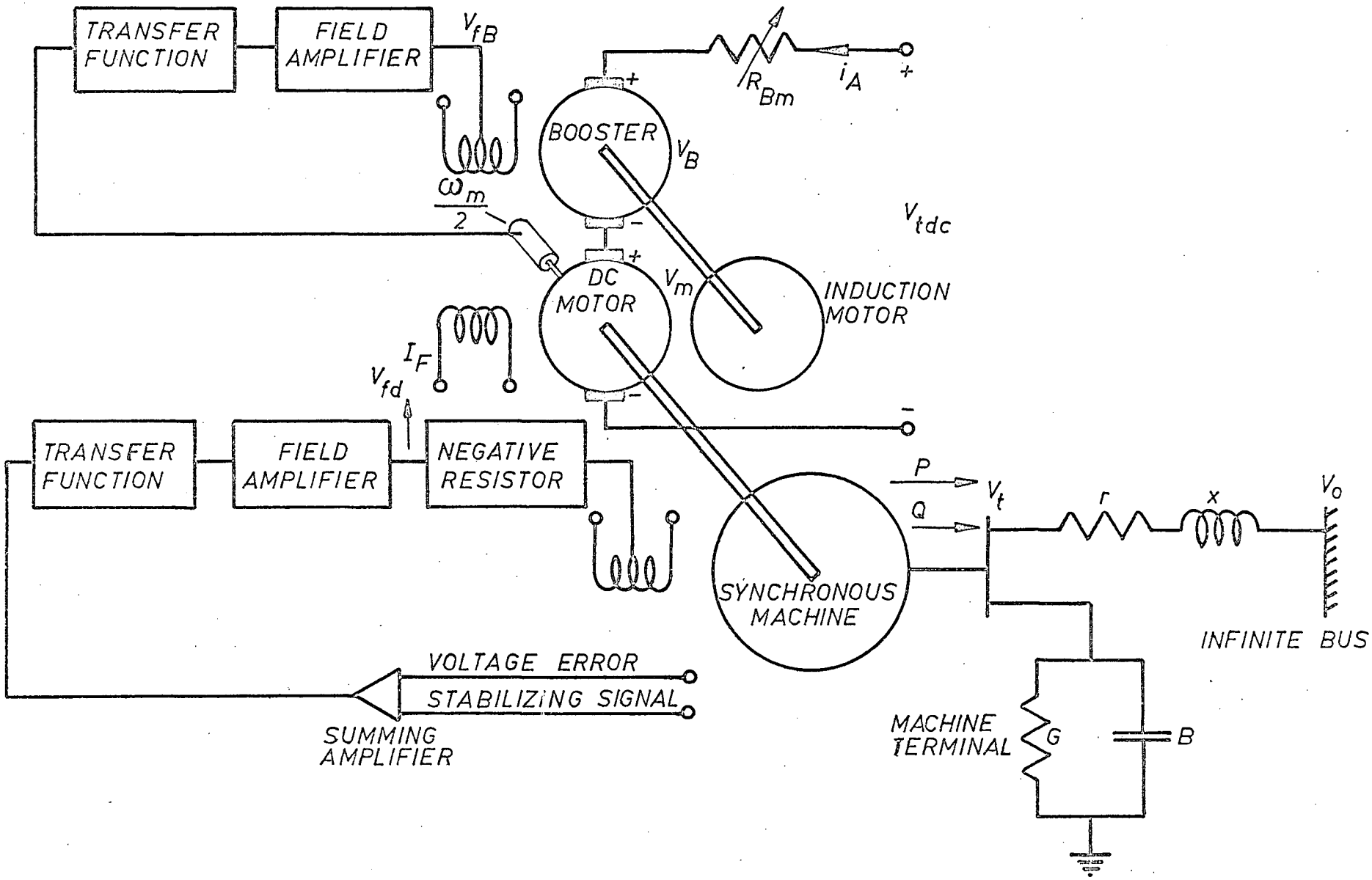

Fig. 3.1. Dynamic Test Model of One Machine-Infinite Bus System

based on Fig. 2.7, and that of the governor-hydraulic system on Fig. 2.4 incorporating the state equation of the d-c motor-booster of Fig. 2.2.

3.1. Seventh Order Synchronous Machine State Equations

Park's equations for a synchronous machine in d-q coordinates[3.1] are:

$$v_d = p\psi_d - \omega_e\psi_q - r_a i_d \tag{3.1}$$

$$v_q = p\psi_q + \omega_e\psi_d - r_a i_q \tag{3.2}$$

$$\psi_d = \frac{1+T_{D1}p}{(1+T'_{do}p)(1+T''_{do}p)} \frac{x_{ad}}{\omega_{eo}R'_f} v_{fd} - \frac{(1+T'_dp)(1+T''_dp)}{(1+T'_{do}p)(1+T''_{do}p)} \frac{x_d}{\omega_{eo}} i_d \tag{3.3}$$

$$\psi_q = -\frac{1+T''_q p}{1+T''_{qo}p} \frac{x_q}{\omega_{eo}} i_q \tag{3.4}$$

which can be rearranged into the following state variable form

$$p\psi_d = v_d + \omega_e\psi_q + r_a i_d \tag{3.5}$$

$$p\psi_q = v_q - \omega_e\psi_d + r_a i_q \tag{3.6}$$

$$p\psi_F = Rv_F - v_{FR} \tag{3.7}$$

$$p\psi_D = -v'_{DR} \tag{3.8}$$

$$p\psi_Q = -v'_{QR} \tag{3.9}$$

where v_{FR}, i_d and v_{DR} are solved from

$$\begin{bmatrix} v_{FR} \\ i_d \\ v_{DR} \end{bmatrix} = \begin{bmatrix} \frac{x_d(T''_{do} + T_D)}{x''_d\, T''_{do}\, T'_{do}} & \frac{-x_d(T'_{do}-T_c)\omega_{eo}}{x''_d\, T'_{do}} & \frac{x_d(T'_{do}-T_c)}{x''_d\, T''_{do}\, T'_{do}} \\ \frac{1}{x''_d\, T'_{do}} & -\frac{\omega_{eo}}{x''_d} & \frac{1}{x''_d\, T''_{do}} \\ -\frac{x_d T_D}{x''_d T''_{do}\, T'_{do}} & \frac{\omega_{eo} x_d\, T_D}{x''_d\, T''_{do}} & \frac{x_d\, T_c}{x''_d\, T''_{do} T'_{do}} \end{bmatrix} \begin{bmatrix} \psi_F \\ \psi_d \\ \psi_D \end{bmatrix} \tag{3.10}$$

and i_q and v'_{QR} from

$$\begin{bmatrix} i_q \\ v'_{QR} \end{bmatrix} = \begin{bmatrix} -\frac{\omega_{eo}}{x_q} & \frac{1}{x''_q\, T''_{qo}} \\ \frac{-\omega_{eo}(x_q - x''_q)}{x''_q} & \frac{x_q}{x''_q\, T''_{qo}} \end{bmatrix} \begin{bmatrix} \psi_q \\ \psi_Q \end{bmatrix} \tag{3.11}$$

The derivation of (3.5) through (3.11) is presented in Appendix 3A.

For the study of the machine-infinite bus system as shown in Fig. 3.1, the d- and q-axis machine terminal voltages can be expressed in terms of the infinite bus voltage and the torque angle between synchronous machine q-axis and infinite bus voltage and the machine d- and q-axis current as follows[3.2]

$$\begin{bmatrix} v_d \\ v_q \end{bmatrix} = \begin{bmatrix} k_1 r + k_2 x & -(k_1 x - k_2 r) \\ k_1 x - k_2 r & k_1 r + k_2 x \end{bmatrix} \begin{bmatrix} i_d \\ i_q \end{bmatrix} + \begin{bmatrix} k_1 & k_2 \\ -k_2 & k_1 \end{bmatrix} \begin{bmatrix} v_o \sin\delta \\ v_o \cos\delta \end{bmatrix} \tag{3.13}$$

$$\text{where } k_1 = (1-xB+rG)/((1-xB+rG)^2 + (xG+rB)^2)$$
$$k_2 = (xG+rB)/((1-xB+rG)^2 + (xG+rB)^2) \qquad (3.12)$$

To complete the description of the synchronous machine dynamics, two additional equations are obtained as follows. From the equilibrium equation for torque

$$p\omega_m = \frac{1}{J}(T_i - D\omega_m - T_e) \qquad (3.13)$$

where the three phase electrical torque is

$$T_e = 3\,\frac{\text{poles}}{2}\,(\psi_d\, i_q - \psi_q\, i_d) \qquad (3.14)$$

From the relation between electrical torque angle and mechanical speed

$$p\delta = \frac{\text{poles}}{2}\,\omega_m - \omega_{eo} \qquad (3.15)$$

Equations (3.5) through (3.9), (3.13) and (3.15) are the seventh order synchronous machine equations in the state variable form and (3.10), (3.11), (3.12) and (3.14) are the auxiliary equations.

3.2. State Equations of Controllers and DC Motor-Booster

The transfer function of the regulator-exciter, Fig. 2.7, in state equation form is

$$pv_R = -\frac{1}{T_{RE}}\,v_R + \frac{K_A}{T_{RE}}(v_{ref}-v_t) \qquad (3.16)$$

for the regulator and

$$pv_{fd} = \frac{1}{T_E} f(v_R) - \frac{1}{T_E} v_{fd} \tag{3.17}$$

for the synchronous machine field voltage. The characteristics of the field voltage limiter are approximated by

$$f(v_R) = a_1 \tanh (a_2 v_R) \tag{3.18}$$

where the values of a_1 and a_2 are determined from a least squares criterion. The terminal voltage is

$$v_t = \sqrt{v_d^2 + v_q^2} \tag{3.19}$$

The transfer function of the governor-hydraulic system, Fig. 2.4, in the state equation are as follows. For the actuator position

$$pa = -\frac{\sigma}{T_A} a - \frac{1}{T_A} a_f - \frac{1}{T_A} \Delta\omega_m \quad , \tag{3.20}$$

for the actuator feedback position

$$pa_f = -\frac{\sigma\delta}{T_A} a - \frac{\delta T_r + T_A}{T_r T_A} a_f - \frac{\delta}{T_A} \Delta\omega_m \tag{3.21}$$

for the gate position

$$pg = \frac{1}{T_G} a - \frac{1}{T_G} g \tag{3.22}$$

and for the turbine torque output

$$pt = -\frac{1}{.5T_G}\,a + \frac{T_G + T_W}{.5T_G T_W}\,g - \frac{1}{.5T_W}\,t \qquad (3.23)$$

The booster armature voltage state equation from (2.13) is

$$pv_B = -\frac{\omega_g L_{af}}{R_{fB}T_{fB}}\,v_{fB} - \frac{1}{T_{fB}}\,v_B \qquad (3.24)$$

where the booster field voltage signal of Fig. 2.2 is computed by

$$v_{fB} = \frac{2}{K_3}\left(\frac{t}{2}\right) - \left(\frac{2\alpha\alpha_R}{K_3}\,\frac{2K_4}{K_3}\right)\frac{\Delta\omega_m}{2} + \frac{2\alpha T_{fB}}{K_3}\,p\left(\frac{t}{2}\right)$$

$$- T_{fB}\left(\frac{2\alpha\alpha_R}{K_3} - \frac{2K_4}{K_3}\right)\,p\left(\frac{\Delta\omega_m}{2}\right) \qquad (3.25)$$

The state equation of the mechanical speed of the test model of (3.13) becomes

$$p\left(\frac{\omega_m}{2}\right) = \frac{L_{aF}i_F}{2J}\,i_A - \frac{K_1}{J}\left(\frac{\omega_m}{2}\right) - \frac{K_2}{2J} - \frac{T_e}{2J} \qquad (3.26)$$

where the d-c motor torque of (3.13) is computed by

$$T_i = L_{aF}i_F i_A \qquad (3.27)$$

the d-c motor and booster armature current by

$$i_A = (v_{tdc} - v_m - v_B) \,/\, R \qquad (3.28)$$

and the motor armature voltage by

$$v_m = 2\, L_{aF}\, i_F \left(\frac{\omega_m}{2}\right) \tag{3.29}$$

The state variable $\frac{\omega_m}{2}$ instead of ω_m is chosen because the tachometer output voltage is 94.25 volts at synchronous speed (188.5 rad/sec). The damping coefficient determined experimentally is

$$D = K_1 + \frac{K_2}{\omega_m} \tag{3.30}$$

Finally, the electrical torque angle state equation from (3.15) becomes

$$p\delta = 4\,\frac{\omega_m}{2} - \omega_{eo} \tag{3.31}$$

3.3. Initial State of a Power System

The initial states of a power system, v_d, v_q, i_d, i_q, v_o and δ, are determined from the operating conditions, i.e., the real power P, the reactive power Q and the voltage V_t at the machine terminal from the following nonlinear algebraic equations.

$$P = v_d\, i_d + v_q\, i_q \tag{3.32}$$

$$Q = v_q\, i_d - v_d\, i_q \tag{3.33}$$

$$v_t^2 = v_d^2 + v_q^2 \tag{3.34}$$

$$v_d = -r_a i_d + x_q i_q \tag{3.35}$$

$$v_d = k_1(v_o \sin\delta + r i_d - x i_q) + k_2(v_o \cos\delta + x i_d + r i_q) \tag{3.36}$$

$$v_q = k_1(v_o \cos\delta + x i_d + r i_q) - k_2(v_o \sin\delta + r i_d - x i_q) \tag{3.37}$$

For the particular cases studied in this thesis, these equations are solved by the method of Fletcher and Powell.[3.3] An initial estimate of the solution of i_q, v_d, v_q and i_d is obtained from the closed form solutions[3.4] which neglects armature resistance and that of v_o and δ from the transmission configuration of Fig. 3.1.

$$i_q = \frac{P V_t}{\sqrt{(P x_q)^2 + (v_t^2 + x_q Q)^2}} \tag{3.38}$$

$$v_d = x_q i_q \tag{3.39}$$

$$v_q = \sqrt{V_t^2 - v_d^2} \tag{3.40}$$

$$i_d = \frac{Q + x_q i_q^2}{v_q} \tag{3.41}$$

$$v_o = \sqrt{[v_d - r(i_d - v_d G + v_q B) + x(i_q - v_d B - v_q G)]^2 + [v_q - r(i_q - v_d B - v_q G) - x(i_d - v_d G + v_q B)]^2} \tag{3.42}$$

$$\delta = \arctan \frac{v_d - r(i_d - v_d G + v_q B) + x(i_q - v_d B - v_q G)}{v_q - r(i_q - v_d B - v_q G) - x(i_d - v_d G + v_q B)} \tag{3.43}$$

The initial value of the field voltage, required for the integration of (3.17), is determined from (3.1) and (3.3),

$$v_{fd} = (v_q + x_d\, i_d + r_a i_q) \quad \frac{R_f'}{x_{ad}} \tag{3.44}$$

where $\omega_e = \omega_{eo}$,

$$\text{and } \frac{R_f'}{x_{ad}} = R_f \sqrt{r_a^2 + x_q^2} \quad /(r_a^2 + x_d\, x_q) \text{ 'slope'} \tag{3.45}$$

The 'slope' is determined by the slope of the steady state short circuit characteristic of the synchronous machine, relating RMS armature phase current and d-c field current. The derivation of the expression for $\frac{R_f'}{x_{ad}}$ is presented in Appendix 3B.

The initial values of ψ_F, ψ_d and ψ_q are determined from (3A.12) and (3A.19) as

$$\begin{bmatrix} \psi_F \\ \psi_d \\ \psi_q \end{bmatrix} = \begin{bmatrix} T_{do}' & -T_{do}'(x_d - x_d') & 0 \\ \frac{1}{\omega_{eo}} & -\frac{x_d}{\omega_{eo}} & 0 \\ 0 & 0 & \frac{-x_q}{\omega_{eo}} \end{bmatrix} \begin{bmatrix} v_{FR} \\ i_d \\ i_q \end{bmatrix} \tag{3.46}$$

The following conditions are applied

$$\begin{aligned} &T_{D1} = 0 \quad T_{do}'' = 0 \quad T_{qo}'' = 0 \quad T_c = T_d' \quad T_D = 0 \\ &v_{DR}' = 0 \quad v_{QR}' = 0 \end{aligned} \tag{3.47}$$

Since $v_{FR} = v_F$ during steady state, the initial regulator voltage is

$$v_R = \frac{1}{a_2} \operatorname{arctanh}\left(\frac{v_{fd}}{a_1}\right) \tag{3.48}$$

and the reference voltage is established from

$$v_{ref} = (v_R + K_A\ v_t) \ / \ K_A \tag{3.49}$$

The initial values of the governor-hydraulic prime mover are

$$a = 0 \tag{3.50}$$

$$a_f = 0 \tag{3.51}$$

$$g = 0 \tag{3.52}$$

$$t = 0 \tag{3.53}$$

The initial value of the booster voltage of (3.24) is

$$v_B = 0 \tag{3.54}$$

since $v_{fB} = 0$, (3.25). The initial real power of the dynamic test model is set by the load setting resistor in the d-c motor-booster armature circuit. The value of resistance is established from (3.28), (3.20) and (3.54)

$$R = (v_{tdc} - \omega_m\ L_{aF}\ i_F) \ / \ i_A \tag{3.55}$$

where i_A is obtained from the steady state torque equation and is equal to

$$i_A = (K_1\ \omega_m + K_2 + \psi_d\ i_q - \psi_q\ i_d) \ / \ L_{aF}\ i_F \tag{3.56}$$

The first two terms on the right hand side of (3.56) are torque terms due to friction and the last two terms are the torque of the synchronous machine. The mechanical synchronous speed of the test model is

$$\omega_m = 188.5 \text{ rad/sec} \tag{3.57}$$

3.4. State Equations of Fifth Order-Synchronous Machine and Controllers

The fifth order-synchronous machine state equations are obtained by neglecting the damper winding effects of the seventh order model. By removing (3.8) and (3.9) and setting

$$T_{D1} = 0 \ , \ T''_{do} = 0 \ , \ T''_{qo} = 0 \ , \ T''_{d} = 0 \ , \ T''_{q} = 0 \tag{3.58}$$

$$A = 1, \ B = 0, \tag{3.59}$$

and

$$T_c = T'_d = \frac{x'_d}{x_d} T'_{do} \ , \ T_D = 0 \tag{3.60}$$

in (3A.2), Park's equations reduce to

$$p\psi_d = v_d + \omega_e \psi_q + r_a i_d \tag{3.61}$$

$$p\psi_q = v_q - \omega_e \psi_d + r_a i_q \tag{3.62}$$

$$p\psi_F = v_F - v_{FR} \tag{3.63}$$

where (3.10) is replaced by

$$\begin{bmatrix} v_{FR} \\ i_d \end{bmatrix} = \begin{bmatrix} \frac{x_d}{x'_d \, T'_{do}} & \frac{-\omega_{eo} \, (x_d - x'_d)}{x'_d} \\ \frac{1}{x'_d \, T'_{do}} & -\frac{\omega_{eo}}{x'_d} \end{bmatrix} \begin{bmatrix} \psi_F \\ \psi_d \end{bmatrix} \tag{3.64}$$

and (3.11) becomes

$$i_q = -\frac{\omega_{eo}}{x_q} \psi_q \tag{3.65}$$

Further elimination of v_d, v_q, i_d, i_q and v_{FR} in (3.61) through (3.63) using (3.12), (3.64) and (3.65) results in the following state equations.

$$p\psi_F = -\frac{x_d}{x'_d\, T'_{do}}\psi_F + \frac{\omega_{eo}(x_d - x'_d)}{x'_d}\psi_d + \frac{(r_a^2 + x_d x_q)\text{'slope'}}{\sqrt{r_a^2 + x_q^2}\; R_f} v_{fd} \tag{3.66}$$

$$p\psi_d = \frac{k_1 r + k_2 x + r_a}{x'_d\, T'_{do}}\psi_F - \frac{k_1 r + k_2 x + r_a}{x'_d}\omega_{eo}\psi_d + \frac{k_1 x - k_2 r}{x_q}\omega_{eo}\psi_q + 4.0\,\frac{\omega_m}{2}\psi_q + k_1 v_o \sin\delta + k_2 v_o \cos\delta \tag{3.67}$$

$$p\psi_q = \frac{k_1 x - k_2 r}{x'_d\, T'_{do}}\psi_F - \frac{k_1 x - k_2 r}{x'_d}\omega_{eo}\psi_d - 4.0\,\frac{\omega_m}{2}\psi_d - \frac{k_1 r + k_2 x + r_a}{x_q}\omega_{eo}\psi_q - k_1 v_o \sin\delta + k_1 v_o \cos\delta \tag{3.68}$$

The state equations (3.26) and (3.31) for machine dynamics, (3.16) and (3.17) for regulator-exciter, (3.20) through (3.23) for governor-hydraulic system, (3.24) for booster armature voltage, and hence the auxiliary equations of them remain unchanged except the electrical torque T_e of (3.26) and (3.14) now equal to

$$T_e = 6\omega_{eo}\left(\frac{1}{x'_d} - \frac{1}{x_q}\right)\psi_d\psi_q - \frac{6}{x'_d\, T'_{do}}\psi_q\psi_F \tag{3.69}$$

the d- and q- axis voltages of (3.19) from 3.61), (3.62), (3.64) and (3.65) now equal to

$$v_d = p\psi_d - \omega_e\psi_q - \frac{r_a}{x'_d\, T'_{do}}\,\psi_F + \frac{r_a\,\omega_{eo}}{x'_d}\,\psi_d \tag{3.70}$$

$$v_q = p\psi_q + \omega_e\psi_d + \frac{r_a\,\omega_{eo}}{x_q}\,\psi_q \tag{3.71}$$

These equations consist of the complete set of state and auxiliary equations for the power system with a fifth order-synchronous machine and controllers.

The initial conditions for the state equations of the fifth order-synchronous and controllers are the same as presented in Section 3.3. The variables i_d, i_q, v_d, v_q, v_t and i_{fd} are calculated from the solution of the state variables at each integration step.

$$i_d = \frac{1}{x'_d\, T'_{do}}\,\psi_F - \frac{\omega_{eo}}{x'_d}\,\psi_d \tag{3.72}$$

$$i_q = -\frac{\omega_{eo}}{x_q}\,\psi_q \tag{3.73}$$

$$v_d = (k_1 r + k_2 x) i_d - (k_1 x - k_2 r) i_q + k_1 v_o \sin\delta + k_2\, v_o \cos\delta \tag{3.74}$$

$$v_q = (k_1 x - k_2 r) i_d + (k_1 r + k_2 x) iq - k_2 v_o \sin\delta + k_1\, v_o \cos\delta \tag{3.75}$$

$$v_t = \sqrt{v_d^2 + v_q^2} \tag{3.19}$$

$$i_{fd} = \frac{\sqrt{r_a^2 + x_q^2}}{(r_a^2 + x_d x_q)\ \text{'slope'}} \left(\frac{x_d}{T'_{do} x'_d} \psi_F - \frac{(x_d - x'_d)}{x'_d} \omega_{eo} \psi_d \right) \tag{3.76}$$

3.5. State Equations of Third Order-Synchronous Machine and Controllers

The third order synchronous machine state equations are obtained from the fifth order model with two more assumptions. First, the speed voltage effects due to speed variation in (3.61) and (3.62) are negligible;

$$\omega_e \psi_d \simeq \omega_{eo} \psi_d \quad , \quad \omega_e \psi_q \simeq \omega_{eo} \psi_q \tag{3.77}$$

Second, the induced voltage effects due to the change of flux linkages are much smaller than the speed voltages;

$$p\psi_d << \omega_{eo} \psi_q \quad , \quad p\psi_q << \omega_{eo} \psi_d \tag{3.78}$$

As a result, the two state equations (3.61) and (3.62) reduce to algebraic equations and may be written

$$\begin{bmatrix} 0 \\ 0 \end{bmatrix} = \begin{bmatrix} 1 & 0 \\ 0 & 1 \end{bmatrix} \begin{bmatrix} v_d \\ v_q \end{bmatrix} + \begin{bmatrix} 0 & \omega_e \\ -\omega_e & 0 \end{bmatrix} \begin{bmatrix} \psi_q \\ \psi_d \end{bmatrix} + \begin{bmatrix} r_a & 0 \\ 0 & r_a \end{bmatrix} \begin{bmatrix} i_d \\ i_q \end{bmatrix} \tag{3.79}$$

where v_d and v_q can be eliminated using (3.12) and i_d and i_q using (3.64) and (3.65). Finally, ψ_d and ψ_q are expressed as

$$\begin{bmatrix} \psi_d \\ \psi_q \end{bmatrix} = \frac{\omega_{eo}}{\Delta} \begin{bmatrix} \dfrac{r_o^2 + x_o(x_o + x_q)}{x_q\, x_d'\, T_{do}'} \\ \dfrac{-r_o\,(x_o+x_d') + r_o x_o}{x_d'^2\, T_{do}'} \end{bmatrix} \begin{bmatrix} \psi_F \\ \psi_F \end{bmatrix} +$$

$$\begin{bmatrix} \dfrac{r_o k_1 - k_2(x_o+x_q)}{x_q} & \dfrac{r_o k_2 + k_1(x_o+x_q)}{x_q} \\ \dfrac{r_o k_2 + k_1(x_o+x_d')}{x_d'} & \dfrac{r_o k_1 - k_2(x_o+x_q)}{x_d'} \end{bmatrix} \begin{bmatrix} v_o \sin\delta \\ v_o \cos\delta \end{bmatrix} \quad (3.80)$$

where $\Delta = \omega_{eo}^2 \dfrac{r_o^2 + (x_o+x_q)(x_o+x_d')}{x_d'\, x_q}$

and
$$\begin{aligned} r_o &= k_1 r + k_2 x + r_a \\ x_o &= k_1 x - k_2 r \end{aligned} \quad (3.81)$$

After eliminating ψ_d, (3.63) reduces to

$$p\psi_F = -\frac{1}{x_d' T_{do}'}\left(x_d - \frac{(x_d-x_d')(r_o^2+x_o(x_o+x_q))}{r_o^2 + (x_o+x_q)(x_o+x_d')}\right)\psi_F + \frac{(r_a^2+x_d x_q)\text{'slope'}}{\sqrt{r_a^2+x_q^2}\quad R_f} v_{fd}$$

$$+\frac{(x_d-x_d')(r_o k_1 - k_2(x_o+x_q))}{r_o^2+(x_o+x_q)(x_o+x_d')} v_o \sin\delta + \frac{(x_d-x_d')(r_o k_2 + k_1(x_o+x_q))}{r_o^2+(x_o+x_q)(x_o+x_d')} v_o \cos\delta \quad (3.82)$$

The other two synchronous machine dynamic state equations (3.26) and (3.31) and the auxiliary equation (3.69) remain unchanged.

The exciter state equations (3.16) and (3.17) and the terminal equation (3.19) remain the same. However, with the conditions (3.77) and (3.78), (3.70) reduces to

$$v_d = -\omega_{eo}\psi_q - \frac{r_a}{x'_d T'_{do}}\psi_F + \frac{r_a \omega_{eo}}{x'_d}\psi_d \qquad (3.83)$$

and (3.71) to

$$v_q = \omega_{eo}\psi_q + \frac{r_a \omega_{eo}}{x_q}\psi_q \qquad (3.84)$$

The state equations describing the governor-hydraulic prime mover (3.20) to (3.23) and the d-c motor-booster state equation (3.24) remain unchanged.

In summary (3.82), (3.26), (3.31), (3.16), (3.17), (3.20) to (3.23) and (3.24) form the state equations of the third order-synchronous machine with controllers, and the auxiliary equations are (3.28), (3.29), (3.69), (3.85), (3.86), (3.18), (3.19), (3.83), (3.84) and (3.25). The method of evaluating the initial conditions is described in Section 3.3. The variables ψ_d, ψ_q, i_d, i_q, v_d, v_q, v_t and i_{fd} are calculated from the solution of state variables at each step as follows

$$\psi_d = \frac{r_o^2 + x_o(x_o+x_q)}{\omega_{eo}T'_{do}(r_o^2+(x_o+x_q)(x_o+x'_d))}\psi_F + \frac{x'_d(r_o k_1 - k_2(x_o+x_q+x_q))}{\omega_{eo}}\sin\delta$$

$$+ \frac{x'_d(r_o k_2 + k_1(x_o+x_q))}{\omega_{eo}}\cos\delta \qquad (3.85)$$

$$\psi_q = \frac{x_q(r_o x_o - r_o(x_o+x'_d))}{\omega_{eo}\, x'_d\, T'_{do}}\ \psi_F + \frac{x_q(r_o k_2 + k_2(x_o+x'_d))}{\omega_{eo}} \sin\delta$$

$$+ \frac{x_q(r_o k_1 - k_2(x_o+x'_d))}{\omega_{eo}} \cos\delta \qquad (3.86)$$

$$i_d = \frac{1}{x'_d T'_{do}}\ \psi_F - \frac{\omega_{eo}}{x'_d}\ \psi_d \qquad (3.87)$$

$$i_q = -\frac{\omega_{eo}}{x_q}\ \psi_q \qquad (3.88)$$

$$v_d = -\omega_{eo}\ \psi_q - r_a i_d \qquad (3.89)$$

$$v_q = \omega_{eo}\ \psi_d - r_a i_q \qquad (3.90)$$

$$v_t = \sqrt{v_d^2 + v_q^2} \qquad (3.91)$$

$$i_{fd} = \frac{\sqrt{r_a^2 + x_q^2}}{(r_a^2 + x_d x_q)\,\text{slope}} \left(\frac{x_d}{x'_d T'_{do}}\ \psi_F - \frac{(x_d - x'_d)}{x'_d}\ \omega_{eo}\psi_d \right) \qquad (3.92)$$

3.6. State Equations of Third Order-Synchronous Machine and Regulator-Exciter but without Governor

For the study of electrical transients of the system, the governor-hydraulic prime mover dynamics are replaced with a constant torque input. The equations (3.82) and (3.31) describing the synchronous machine and (3.16) and (3.17) describing the regulator-exciter remain unchanged. The state equation for mechanical speed (3.26) becomes

$$p\left(\frac{\omega_m}{2}\right) = \frac{P_{3\phi}}{2J\omega_{mb}} + \frac{K_1}{J}\frac{\omega_{mb}}{2} - \frac{K_1}{J}\frac{\omega_m}{2}$$

$$- \frac{3\omega_{eo}}{J}\left(\frac{1}{x'_d} - \frac{1}{x_q}\right)\psi_d\psi_q + \frac{3}{x'_d T'_{do}}\psi_q\psi_F \qquad (3.93)$$

The auxiliary equations are (3.85), (3.86), (3.18), (3.19), (3.83) and (3.84). The initial conditions are evaluated by the techniques described in Section 3.3 and the variables ψ_d, ψ_q, i_d, i_q, v_q, v_t and i_{fd} (3.85) through (3.92).

3.7. Computation and Test Results of the Dynamic Test Model

In this Section, computation results of various state variable models of Section 3.4, 3.5 and 3.6 and results from actual tests are summarized and a comparison is made in order to verify the mathematical models.

A transient test is carried out on the power system described in Chapter 2 simulated on the dynamic test model. The system has a three-phase fault before the fault line of a double circuit transmission system is isolated at 5 cycles. The fault is cleared and the system restored after 30 cycles. The test responses of the torque angle δ, governor actuator position a, governor actuator feedback a_f, gate $_g$, turbine torque t, booster armature voltage v_B, terminal voltage v_t, regulator voltage v_{fd} and field current i_{fd} are recorded on a visicorder. The results are plotted along with the computation results of the three different state variable models.

The curves in Fig. 3.2 through 3.11 are identified as follows:

1. third order machine with exciter,
2. third order machine with exciter and governor,
3. fifth order machine with exciter and governor,
4. dynamic model test results.

Hamming's numerical integration method[3.5] is used for computation with an integration step size of 0.00025 seconds for the fifth order machine which includes $p\Psi_d$ and $p\Psi_q$ and 0.005 seconds for the other two models. The computation results of all three models are very close except the terminal voltage response of the fifth order machine model, curve 3, Fig. 3.8. The fifth order model predicts the voltage spikes due to line switching at fault cleared and system restored which is substantiated by actual test results. It is also observed that both the third and fifth order models with governor, curves 2 and 3, Fig. 3.2, are slightly more unstable than the third order without governor, curve 1, Fig.3.2. This phenomena is observed also from direct model tests.

A close correlation between computational and test model results is observed except for the regulator voltage, Fig. 3.9, and the field voltage, Fig. 3.10, at the instant the system is restored. This may be attributed to the imperfect mathematical model. For example, it does not include transmission line switching, since it is described by steady state equations. However, the prevailing frequency of oscillation is the same.

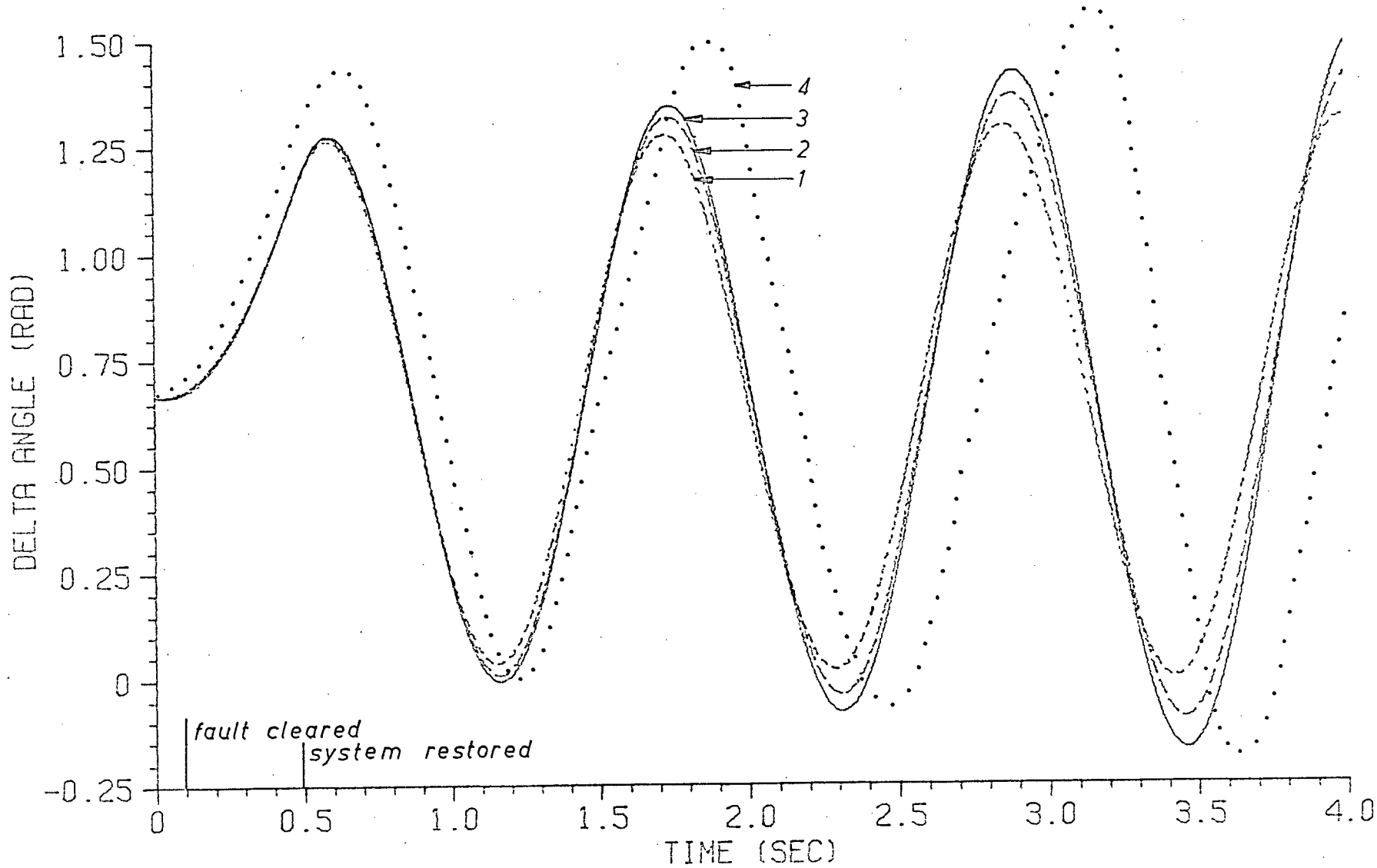

Fig. 3.2. Torque Angle Transient Responses

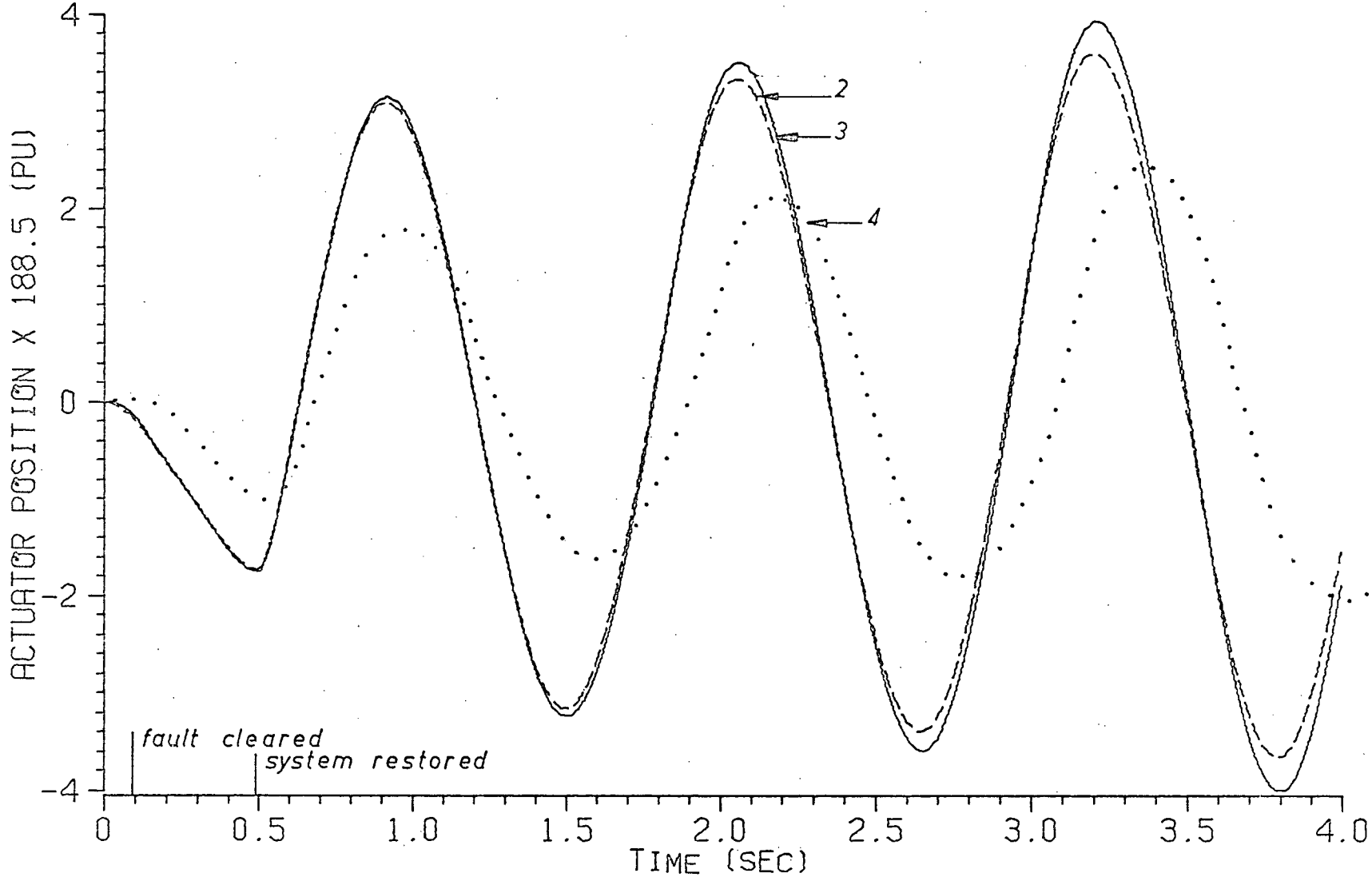

Fig. 3.3. Governor Actuator Position Transient Responses

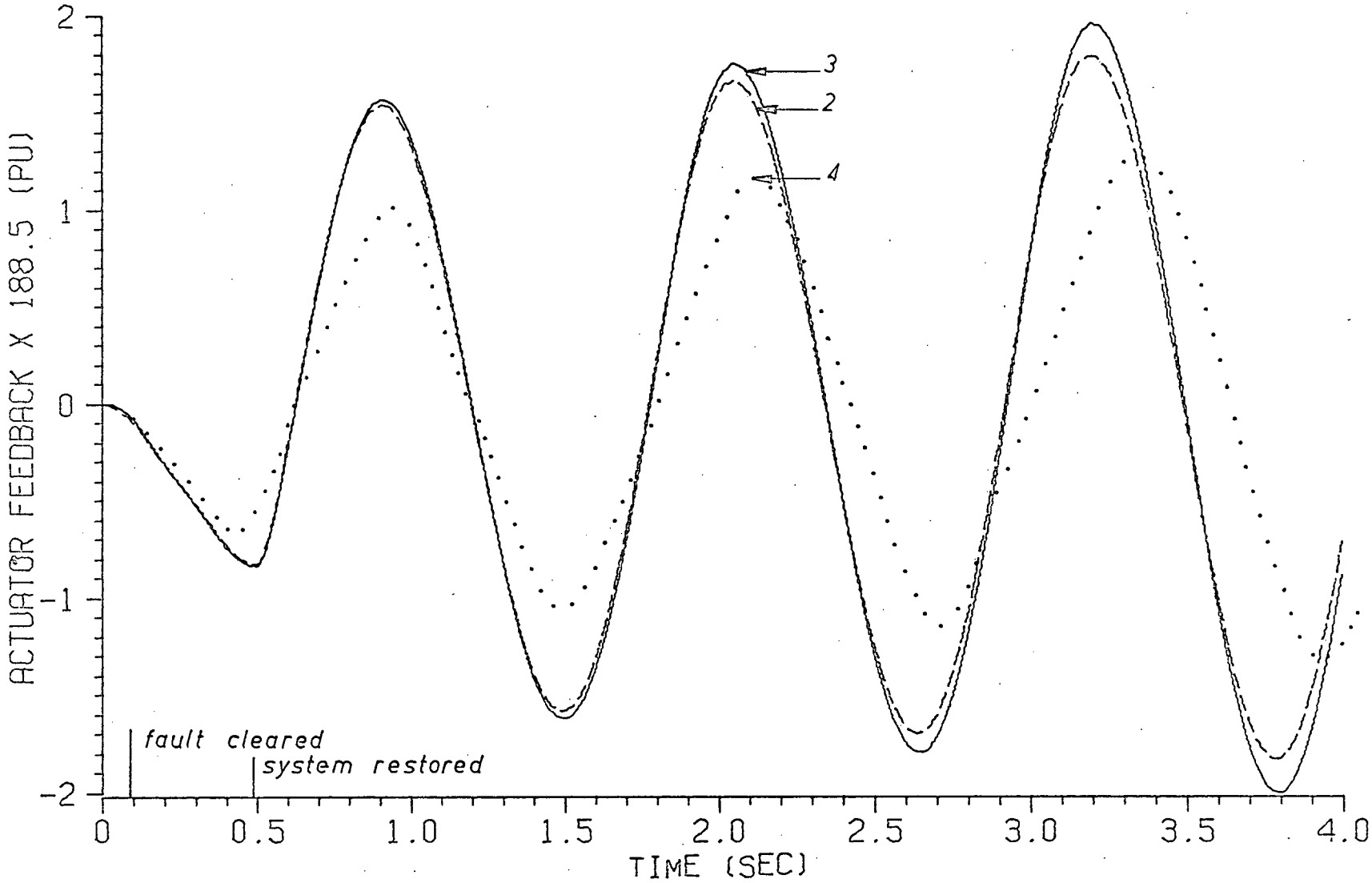

Fig. 3.4. Governor Actuator Feedback Transient Responses

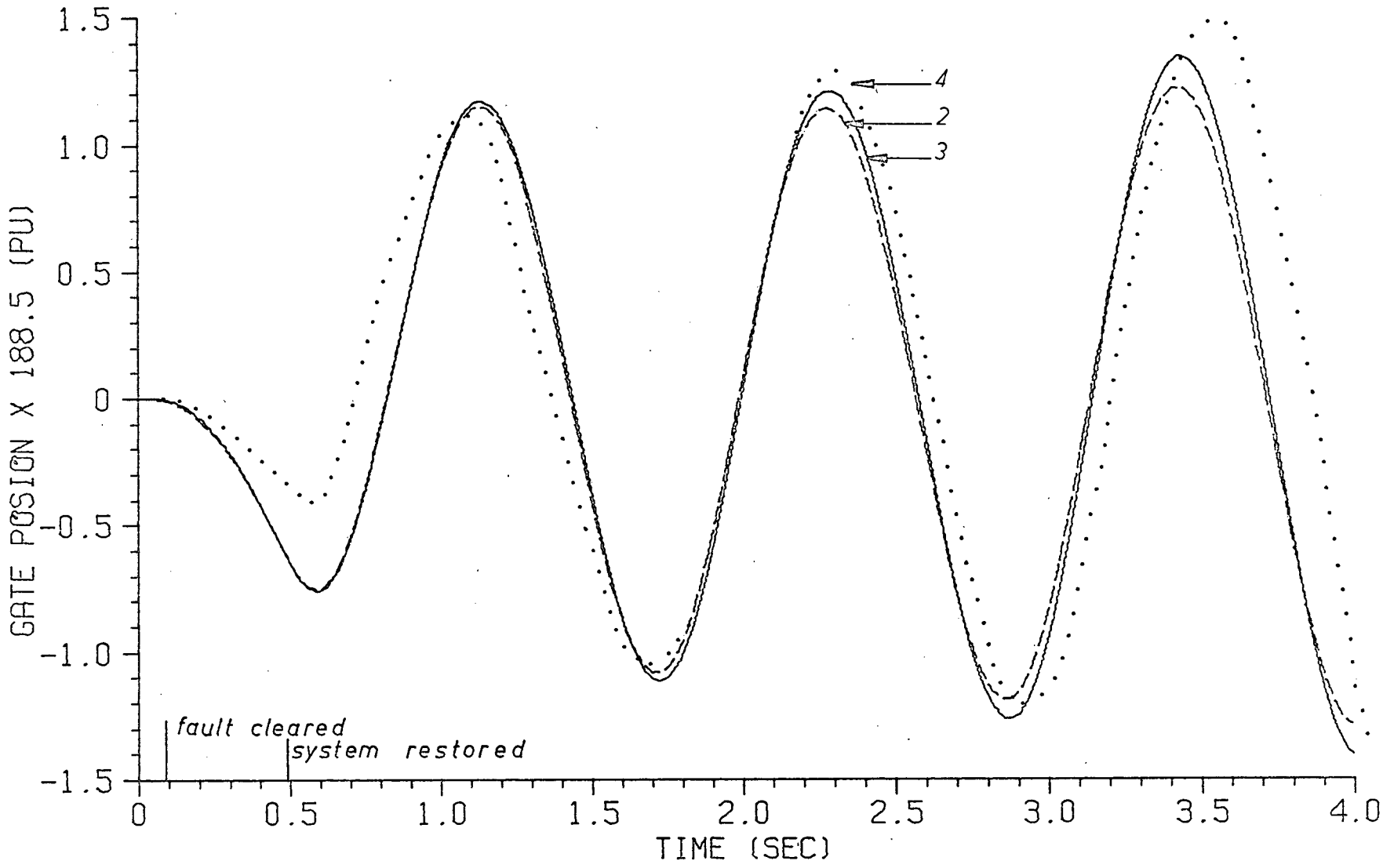

Fig. 3.5. Governor Gate Position Transient Responses

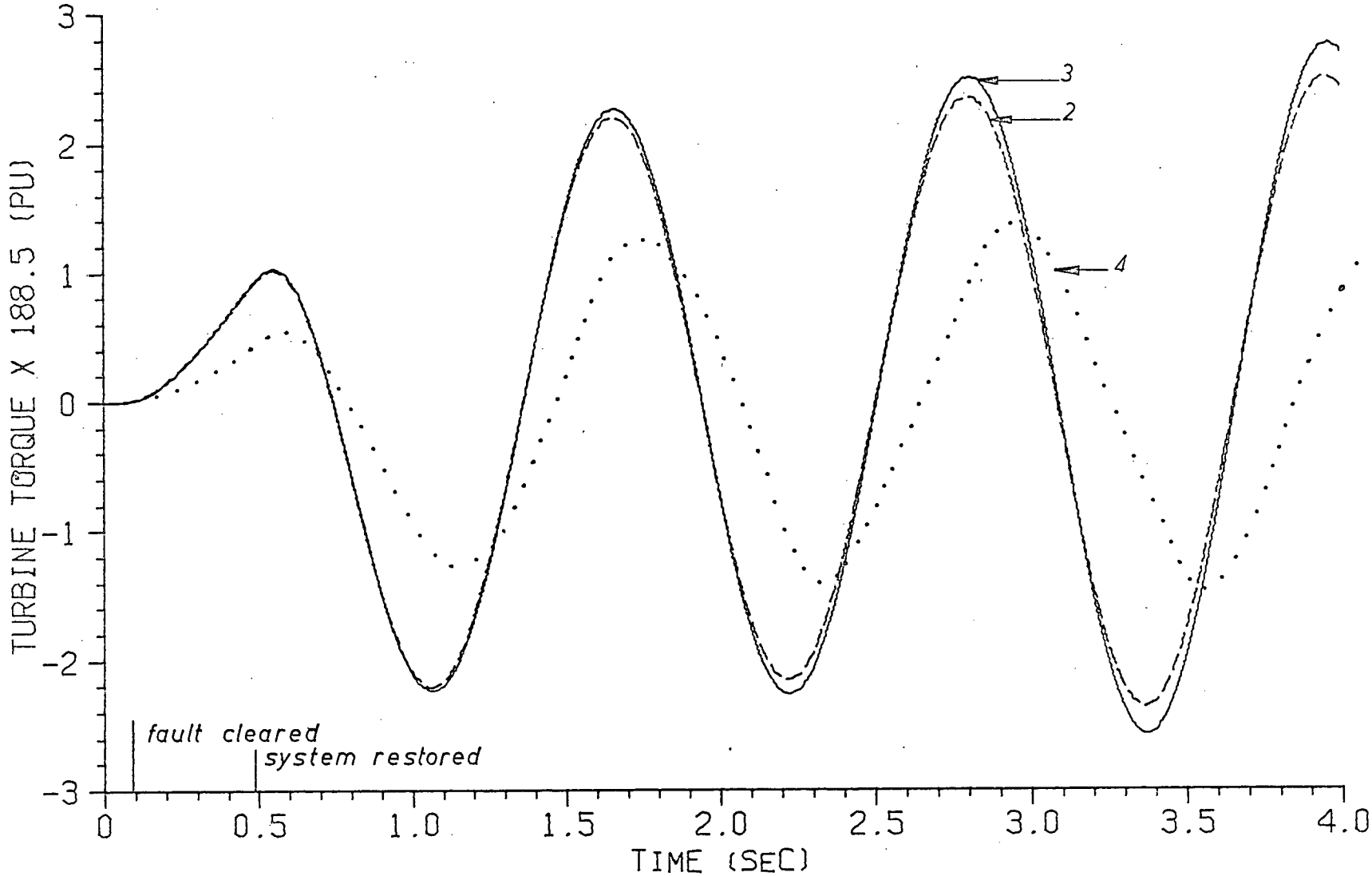

Fig. 3.6. Turbine Torque Transient Responses

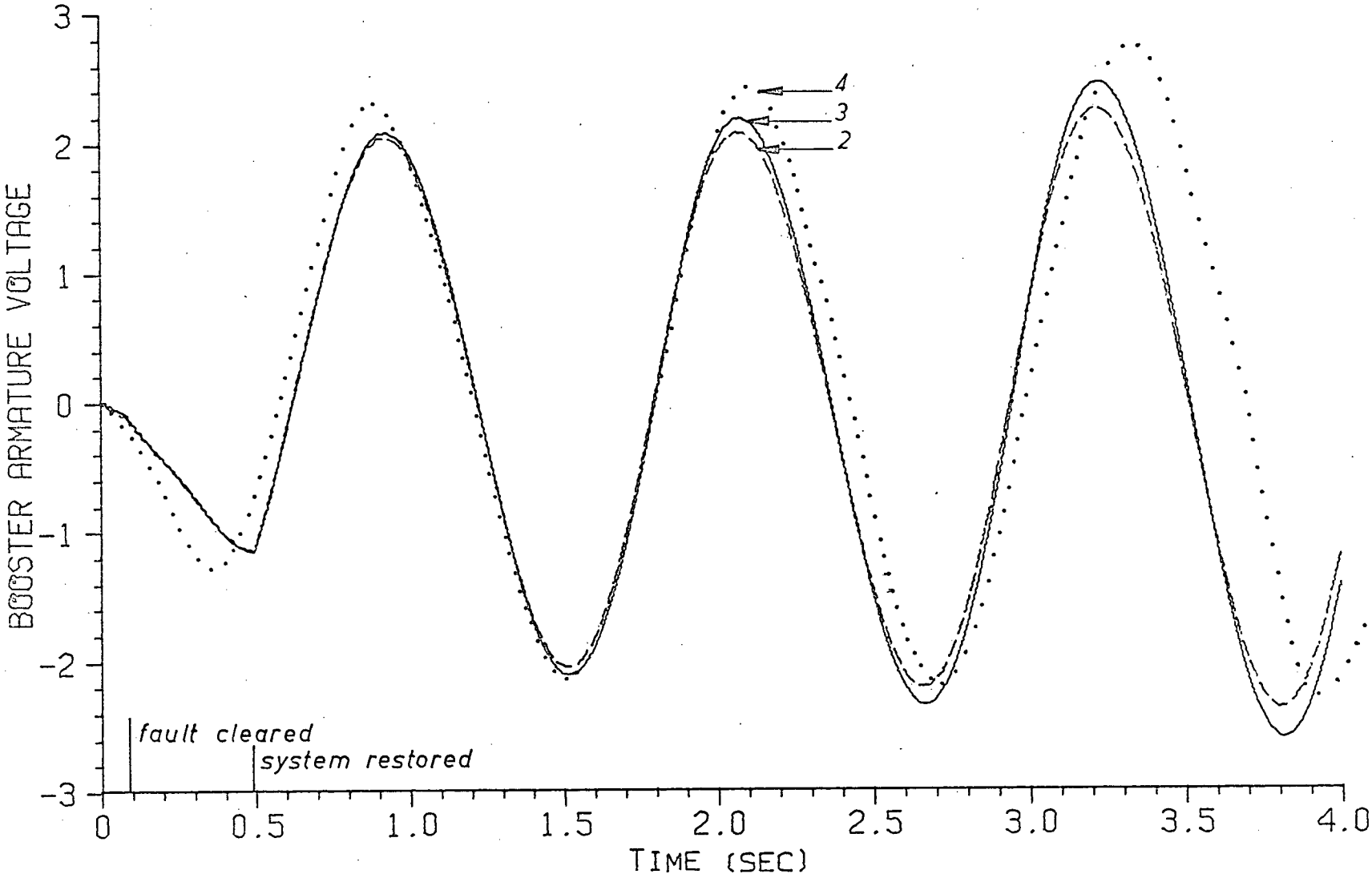

Fig. 3.7. Booster Armature Voltage Transient Responses

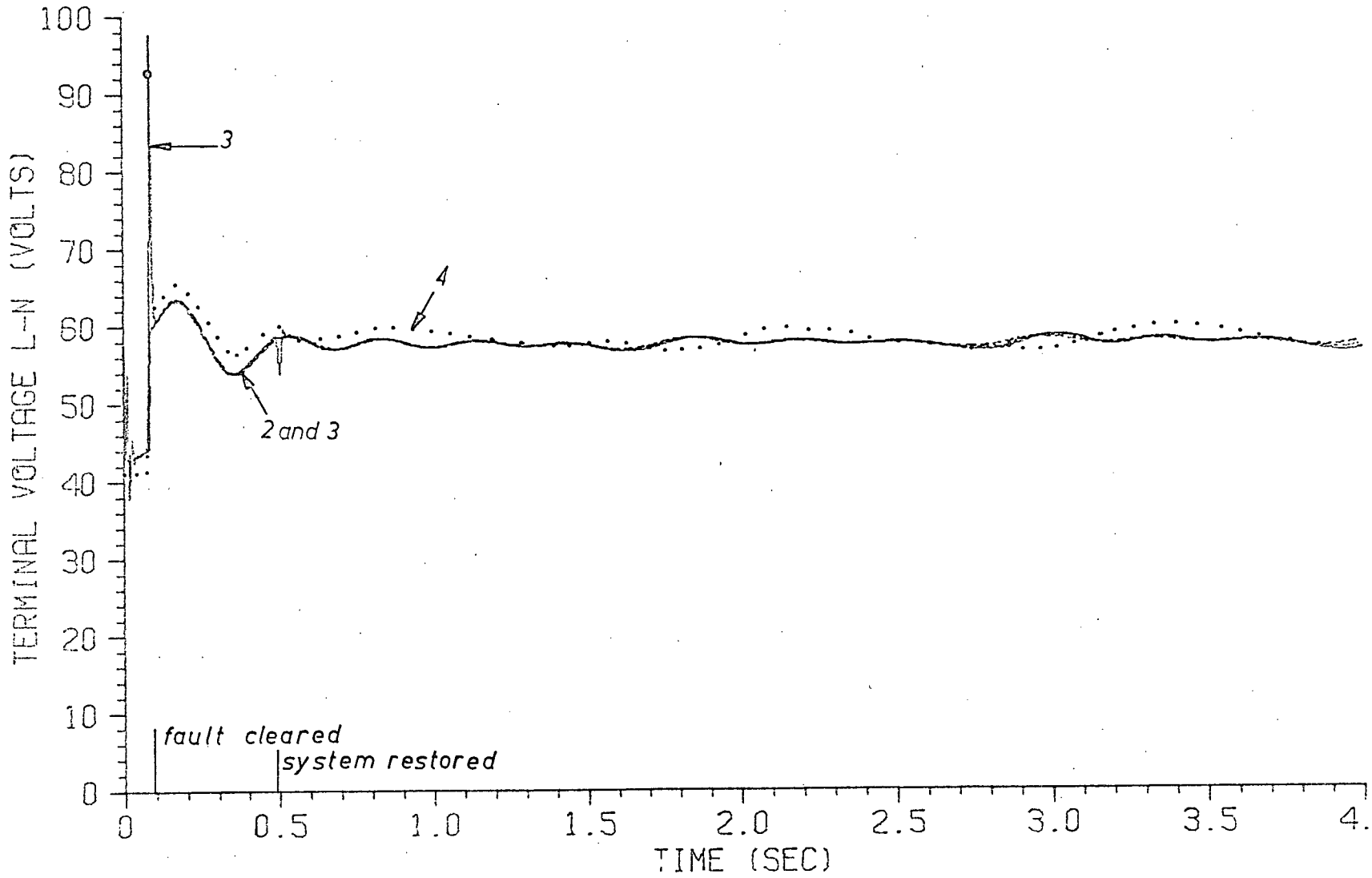

Fig. 3.8. Terminal Voltage Transient Responses

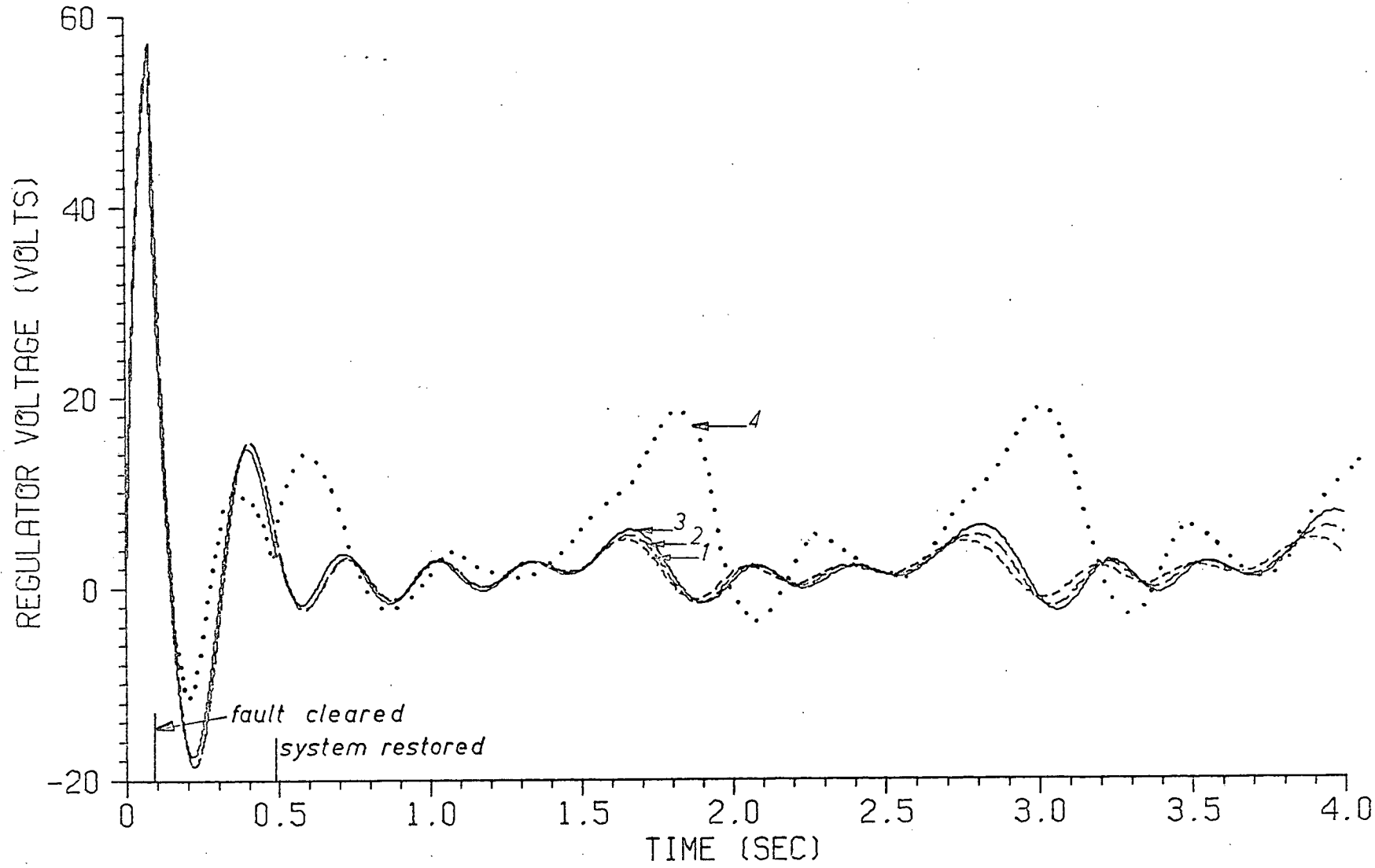

Fig. 3.9. Regulator Voltage Transient Responses

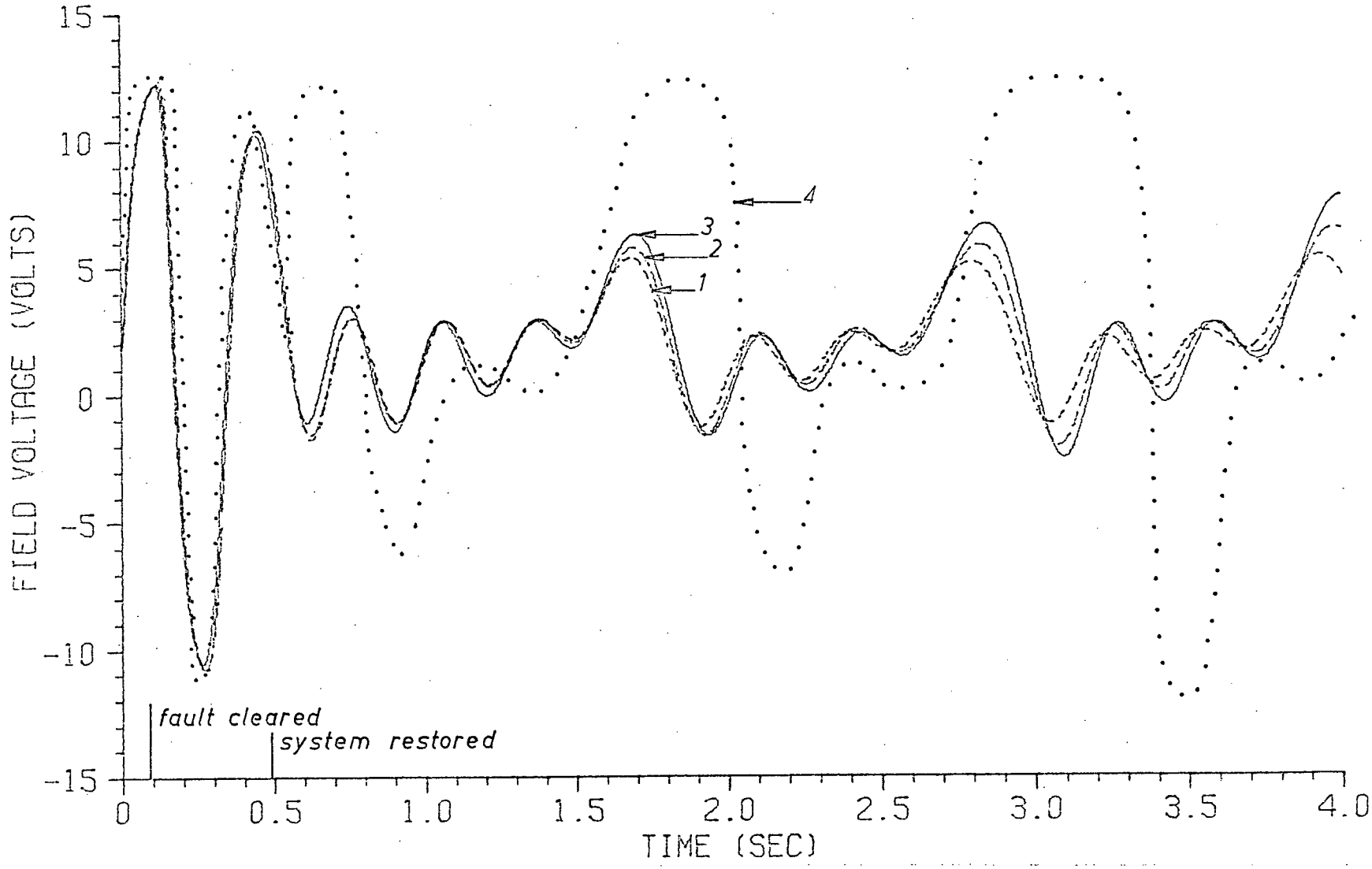

Fig. 3.10. Field Voltage Transient Responses

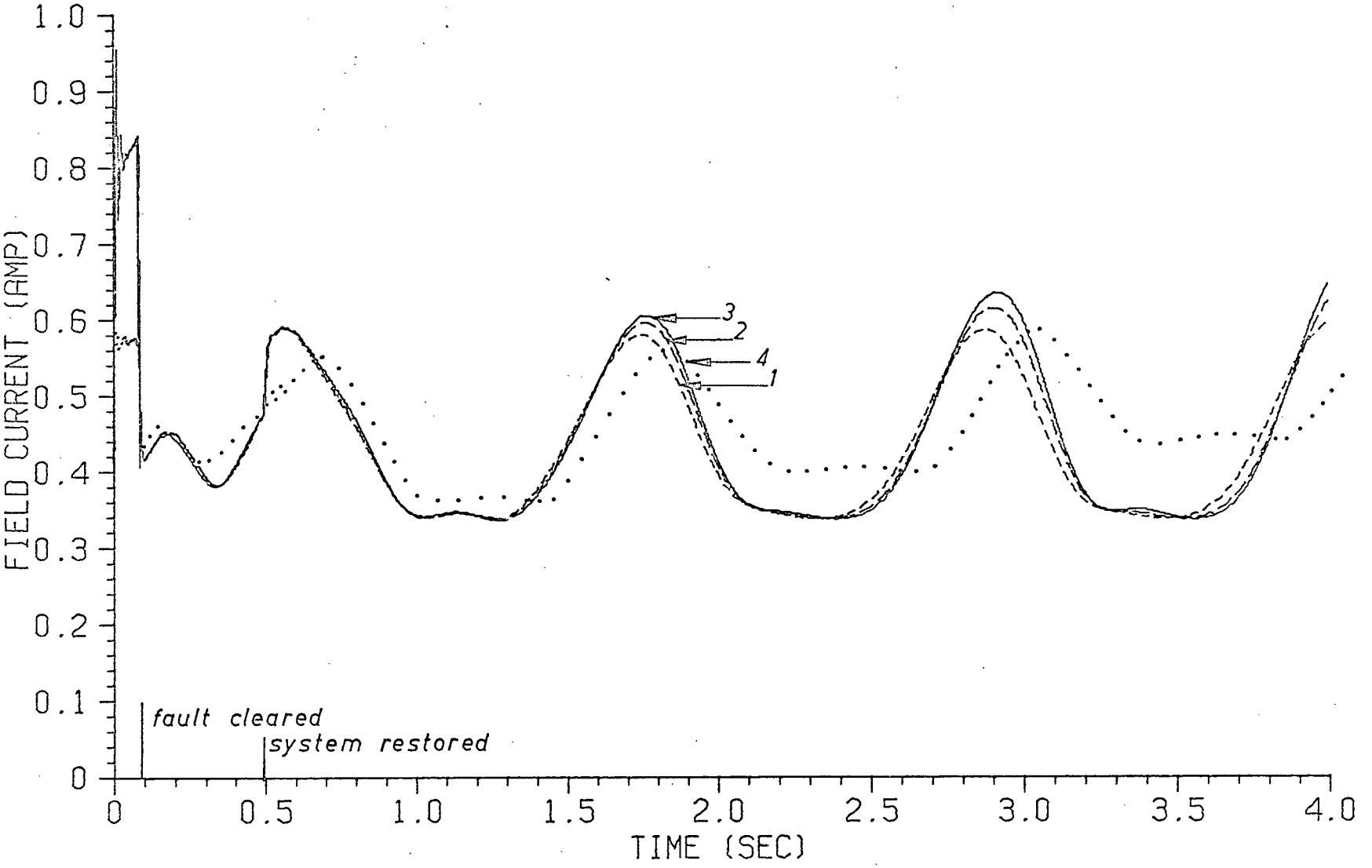

Fig. 3.11. Field Current Transient Responses

4. PARAMETER SENSITIVITY OF THE TEST MODEL

Sensitivity analysis[4.1, 4.2] is applied in this chapter to investigate the effect of model parameters on system response. As shown in Section 2.3.3, only important model parameters, not all of them, can be matched simultaneously with actual system values (Table 2.1). The model base impedance chosen is a compromise. Sensitivity analysis is applied to see whether this approach is justified. The controllers are included in the investigation. The state equations for the synchronous machine and controllers are given in Section 3.4.

4.1. Sensitivity Equation

The state variable equation is written as

$$\dot{x}_i = f_i(x, q_r) \quad , \quad q_r = q \,/\, q_o \tag{4.1}$$

where q_r is the relative value of the parameter, q the true value and q_o a constant equal to initial value of the parameter. The sensitivity equation for small parameter perturbations becomes

$$\dot{x}_{i,q_r} = \sum_{k=1}^{n} \frac{\partial f_i}{\partial x_k} \; x_{k,q_r} + q_o \frac{\partial f_i}{\partial q} \tag{4.2}$$

where $$x_{k,q_r} \triangleq \frac{dx_k}{dq_r} \tag{4.3}$$

The right hand side of the sensitivity equation (4.2) consists of two terms; the first term includes the state variable sensitivity coefficients only and the second term depends upon parameters explicitly. The two terms will be identified as $fl_{i,q_r}(x,x_k,q_r)$ and $f2_{i,q_r}(x)$ respectively, where

$$fl_{i,q_r}(x,x_k,q_r) = \sum_{k=1}^{n} \frac{\partial f_i}{\partial x_k} x_{k,q_r} \tag{4.4}$$

and $$f2_{i,q_r}(x) = q_o \frac{\partial f_i}{\partial q} \tag{4.5}$$

When the results are applied to system equations of Section 3.4, the terms independent of parameters are

$$fl_{\psi_F,q_r} = \frac{x_d}{x'_d T'_{do}} x_{\psi_F,q_r} + \omega_{eo}(x_d - x'_d) x_{\psi_d,q_r} + \frac{(r_a^2 + x_d x_q)\ \text{'slope'}}{\sqrt{r_a^2 + x_q^2}\ R_f} x_{v_{fd},q_r} \tag{4.6}$$

$$fl_{\psi_d,q_r} = \frac{r_o}{x'_d T'_{do}} x_{\psi_F,q_r} - \frac{r_o}{x'_d} \omega_{eo} x_{\psi_d,q_r} + \frac{x_o}{x_q} \omega_{eo} x_{\psi_q,q_r} + 4\frac{\omega_m}{2} x_{\psi_q,q_r} + 4\psi_q x_{\frac{\omega_m}{2},q_r} + k_1 v_o \cos\delta \sin(x_{\delta,q_r}) - k_2 v_o \sin\delta \cos(x_{\delta,q_r}) \tag{4.7}$$

$$fl_{\psi_q,q_r} = \frac{x_o}{x'_d T'_{do}} x_{\psi_F,q_r} - \frac{x_o}{x'_d} \omega_{eo} x_{\psi_d,q_r}$$

$$- 4 \frac{\omega_m}{2} x_{\psi_d,q_r} - 4 \psi_d x_{\frac{\omega_m}{2},q_r} - \frac{r_o}{x_q} \omega_{eo} x_{\psi_q,q_r}$$

$$- k_1 v_o \cos\delta \sin (x_{\delta,q_r}) - k_1 v_o \sin\delta \cos (x_{\delta,q_r}) \qquad (4.8)$$

$$fl_{\frac{\omega_m}{2},q_r} = \left(\frac{K_1}{J} - \frac{(L_{aF} i_F)^2}{JR}\right) x_{\frac{\omega_m}{2},q_r} - \frac{L_{aF} i_F}{2JR} x_{v_B,q_r}$$

$$- \frac{3\omega_{eo}}{J} \left(\frac{1}{x'_d} - \frac{1}{x_q}\right)\left(\psi_d x_{\psi_q,q_r} + \psi_q x_{\psi_d,q_r}\right)$$

$$+ \frac{3}{J x'_d T'_{do}} \left(\psi_F x_{\psi_q,q_r} + \psi_q x_{\psi_F,q_r}\right) \qquad (4.9)$$

$$fl_{\delta,q_r} = 4 x_{\frac{\omega_m}{2},q_r}$$

$$fl_{v_R,q_r} = - \frac{1}{T_{RE}} x_{v_R,q_r} - \frac{K_A}{T_{RE} v_t} \left[\frac{1}{x'_d T'_{do}} (v_d(r_o - r_a) + v_q x_o) x_{\psi_F,q_r}\right.$$

$$- \frac{\omega_{eo}}{x'_d} (v_d(r_o - r_a) + v_q x_o) x_{\psi_d,q_r} + \frac{\omega_{eo}}{x_q} (v_d x_o - v_q(r_o - r_a))$$

$$x_{\psi_q,q_r}$$

$$\left. + (v_d(k_1 v_o \cos\delta - k_2 v_o \sin\delta) + v_q(-k_2 v_o \cos\delta - k_1 v_o \sin\delta)) \right.$$

$$\left. x_{\delta,q_r}\right] \qquad (4.11)$$

$$fl_{v_{fd},q_r} = -\frac{1}{T_E} x_{v_{fd},q_r} + \frac{a_1 a_2}{T_E} \operatorname{sech}^2(a_2 v_R)\, x_{v_R,q_r} \qquad (4.12)$$

$$fl_{a,q_r} = -\frac{\sigma}{T_A} x_{a,q_r} - \frac{1}{T_A} x_{a_f,q_r} - \frac{2}{T_A} x_{\frac{\omega_m}{2},q_r} \qquad (4.13)$$

$$fl_{a_f,q_r} = -\frac{\sigma\delta}{T_A} x_{a,q_r} - \frac{\delta T_r + T_A}{T_r T_A} x_{a_f,q_r} - \frac{2}{T_A} x_{\frac{\omega_m}{2},q_r} \qquad (4.14)$$

$$fl_{g,q_r} = \frac{1}{T_G} x_{a,q_r} - \frac{1}{T_G} x_{g,q_r} \qquad (4.15)$$

$$fl_{t,q_r} = -\frac{1}{.5T_G} x_{a,q_r} + \frac{T_G + T_W}{.5T_G T_W} x_{g,q_r} - \frac{1}{.5T_W} x_{t,q_r} \qquad (4.16)$$

$$\begin{aligned} fl_{v_B,q_r} = &-\frac{2\alpha}{K_3}\frac{\omega_g L_{af}}{R_{fB}T_{fB}}\frac{1}{2} x_{t,q_r} + \left(\frac{2\alpha\alpha_R}{K_3} - \frac{2K_4}{K_3}\right)\frac{\omega_g L_{af}}{R_{fB}T_{fB}} x_{\frac{\omega_m}{2},q_r} \\ &- \frac{2\alpha T_{fB}}{K_3}\frac{\omega_g L_{af}}{R_{fB}T_{fB}}\frac{1}{2} fl_{t,q_r} + T_{fB}\left(\frac{2\alpha\alpha_R}{K_3} - \frac{2K_4}{K_3}\right)\frac{\omega_g L_{af}}{R_{fB}T_{fB}} fl_{\frac{\omega_m}{2},q_r} \\ &- \frac{1}{T_{fB}} x_{v_B,q_r} \end{aligned} \qquad (4.17)$$

The parameters involved in the sensitivity investigation are r_a, x_d, x_q, x'_d, T'_{do} and J of the synchronous machine, K_A, T_{RE} and T_E of the regulator-exciter and δ, σ, T_A, T_R, T_G and T_W of the governor-hydraulic operator.

For the armature resistance r_a, (4.5) yields

$$f2_{\psi_F,r_a} = \frac{r_a \text{'slope'}}{R_f(r_a^2+x_q^2)}\left(2r_a\sqrt{r_a^2+x_q^2} - \frac{r_a(r_a^2+x_d x_2)}{\sqrt{r_a^2+x_q^2}}\right) v_{fd} \qquad (4.18)$$

$$f2_{\psi_d, r_a} = \frac{r_a}{x_d' T_{do}'} \psi_F - \frac{r_a \omega_{eo}}{x_d'} \psi_d \tag{4.19}$$

$$f2_{\psi_q, r_a} = - \frac{r_a \omega_{eo}}{x_q} \psi_q \tag{4.20}$$

for the d-axis synchronous reactance

$$f2_{\psi_F, x_d} = - \frac{x_d}{x_d' T_{do}'} \psi_F + \frac{x_{d\ eo}}{x_d'} \psi_d + \frac{x_d x_q \text{'slope'}}{R_f \quad r_a^2 + x_q^2} v_{fd} \tag{4.21}$$

for the q-axis synchronous reactance

$$f2_{\psi_F, x_q} = \frac{x_q \text{'slope'}}{R_f (r_a^2 + x_q^2)} \left(x_d \sqrt{r_a^2 + x_q^2} - \frac{x_q (r_a^2 + x_d x_q)}{\sqrt{r_a^2 + x_q^2}} \right) v_{fd} \tag{4.22}$$

$$f2_{\psi_d, x_q} = - \frac{x_o \omega_{eo}}{x_q} \psi_q \tag{4.23}$$

$$f2_{\psi_q, x_q} = \frac{r_o \omega_{eo}}{x_q} \psi_q \tag{4.24}$$

$$f2_{v_R, x_q} = \frac{K_A x_q}{T_{RE} v_t} \left(v_d f_{2\psi_d, x_q} + v_q \left(f2_{\psi_q, x_q} - \frac{r_a \omega_{eo}}{x_q^2} \psi_q \right) \right) \tag{4.25}$$

$$f2_{\frac{\omega_m}{2}, x_q} = - \frac{3 \omega_{eo}}{J x_q} \psi_d \psi_q \tag{4.26}$$

$$f2_{v_B, x_q} = x_q T_{fB} \left(\frac{2 \alpha \alpha_R}{K_3} - \frac{2 K_4}{K_3} \frac{\omega_g L_{af}}{R_{fB} T_{fB}} \right) f2_{\frac{\omega_m}{2}, x_q} \tag{4.27}$$

for the d-axis transient reactance

$$f2_{\psi_F, x'_d} = \frac{x_d}{x'_d T'_{do}} \psi_F - \frac{x_d \omega_{eo}}{x'_d} \psi_d \tag{4.28}$$

$$f2_{\psi_d, x'_d} = - \frac{r_o}{x'_d T'_{do}} \psi_F + \frac{r_o \omega_{eo}}{x'_d} \psi_d \tag{4.29}$$

$$f2_{\psi_q, x'_d} = - \frac{x_o}{x'_d T'_{do}} \psi_F + \frac{x_o \omega_{eo}}{x'_d} \psi_d \tag{4.30}$$

$$f2_{v_R, x'_d} = - \frac{K_A x'_d}{T_{RE} v_t} \left(v_d \left(f2_{\psi_d, x'_d} + \frac{r_a}{x'^2_d T'_{do}} \psi_F - \frac{r_a \omega_{eo} \psi_d}{x'^2_d} \right) \right.$$

$$\left. + v_q f2_{\psi_q, x'_d} \right) \tag{4.31}$$

$$f2_{\frac{\omega_m}{2}, x'_d} = \frac{3 \omega_{eo}}{J x'_d} \psi_d \psi_q - \frac{3}{J x'_d T'_{do}} \psi_F \psi_q \tag{4.32}$$

$$f2_{v_B, x'_d} = x'_d T_{fB} \left(\frac{2 \alpha \alpha_R}{K_3} - \frac{2 K_4}{K_3} \right) \frac{\omega_g L_{af}}{R_{fB} T_{fB}} f2_{\frac{\omega_m}{2}, x'_d} \tag{4.33}$$

for the d-axis open-circuit transient time constant

$$f2_{\psi_F, T'_{do}} = \frac{x_d}{x'_d T'_{do}} \psi_F \tag{4.34}$$

$$f2_{\psi_d, T'_{do}} = - \frac{r_o}{x'_d T'_{do}} \psi_F \tag{4.35}$$

$$f2_{\psi_q, T'_{do}} = - \frac{x_o}{x'_d T'_{do}} \psi_F \tag{4.36}$$

$$f2_{v_R,T'_{do}} = -\frac{K_A T'_{do}}{T_{RE} v_t}\left(v_d\left(f2_{\psi_d,T'_{do}} + \frac{r_a}{x'_d T'_{do}}\psi_F\right) + v_q f2_{\psi_q,T'_{do}}\right) \tag{4.37}$$

$$f2_{\frac{\omega_m}{2},T'_{do}} = -\frac{3}{J x'_d T'_{do}}\psi_F\,\psi_q \tag{4.38}$$

$$f2_{v_B,T'_{do}} = T'_{do} T_{fB}\left(\frac{2\alpha\alpha_R}{K_3} - \frac{2K_4}{K_3}\right)\frac{\omega_g L_{AF}}{R_{fB} T_{fB}}\; f2_{\frac{\omega_m}{2},T'_{do}} \tag{4.39}$$

and for the moment of inertia J

$$i_A = \frac{1}{R}\left(v_t - 2L_{aF} i_F \frac{\omega_m}{2} - v_B\right) \tag{4.40}$$

$$f2_{\frac{\omega_m}{2},J} = \frac{K_1}{J}\frac{\omega_m}{2} - \frac{L_{aF} i_F}{2J} i_A + \frac{K_2}{2J} + \frac{3\omega_{eo}}{J}\left(\frac{1}{x'_d} - \frac{1}{x_q}\right)\psi_d\,\psi_q$$

$$- \frac{3}{J x'_d T'_{do}}\psi_F\,\psi_q \tag{4.41}$$

$$\frac{\Delta\omega_m}{2} = \frac{\omega_m}{2} - 94.25 \tag{4.42}$$

$$f2_{v_B,J} = -\frac{J}{K_3 T_m}\frac{\omega_g L_{af}}{R_{fB} T_{fB}} t + \frac{2\alpha_R J}{K_3 T_m}\frac{\omega_g L_{af}}{R_{fB} T_{fB}}\frac{\Delta\omega_m}{2}$$

$$+ JT_{fB}\left(\frac{2\alpha\alpha_R}{K_3} - \frac{2K_4}{K_3}\right)\frac{\omega_g L_{af}}{R_{fB} T_{fB}}\; f2_{\frac{\omega_m}{2},J} \tag{4.43}$$

Next for the gain K_A of the regulator-exciter, (4.5) yields

$$f2_{v_R,K_A} = -\frac{K_A}{T_{RE}}\left(v_{ref} - v_t\right) \tag{4.44}$$

for the regulator time constant T_{RE}

$$f2_{v_R, T_{RE}} = \frac{1}{T_{RE}} v_R - \frac{K_A}{T_{RE}} (v_{ref} - v_t) \tag{4.45}$$

and for the exciter time constant T_E

$$f2_{v_{fd}, T_E} = \frac{1}{T_E} v_{fd} - \frac{a_1}{T_E} \tanh (a_2 v_R) \tag{4.46}$$

Finally, for the transient droop δ of the governor-hydraulic operator, (4.5) yields

$$\frac{\Delta\omega_m}{2} = \frac{\omega_m}{2} - 94.25 \tag{4.47}$$

$$f2_{a_f, \delta} = -\frac{\sigma\delta}{T_A} a - \frac{\delta}{T_A} a_f - \frac{2\delta}{T_A} \frac{\Delta\omega_m}{2} \tag{4.48}$$

for the permanent droop

$$f2_{a, \sigma} = -\frac{\sigma}{T_A} a \tag{4.49}$$

$$f2_{a_f, \sigma} = -\frac{\sigma\delta}{T_A} a \tag{4.50}$$

for the actuator servomotor time constant T_A

$$f2_{a, T_A} = \frac{\sigma}{T_A} a + \frac{1}{T_A} a_f + \frac{2}{T_A} \frac{\Delta\omega_m}{2} \tag{4.51}$$

$$f2_{a_f, T_A} = \frac{\sigma\delta}{T_A} a + \frac{\delta}{T_A} a_f + \frac{2\delta}{T_A} \frac{\Delta\omega_m}{2} \tag{4.52}$$

for the dashpot damping time constant T_R

$$f2_{a_f,T_R} = \frac{1}{T_R} a_f \tag{4.53}$$

for the gate servomotor time constant T_G

$$f2_{g,T_G} = -\frac{1}{T_G} (a-g) \tag{4.54}$$

$$f2_{t,T_G} = \frac{2}{T_G} (a-g) \tag{4.55}$$

and for the water starting time constant T_W

$$f2_{t,T_W} = -\frac{2}{T_W} (g-t) \tag{4.56}$$

The equations, (4.6) through (4.56), are used for the computation.

4.2. Parameter Sensitivity of System Response

Parameter sensitivity of system response is investigated in this section. There are fifteen parameters and twelve state variables involved. From each sensitivity curve the maximum and minimum are found. A convenient criteria is set that any parameter whose sensitivity curve maximum and minimum for a state variable are less than one-seventh of those of all the sensitivity curves will be considered insensitive.

The results can be summarized in three categories. One, parameters are very sensitive in the beginning and remain sensi-

tive for the rest of the time period. Two, parameters are very sensitive in the beginning but not towards the end. Three, parameters are insensitive in the beginning but become sensitive towards the end.

In the first category, it is noted that the sensitivity curves ψ_{F,x_q} (Fig. 4.1), ψ_{d,x_q} (Fig. 4.2), v_{R,x_q} (Fig. 4.10), and v_{fd,x_q} (Fig. 4.11), all with respect to x_q, have their maximum during the fault and fault cleared period and remain sensitive after the system has been restored. A similar result is observed for the parameter T'_{do} except for $\psi_{F,T'_{do}}$ (Fig. 4.1), which increases during the first 0.2 seconds and remains large throughout the remaining period.

In the second category, it is observed that ψ_{d,x'_d} (Fig. 4.2), ψ_{q,x'_d} (Fig. 4.3) and v_{R,K_A} (Fig. 4.10) are large only during the fault period ($\lesssim 0.08$ seconds).

In the third category, it is noticed that the moment of inertia J is insensitive during the fault and fault cleared period but becomes very sensitive towards the end.

It is found, in general, from this study that x_q, T'_{do} and J are the most sensitive parameters and that to a certain extent x'_d, K_A, and T_{RE} but not r_a, x_d, T_E and the governor-hydraulic operator parameters.

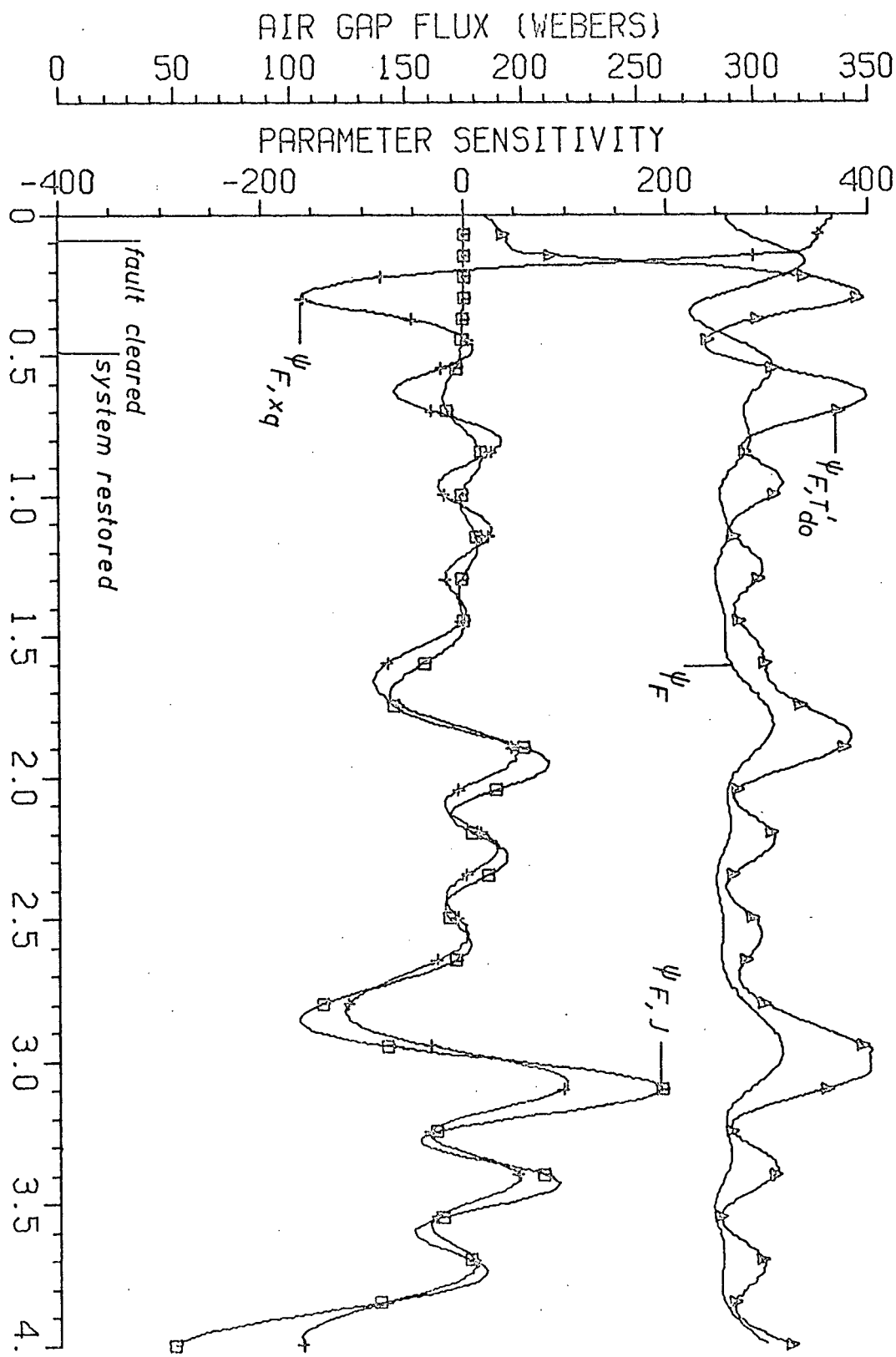

Fig. 4.1. Parameter Sensitivity of Air Gap Flux

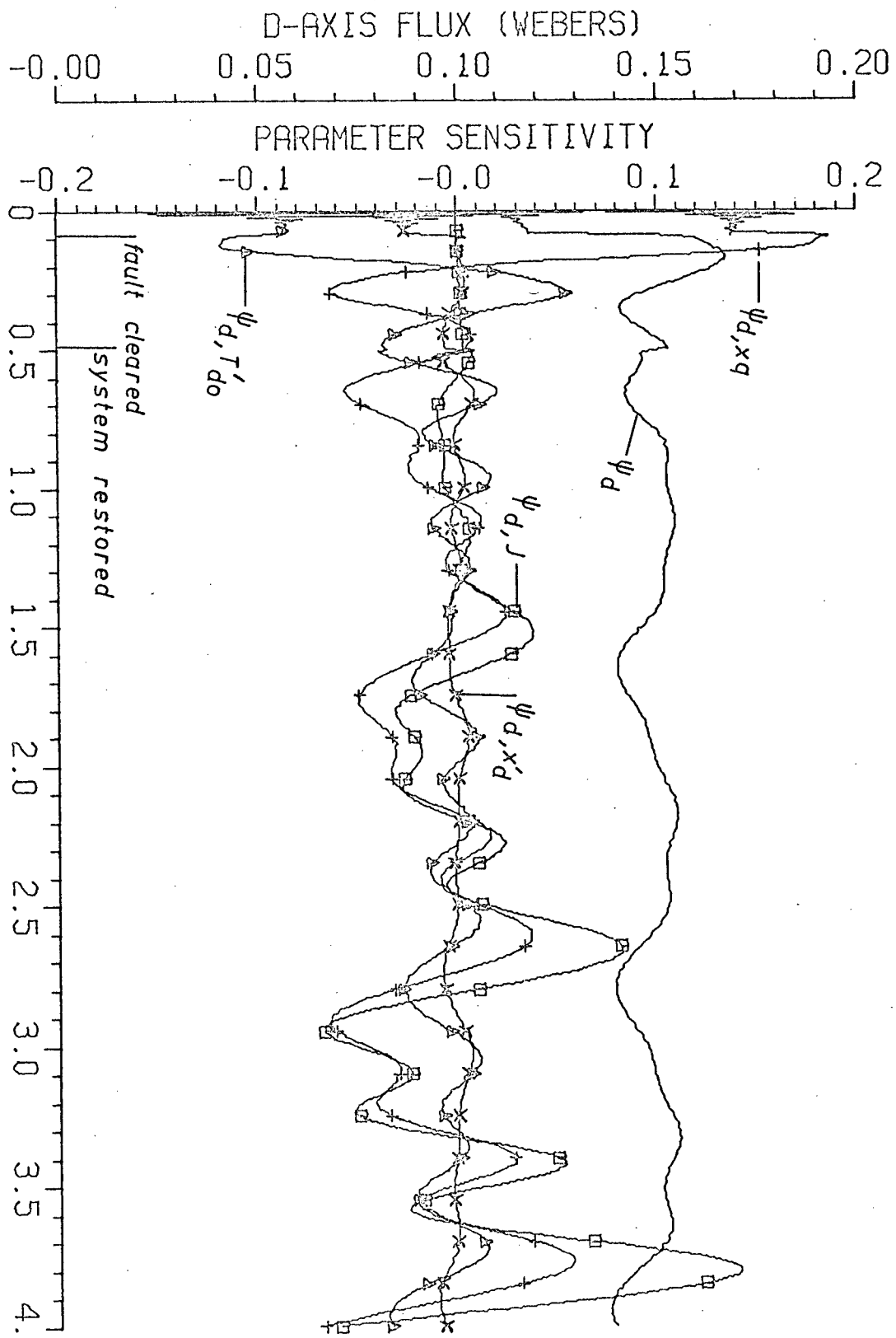

Fig. 4.2. Parameter Sensitivity of D-Axis Flux

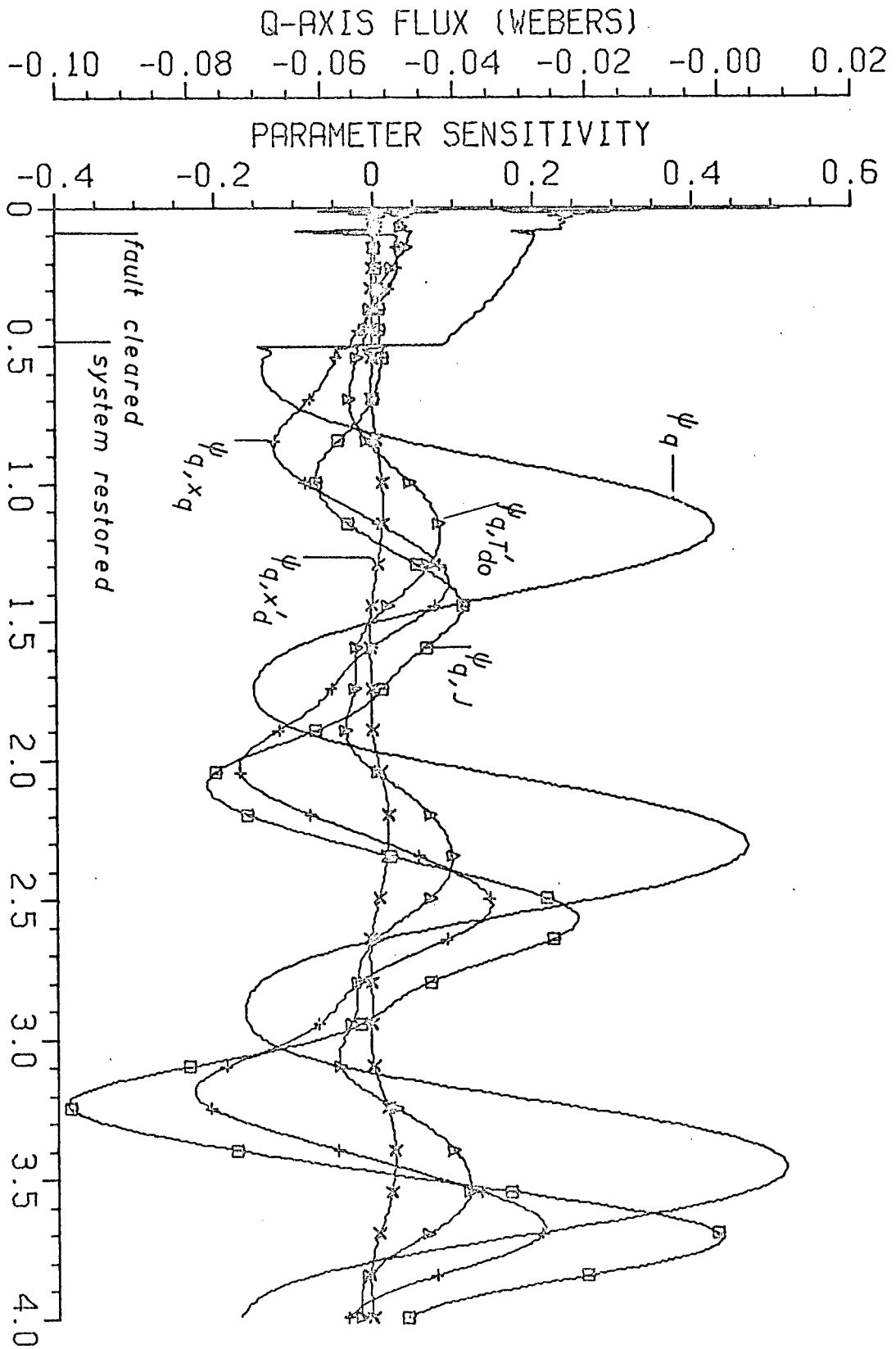

Fig. 4.3. Parameter Sensitivity of Q-Axis Flux

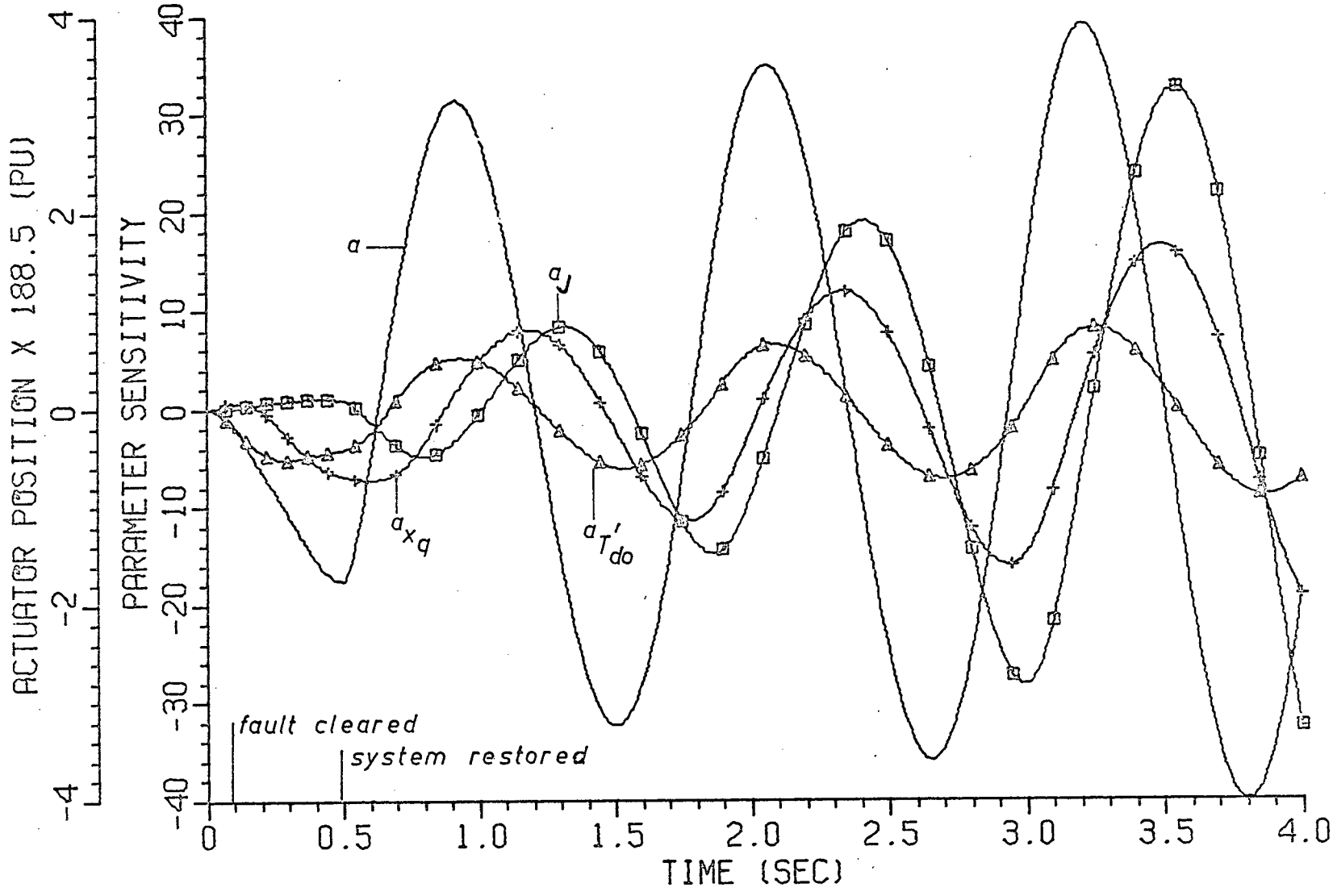

Fig. 4.4. Parameter Sensitivity of Actuator Position

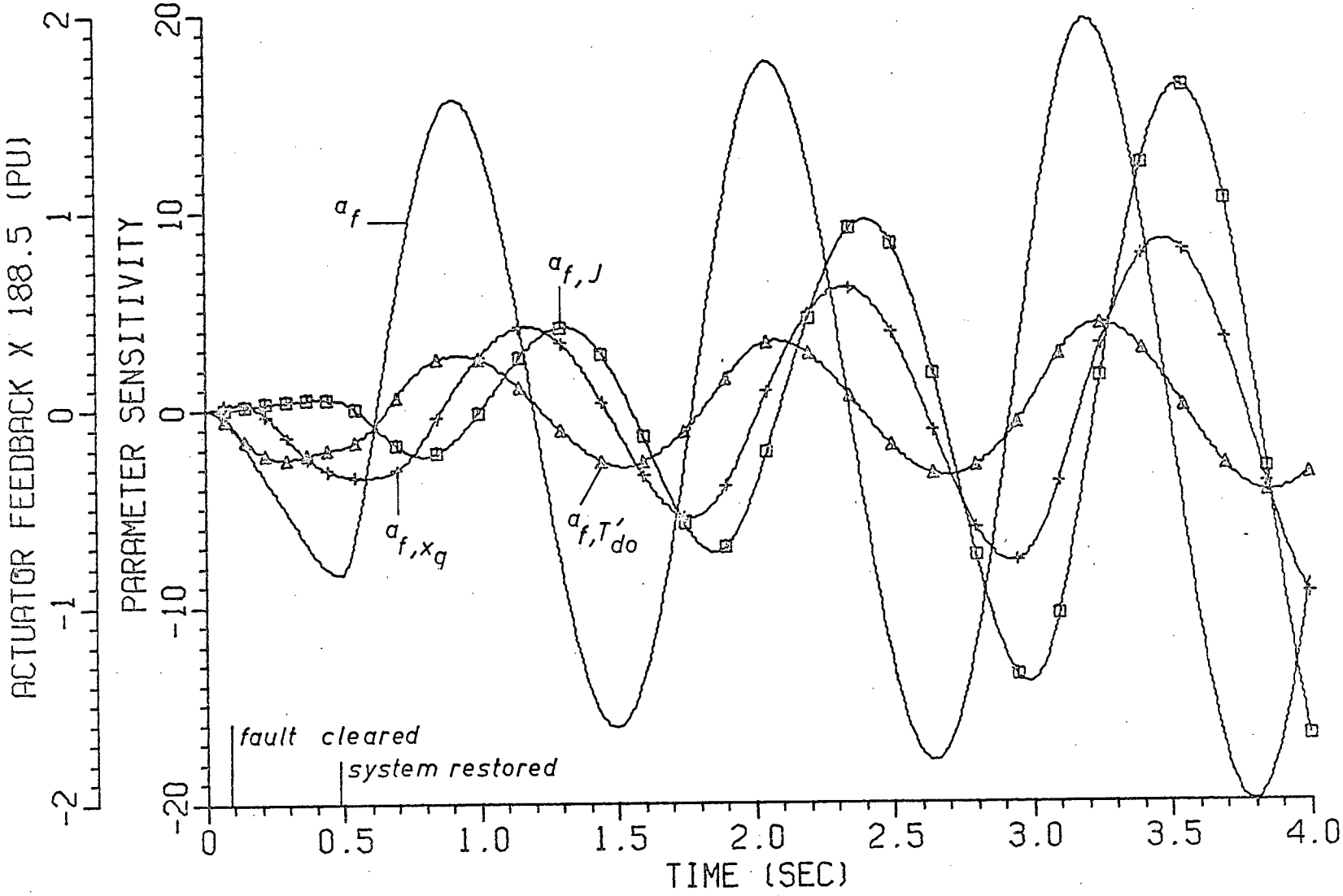

Fig. 4.5. Parameter Sensitivity of Actuator Feedback

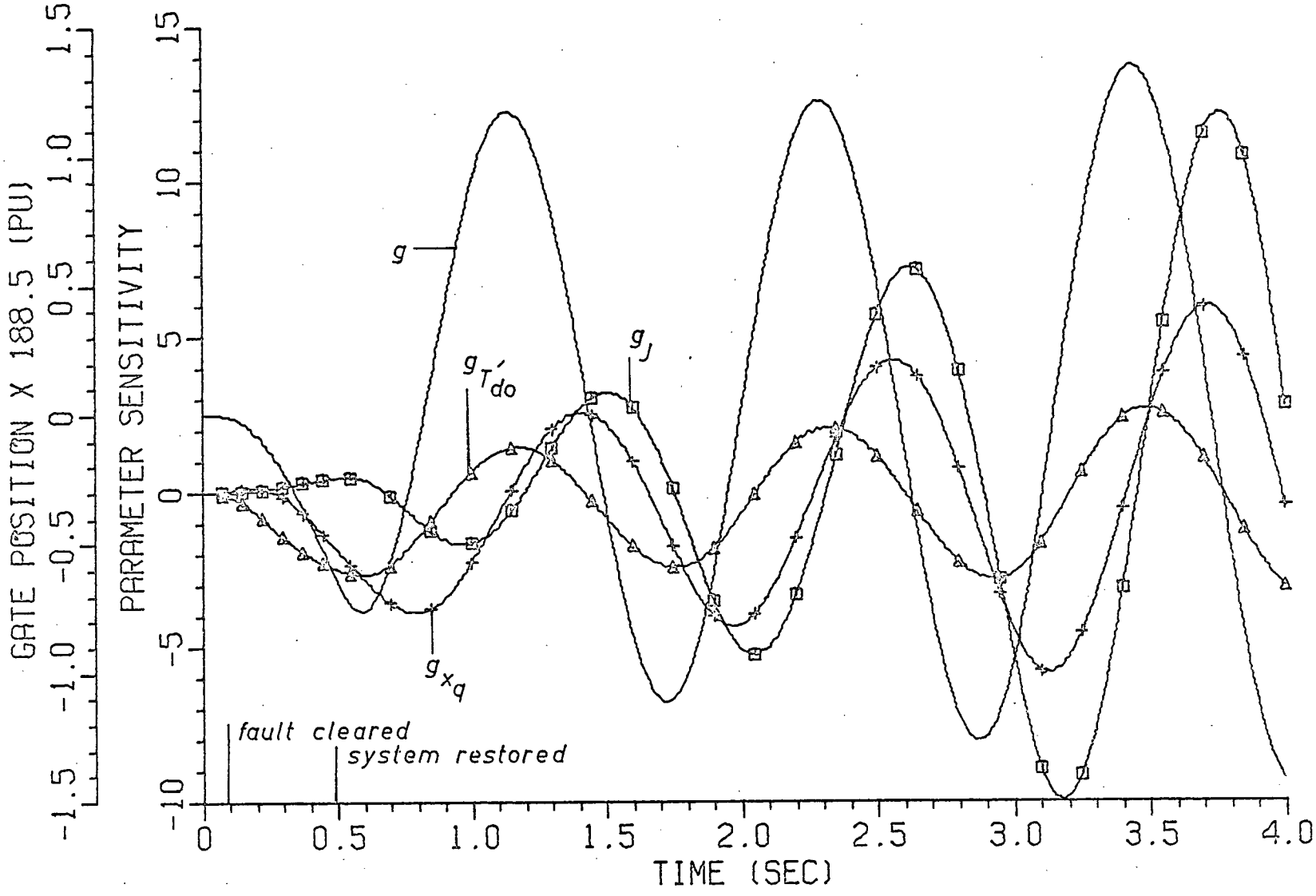

Fig. 4.6. Parameter Sensitivity of Gate Position

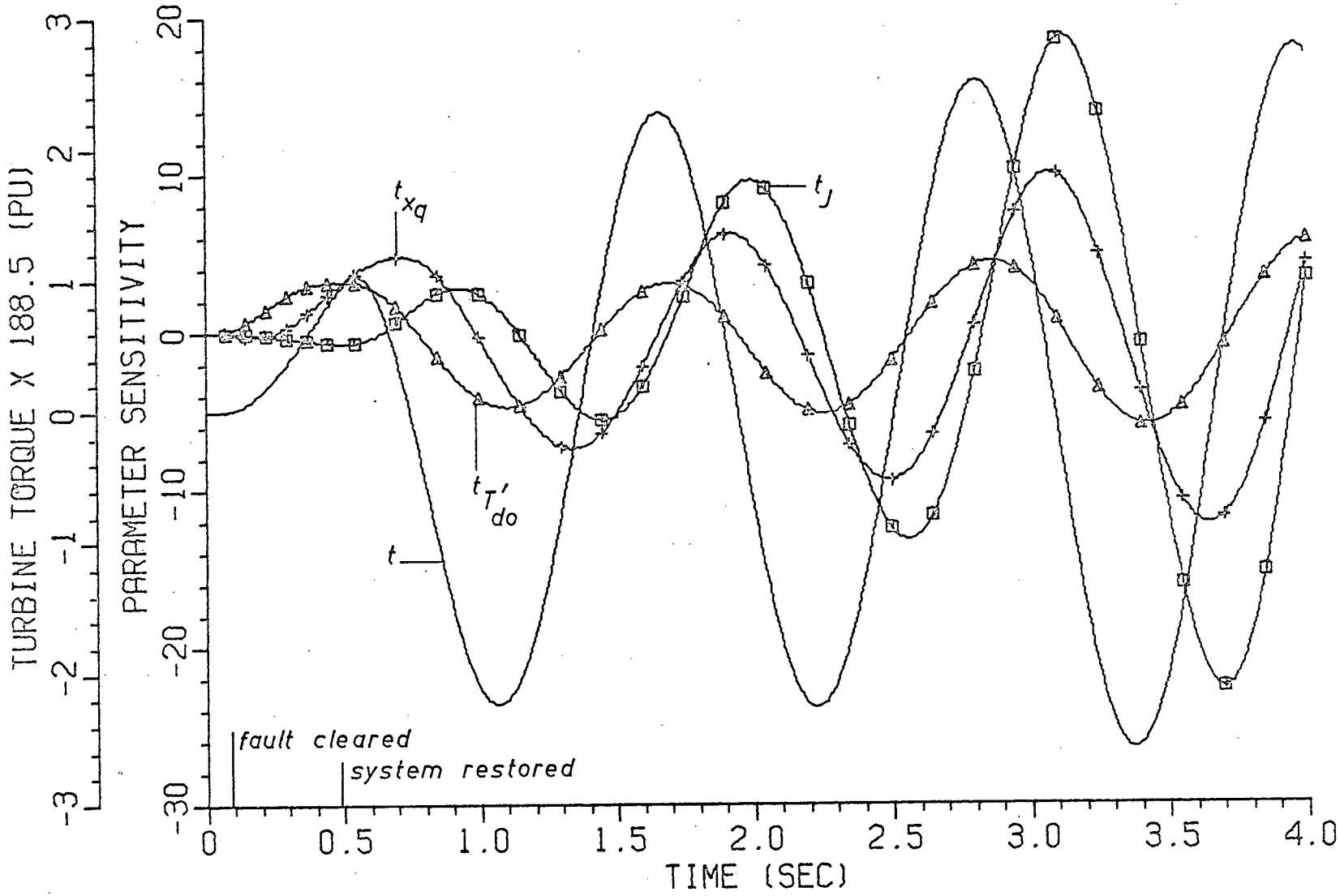

Fig. 4.7. Parameter Sensitivity of Turbine Torque

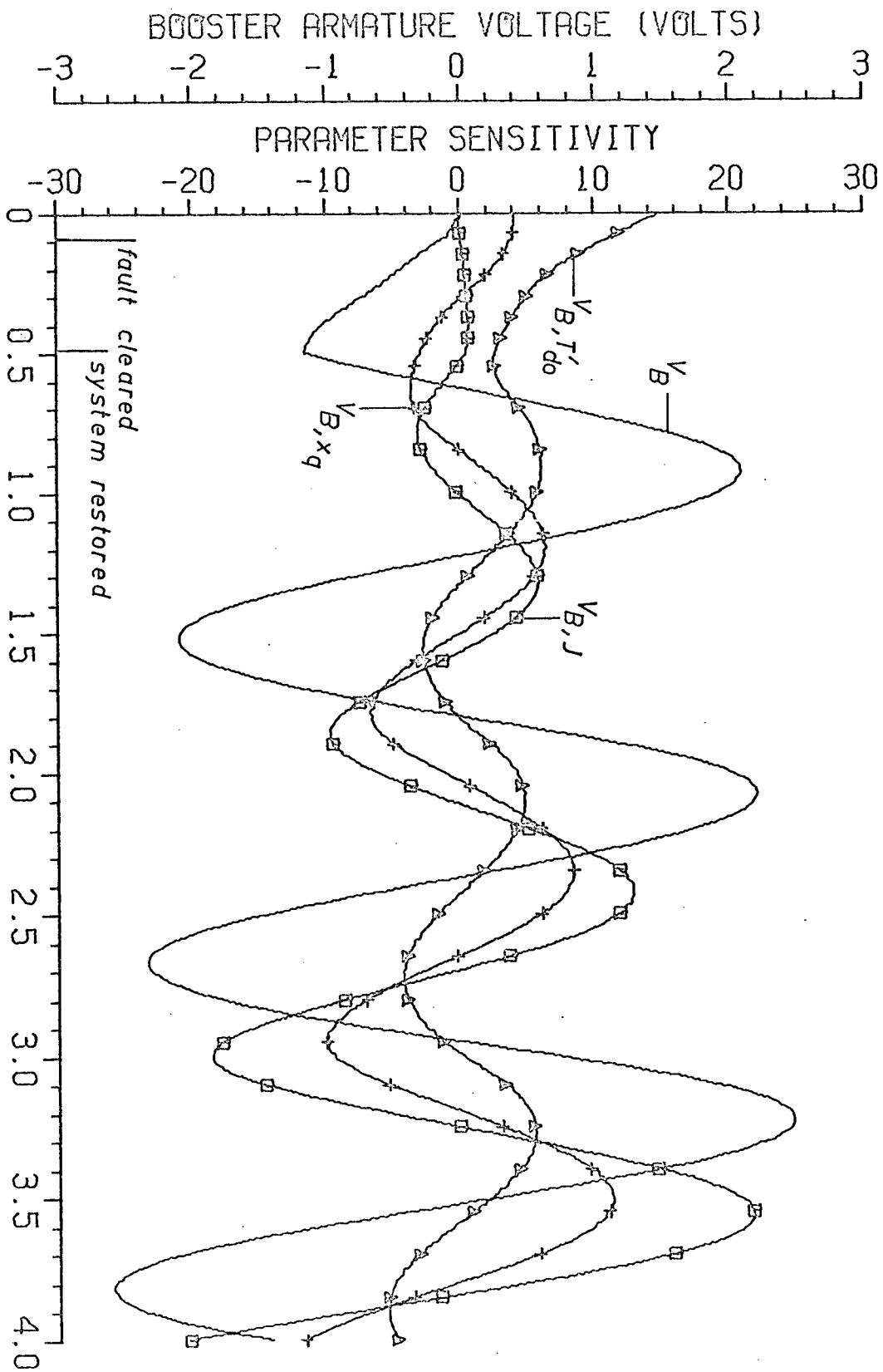

Fig. 4.8. Parameter Sensitivity of Booster Armature Voltage

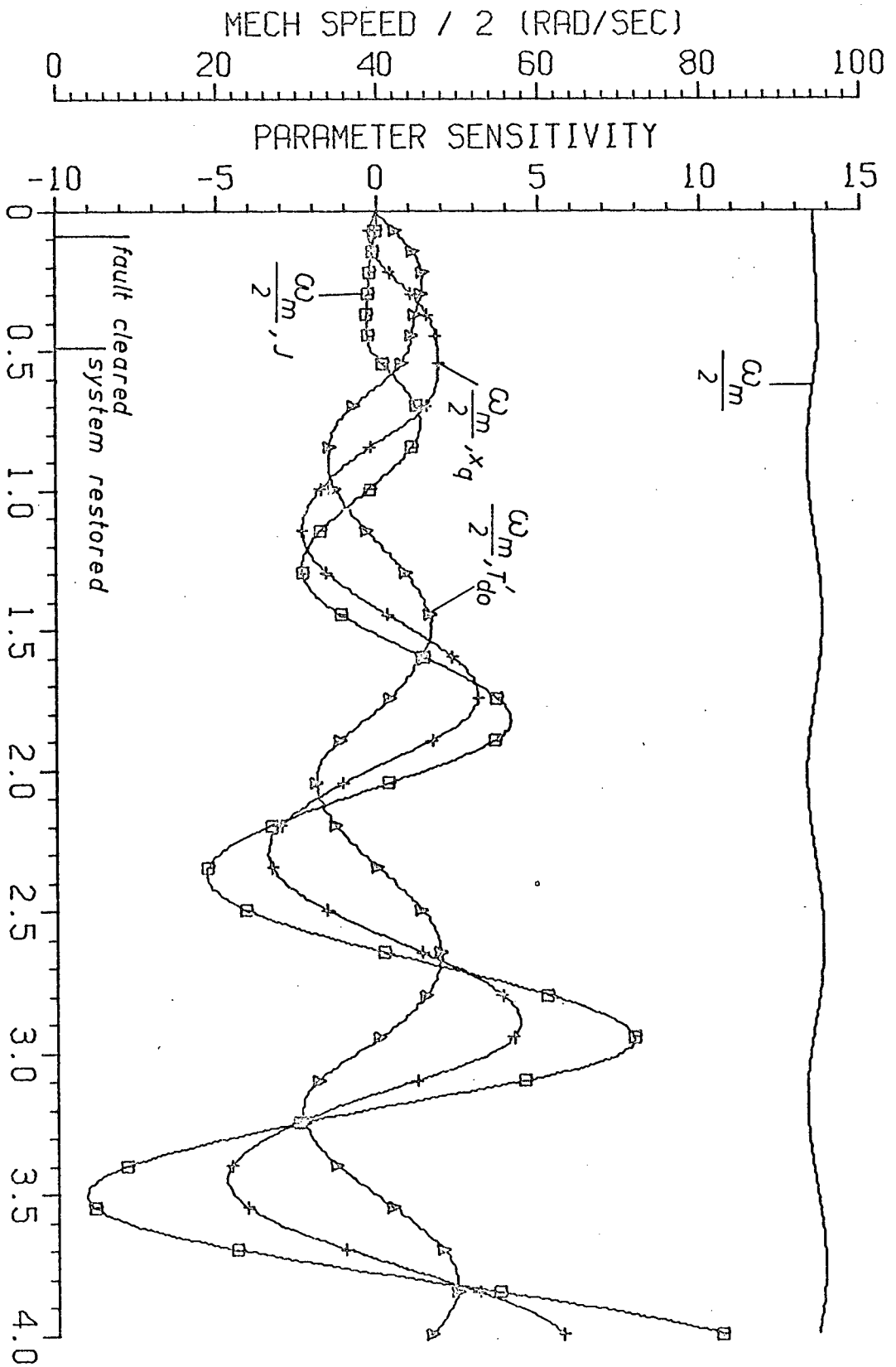

Fig. 4.9. Parameter Sensitivity of Mechanical Speed

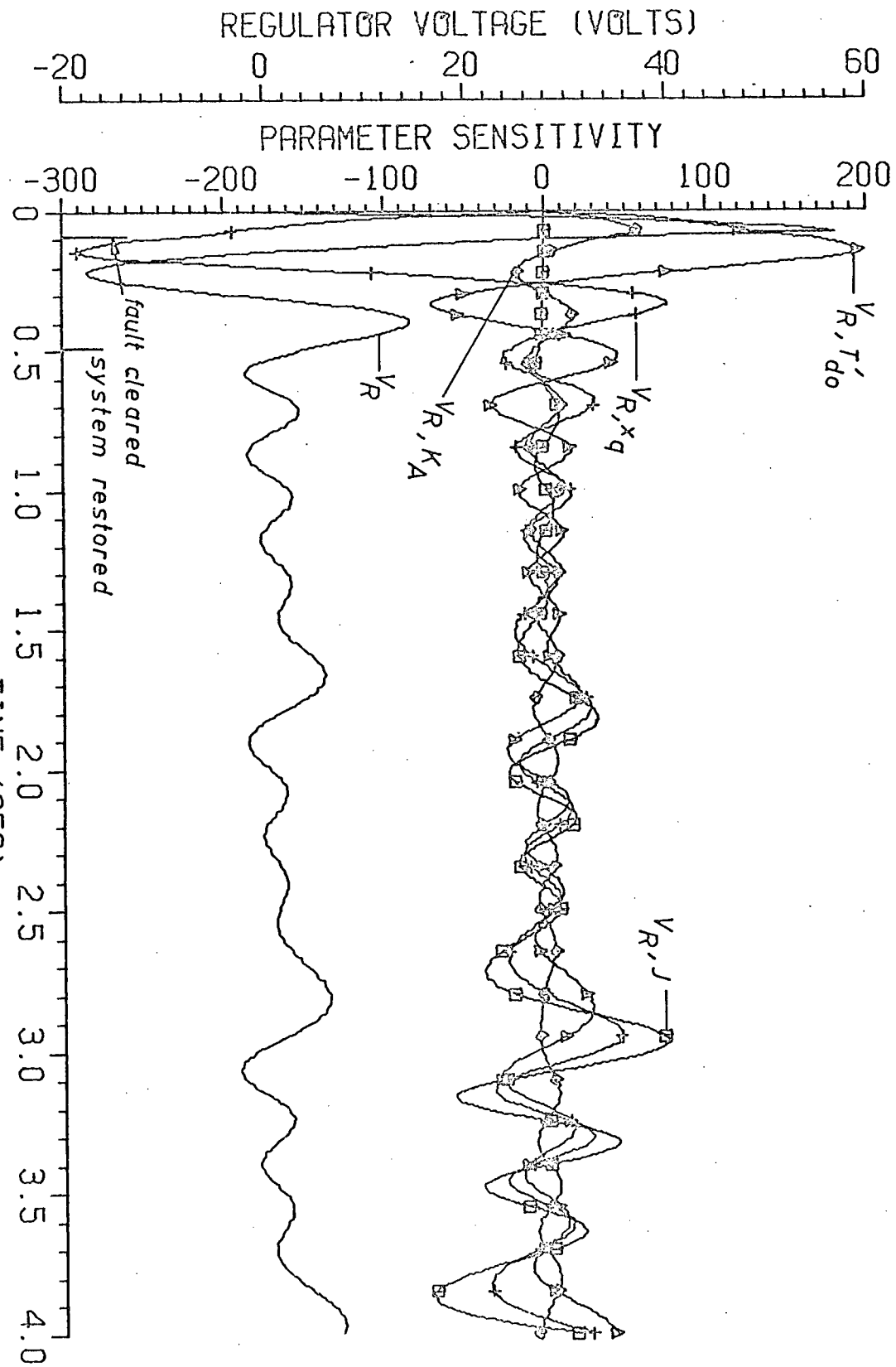

Fig. 4.10. Parameter Sensitivity of Regulator Voltage

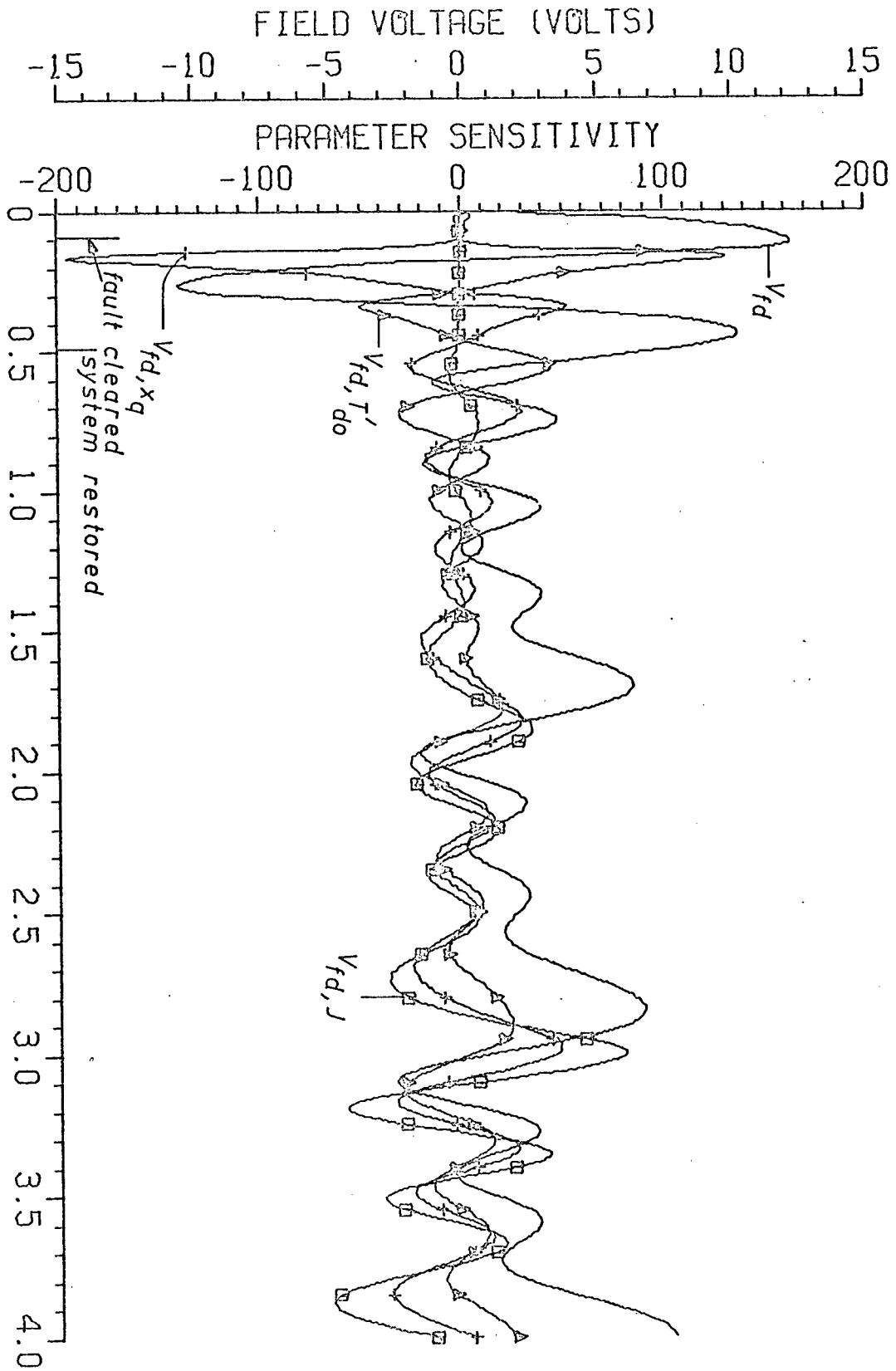

Fig. 4.11. Parameter Sensitivity of Field Voltage

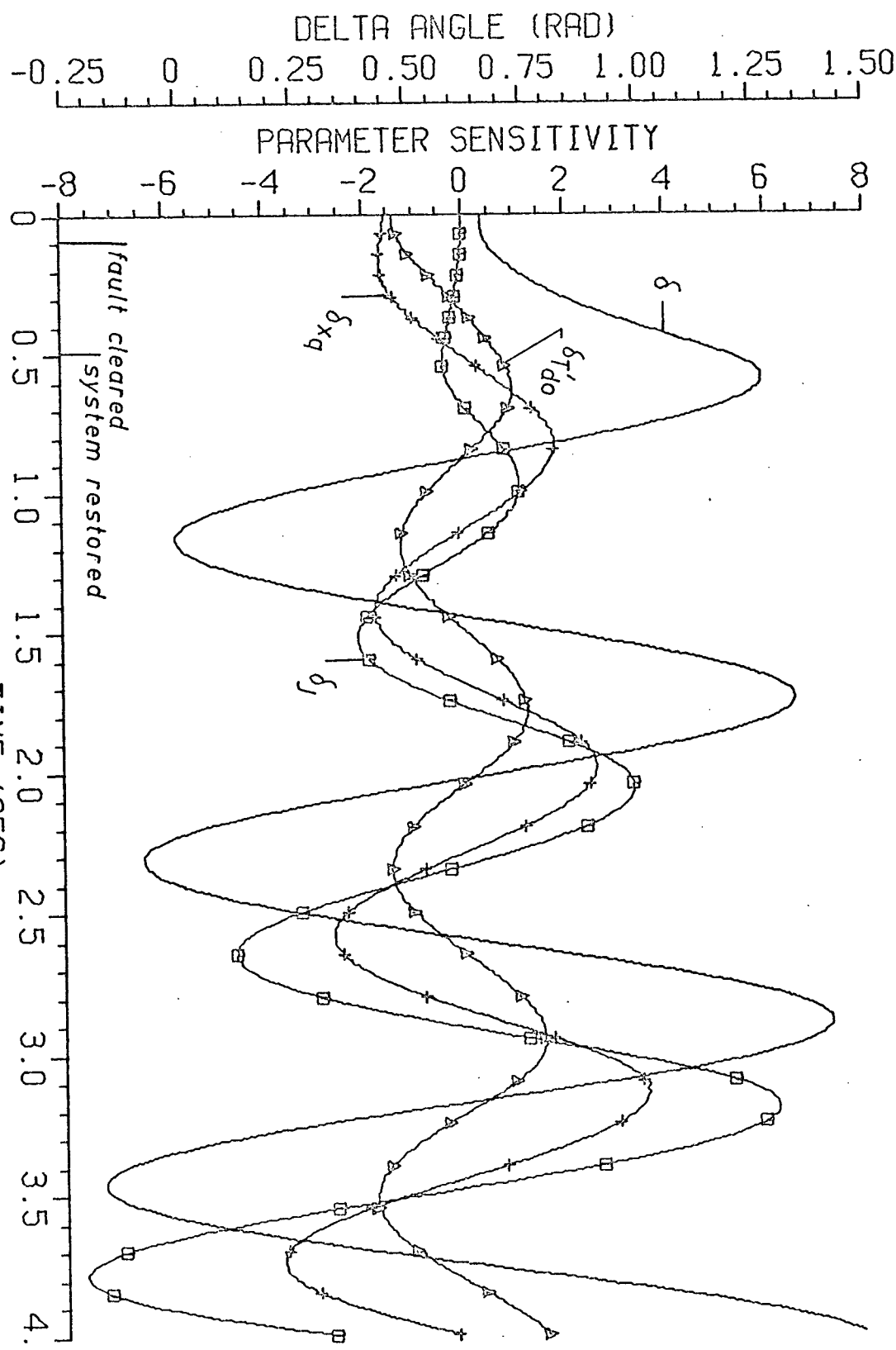

Fig. 4.12. Parameter Sensitivity of Delta Angle

5. NONLINEAR OPTIMAL STABILIZATION OF A POWER SYSTEM AND DYNAMIC MODEL TESTS

5.1. Power System Stabilizing Signal

The main purposes of a stabilizing signal are to provide additional synchronizing torque during the first torque angle swing after a transient disturbance and to provide damping torque for subsequent oscillations. Ellis and others[5.1,5.2,5.3] were able to obtain effective stabilization using speed, accelerating power and frequency deviation signals. The theoretical basis is found from a linear model by deMello and Concordia.[5.4] These are the conventional stabilization techniques. Jones[5.5] did a bang-bang control test on a model power system. In this Chapter, optimal control theory is applied to a power system described by nonlinear state equations including field voltage and stabilizing signal limits. The power system is shown in Fig. 3.1.

5.2. Dynamic Optimization and Computational Method

The problem being considered is to find an optimum control $u^*(t)$ which minimizes the performance functional

$$J = \phi(x(t_f)) + \int_{t_o}^{t_f} F(x)\, dt \qquad (5.1)$$

subject to the dynamical constraints or system equations

$$\dot{x} = f(x,u) \qquad (5.2)$$

The variational calculus method of Lagrange Multipliers[5.6] is used to form an augmented functional

$$J_a = \phi(x(t_f)) + \int_{t_o}^{t_f} (-H(x, \lambda, u) + \lambda^T \dot{x})dt \qquad (5.3)$$

where H is the Hamiltonian

$$H(x, \lambda, u) = -F(x) + \lambda^T f(x,u) \qquad (5.4)$$

and λ is a time-varying costate variable vector. The conditions which must be satisfied at the optimum are[5.7]

$$\dot{x} = f(x, u) \qquad x(t_o) = x_o \qquad \text{state equations} \qquad (5.5)$$

$$\dot{\lambda} = -H_x(x, \lambda, u) \qquad \text{costate equations} \qquad (5.6)$$

$$0 = H_u(x, \lambda, u) \qquad \text{gradient condition} \qquad (5.7)$$

$$\lambda(t_f) = -\phi_x(x(t_f)) \qquad \text{transversality condition} \qquad (5.8)$$

Equations (5.5) through (5.8) represent a nonlinear two-point boundary-value problem (TPBVP).

For the solution of the TPBVP, the gradient[5.6] and Newton-Raphson with Ricatti Transformation[5.7] methods are tested first on a simplified third-order power system. There is no difficulty with the computation. The method of Newton-Raphson with Ricatti transformation is then applied to the fifth-order system using the gradient method to start. Numerical instability in the solution of the Ricatti equation is experienced. The solution of the TPBVP is finally obtained with the gradient method. It takes fifty iterations or less.

Three different performance functions are chosen and tested for each step of the line fault, fault cleared (one circuit of a double circuit removed), and line restored (successful reclosure of circuit). The general form of the performance function from (5.1) is

$$\phi(x(t_f)) = W_1\left(\frac{\Delta\omega_m}{2}\right)^2 + W_2\ (\Delta\delta)^2 \qquad (5.9)$$

$$F(x) = W_3\left(\frac{\Delta\omega_m}{2}\right)^2 + W_4\ (\Delta\delta)^2 + W_5\left(\frac{\Delta\dot{\omega}_m}{2}\right)^2 \qquad (5.10)$$

The first two steps are of fixed time established by the circuit breaker settings. In these two steps, $\phi(x(t_f))$ is set to zero. Studies are made of alternatively considering the weighting factors W_3, W_4 or W_5 alone. The same procedures are repeated for the final step but including W_1 and W_2. To emphasize small deviations of speed and torque angle at the final time W_1 and W_2 are set equal to ten, $W_1 = W_2 = 10$. The final time of the system restored step is estimated from a stabilizing signal study (≈ 1.7 seconds) anticipating a shorter settling time (1.25 seconds).

The Hamiltonian is

$$H = -F(x) + \lambda_1(p\psi_F) + \lambda_2(p\ \frac{\omega_m}{2}) + \lambda_3\ (p\delta)$$
$$+ \lambda_4\left(pv_R + \frac{K_A}{T_{RE}'}u\right) + \lambda_5\ (pv_{fd}) \qquad (5.11)$$

where $p\psi_F$, pv_R are given by (3.82) and (3.16) respectively. The Hamiltonian is maximized or the performance functional is minimized with respect to u if the condition

$$u = U_{max} \text{ sgn } \lambda_4$$

is satisfied. This is a "bang-bang" type of optimal control. The solution of u is obtained indirectly by optimizing the unconstrained value $\underline{u}$ related by Box's transformation[5.8] as follows

$$u = U_{max} \sin (\underline{u}) \tag{5.12}$$

In the gradient method, the correction applied to $\underline{u}$ at each point is

$$\Delta \underline{u} = -k \, H\underline{u} \tag{5.13}$$

It is rather difficult to choose k[5.6]. In this computation the following value of k[5.9] is chosen

$$k = \frac{\delta 1}{\sqrt{\int H_{\underline{u}}^T \, H_{\underline{u}} dt}} \tag{5.14}$$

where $\delta 1$ is a step size constraint.

5.3. Computation and Test Results

Computation results from an IBM 360 Model 67 and test results from the dynamic test model are summarized in this Section as follows.

For the computation, investigation of the various performance functions outlined in Section 5.2 reveals that for the fault step, the three performance functions yield the same optimal control and for the fault cleared and system restored steps, the optimal control is the same for $F = \left(\frac{\Delta\omega_m}{2}\right)^2$ and $F = (\Delta\delta)^2$ but different for $F = \left(\frac{\dot{\omega}_m}{2}\right)^2$. Thus, a single trajectory for the system variables is obtained during the fault step, two trajectories during the fault cleared step, and two trajectories from each of the previous two during the system restored step. These results are presented in Fig. 5.1 with the performance functions summarized in Table 5.1.

Curve Fig.5.1.	Fault	Fault Cleared	System Restored
1	$\int\left(\frac{\Delta\omega_m}{2}\right)^2 dt$	$\int\left(\frac{\Delta\omega_m}{2}\right)^2 dt$	$10\left(\frac{\Delta\omega_m}{2}\right)^2 + 10\,(\Delta\delta)^2 + \int\left(\frac{\Delta\omega_m}{2}\right)^2 dt$
2	$\int\left(\frac{\Delta\omega_m}{2}\right)^2 dt$	$\int\left(\frac{\Delta\omega_m}{2}\right)^2 dt$	$10\left(\frac{\Delta\omega_m}{2}\right)^2 + 10\,(\Delta\delta)^2 + \int\left(\frac{\dot{\omega}_m}{2}\right)^2 dt$
3	$\int\left(\frac{\Delta\omega_m}{2}\right)^2 dt$	$\int\left(\frac{\dot{\omega}_m}{2}\right)^2 dt$	$10\left(\frac{\Delta\omega_m}{2}\right)^2 + 10\,(\Delta\delta)^2 + \int\left(\frac{\Delta\omega_m}{2}\right)^2 dt$
4	$\int\left(\frac{\Delta\omega_m}{2}\right)^2 dt$	$\int\left(\frac{\dot{\omega}_m}{2}\right)^2 dt$	$10\left(\frac{\Delta\omega_m}{2}\right)^2 + 10\,(\Delta\delta)^2 + \int\left(\frac{\dot{\omega}_m}{2}\right)^2 dt$

Table 5.1. Performance Functions Used During Transient Steps

Comparisons are then made between the system responses with optimal control signals and those without. It is observed that the system responses with optimal control signals are much more damped than those without. Once the control is removed after 1.25 seconds the system oscillates with a reduced magnitude. It is observed also that all the system responses with optimal control signals stay very close. The speed deviation, torque angle and field voltage responses are shown in Fig. 5.1a, b, and c respectively.

Comparison is then made between conventional speed deviation and accelerating power stabilizing signal responses and one of the optimal controls (curve 3, Fig. 5.1) responses. In general, it seems that the optimal control yields a better damping effect, speed deviation in Fig. 5.2a and torque angle Fig. 5.2b, than the stabilizing signals except for the field voltage in Fig. 5.2c because of the nature of the forced excitation.

Power stabilization test results obtained directly from the dynamic test model are plotted along with computation results in Fig. 5.3a, 5.3b, and 5.3c for comparison. All system responses are close.

Similar comparisons of computation and test results are made in Fig. 5.4a, b and c for system responses with a speed stabilizing signal. In both cases steady state oscillations are observed as experienced in practice. However, because of the very nature of the steady state oscillations

it is difficult to realize the same initial condition for computation on the test model.

Comparison is then made between test and computation of system responses with optimal control. They agree with each other very well, Fig. 5.5a and 5.5b, except the switching transient disturbance in the field voltage Fig. 5.5c which is observed also in Fig. 3.8.

The last comparisons of test and computation results are carried out on system responses with optimal control for the first 1.25 seconds and power stabilizing signal for the remaining period, Fig. 5.6a, b, and c. Note that the comparison of the first 1.25 seconds is made in Fig. 5.5a, b and c. It is observed that the overall responses of the test and computation are very close.

In Fig. 5.7, system responses with optimal control and power stabilizing signal are plotted along with system responses with power stabilizing signal alone. It is interesting to note that the composite signal yields the best overall system response and this is realized to a lesser degree on the test model.

From the comparisons made above it is concluded the dynamic test model can be used to perform complicated power system tests, such as stabilizing signal control, and used to check computational predictions.

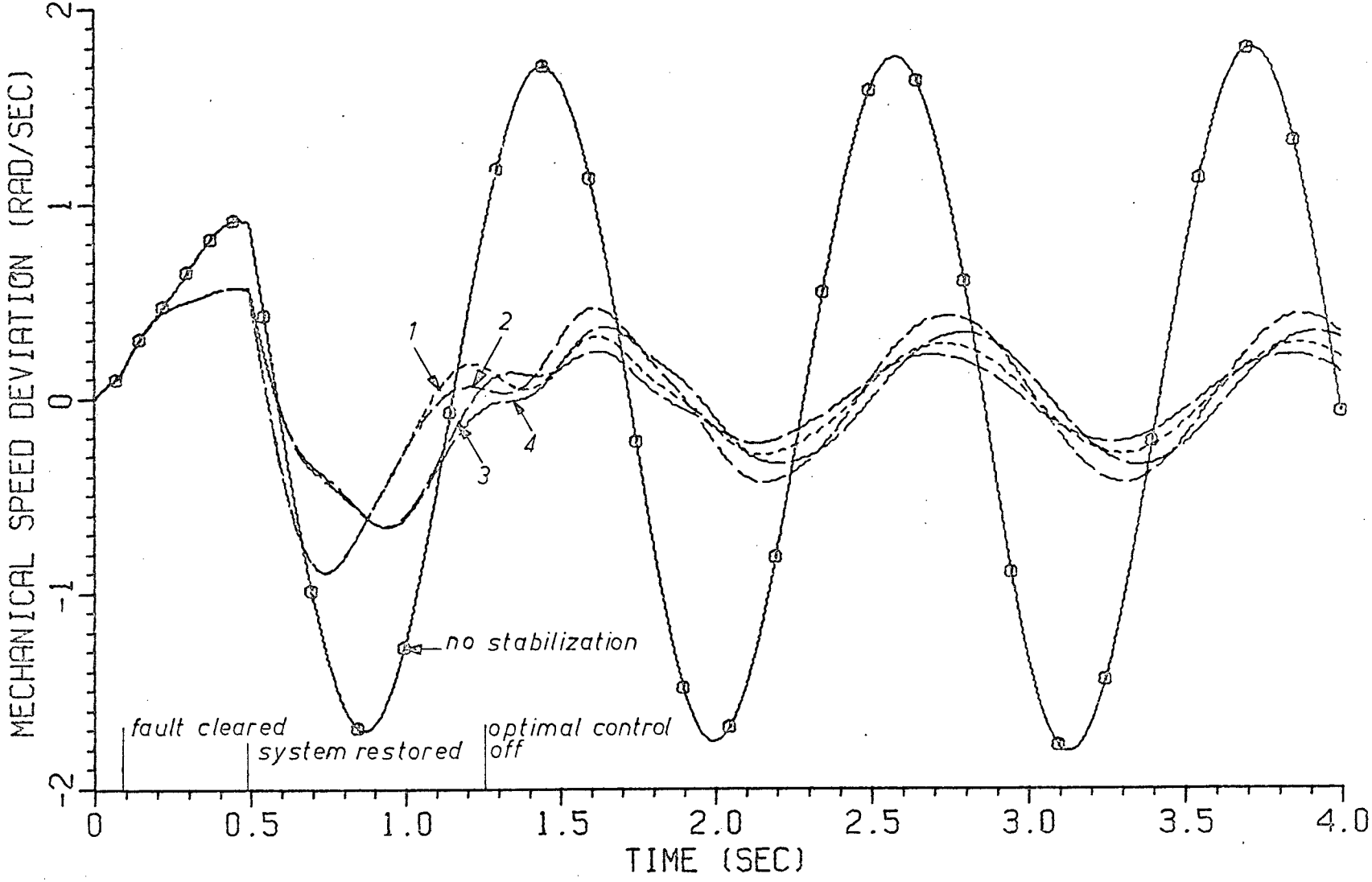

(a) Mechanical Speed Deviation

Fig. 5.1 Calculated Transient Responses of Various Performance Functions

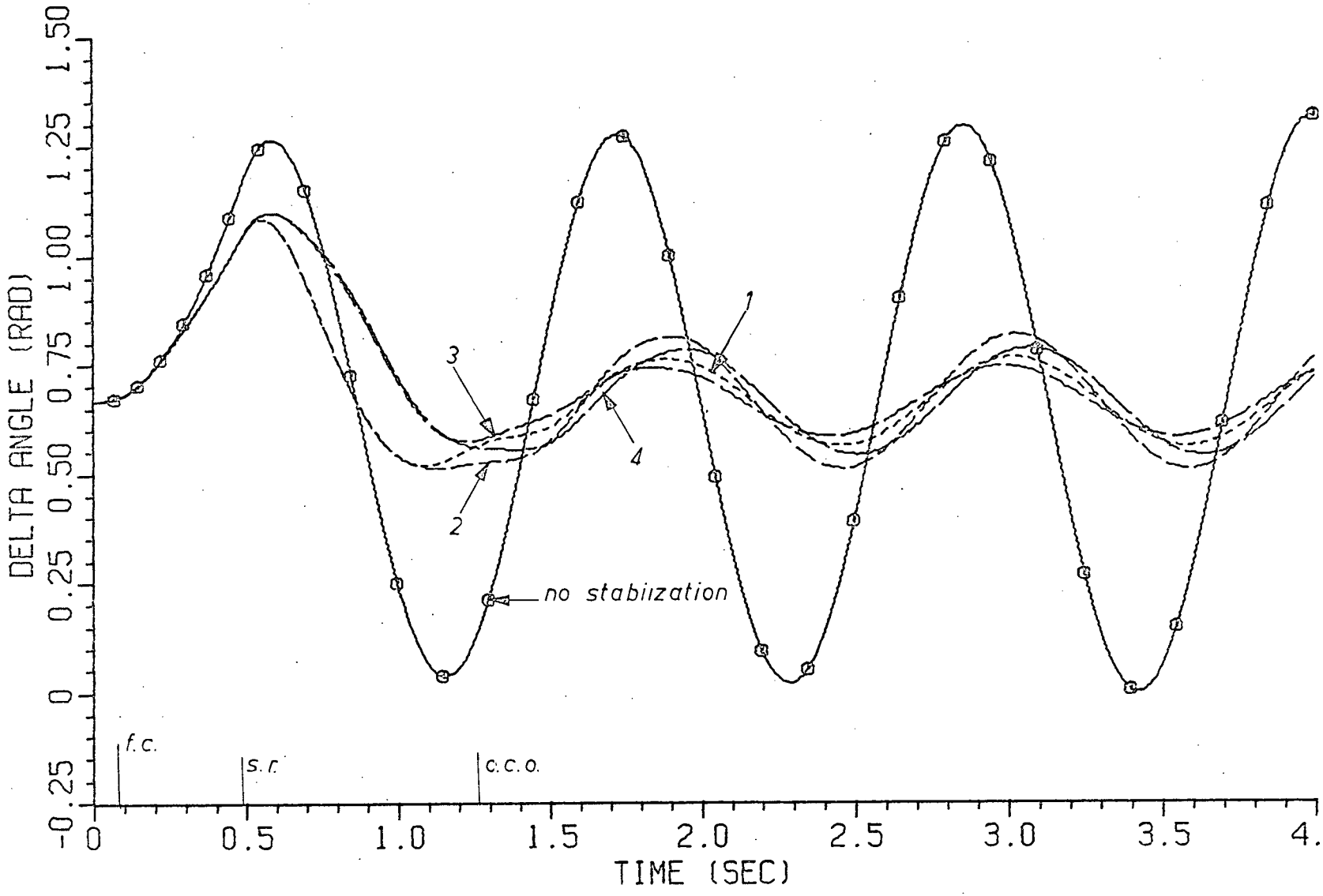

(b) Torque Angle

Fig. 5.1 Calculated Transient Responses of Various Performance Functions

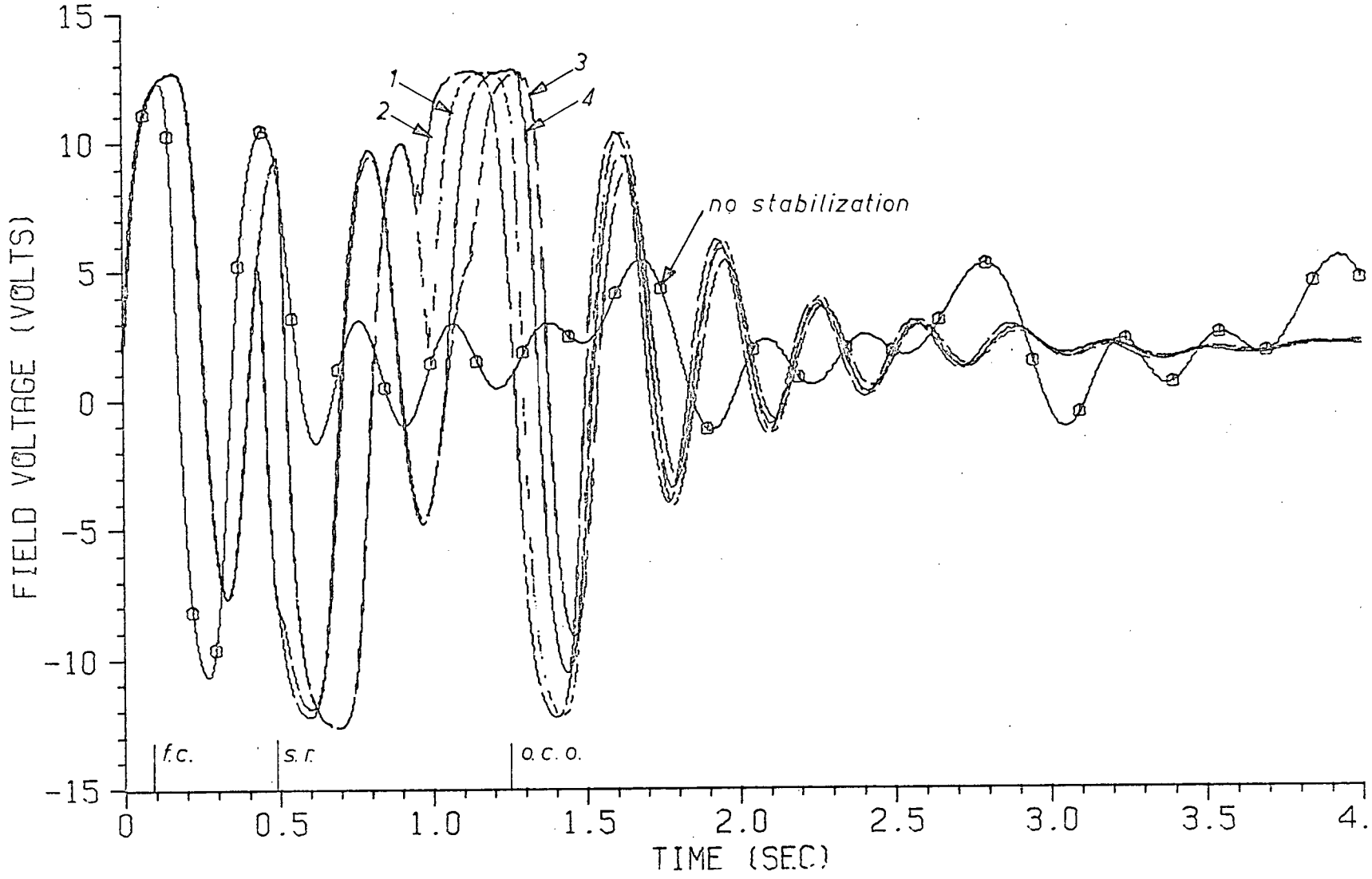

(c) Field Voltage

Fig. 5.1 Calculated Transient Responses of Various Performance Functions

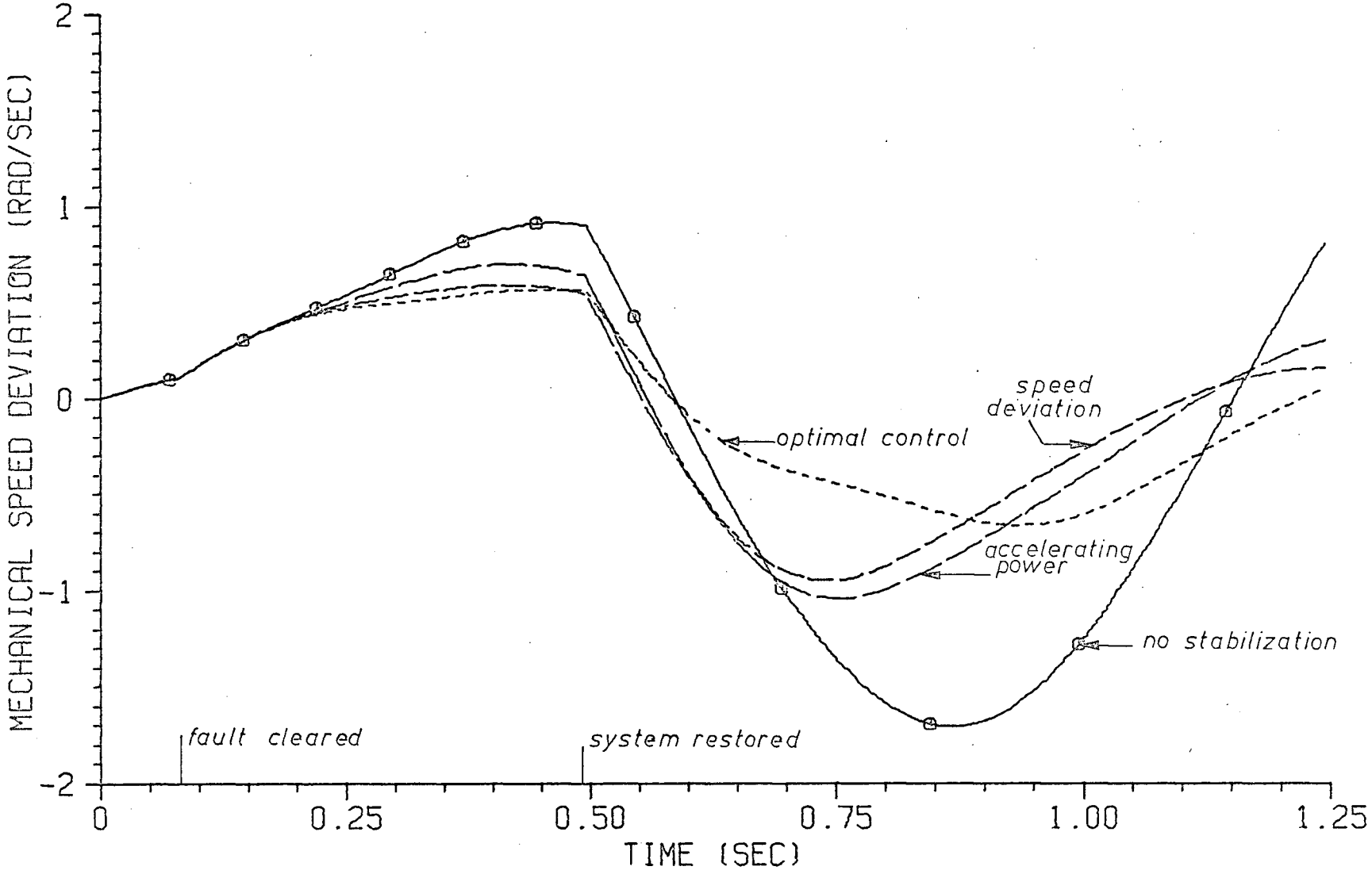

(a) Mechanical Speed Deviation

Fig. 5.2 Calculated Transient Responses of Various Stabilizing Signals

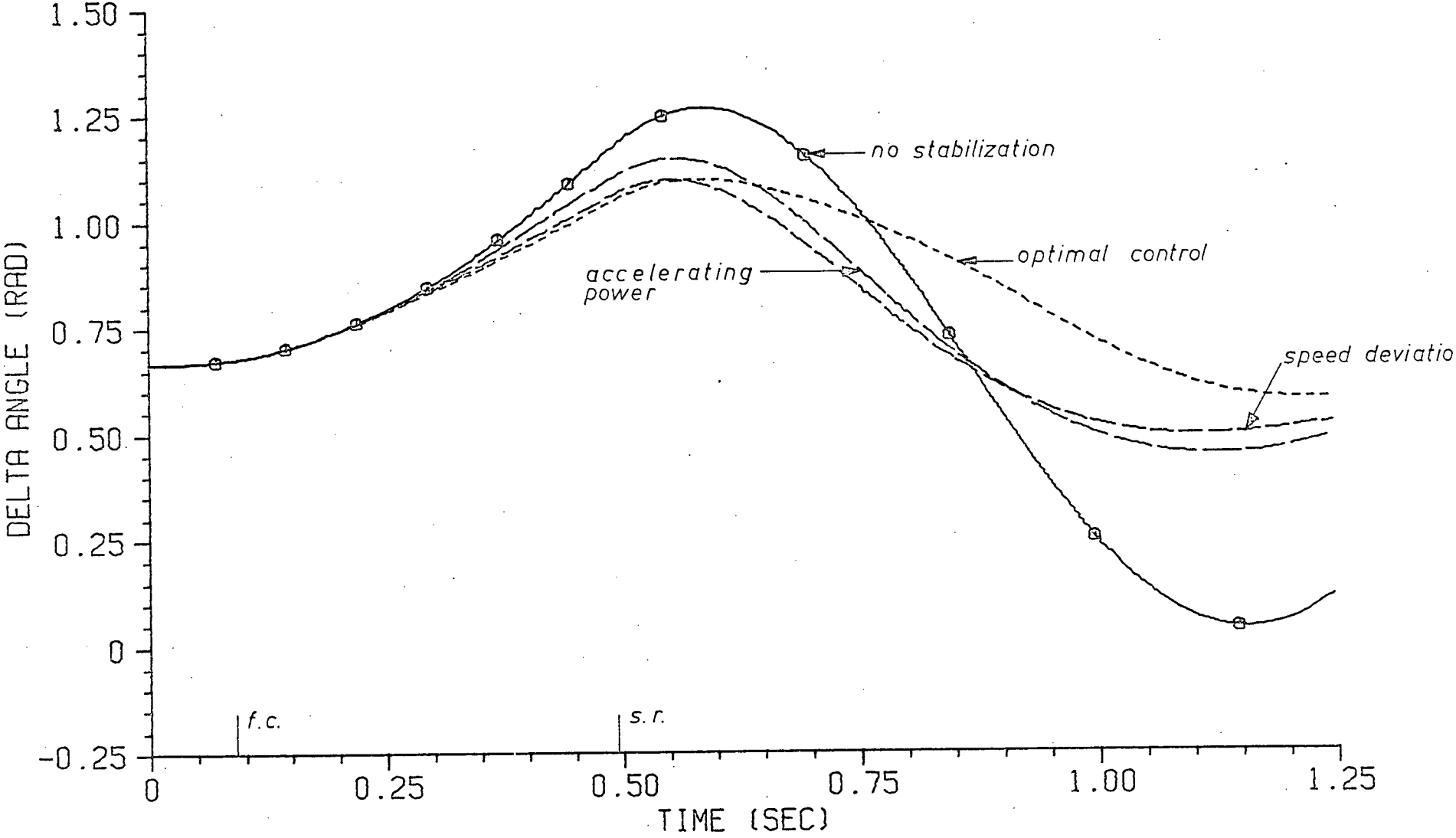

(b) Torque Angle

Fig. 5.2 Calculated Transient Responses of Various Stabilizing Signals

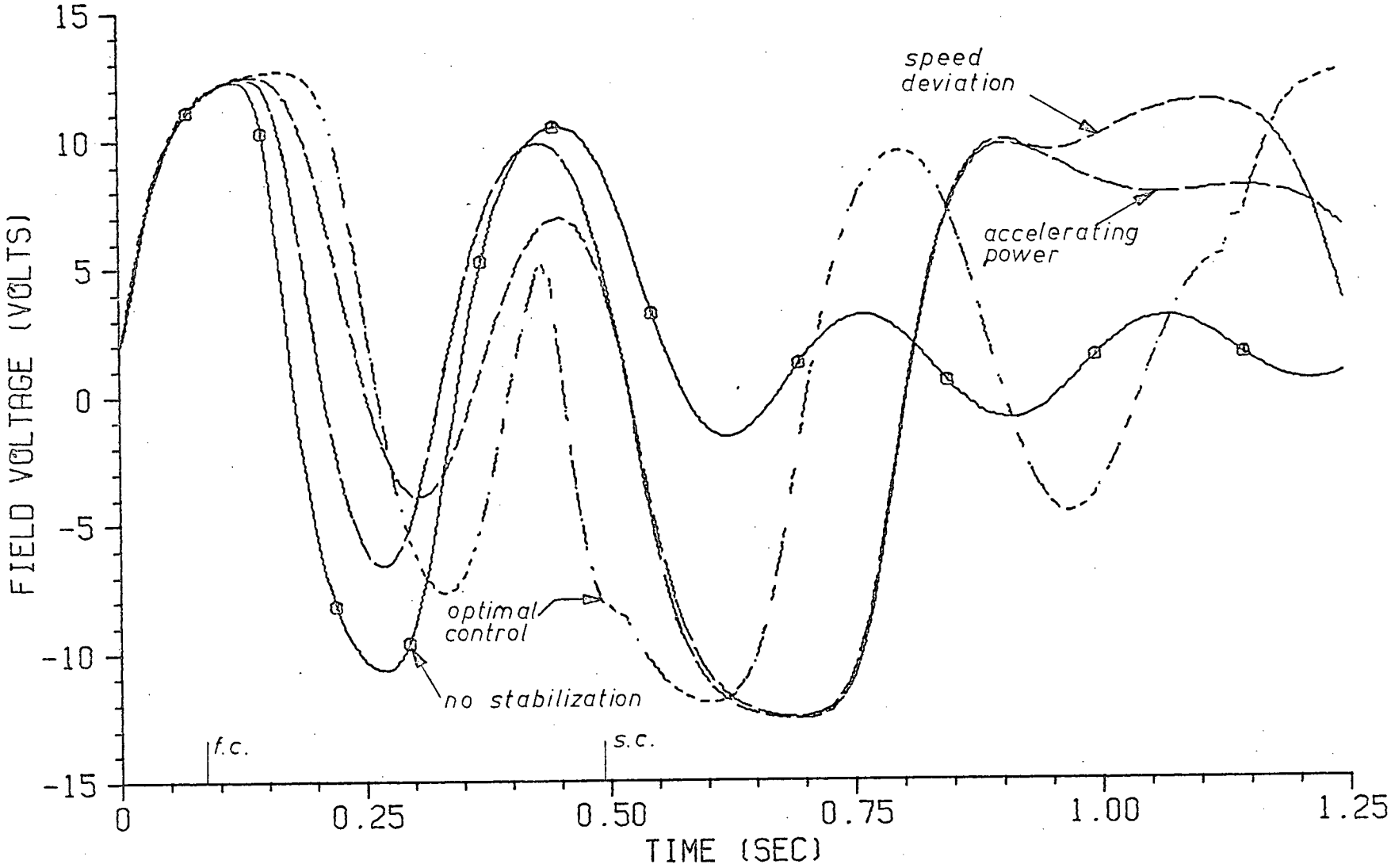

(c) Field Voltage

Fig. 5.2 Calculated Transient Responses of Various Stabilizing Signals

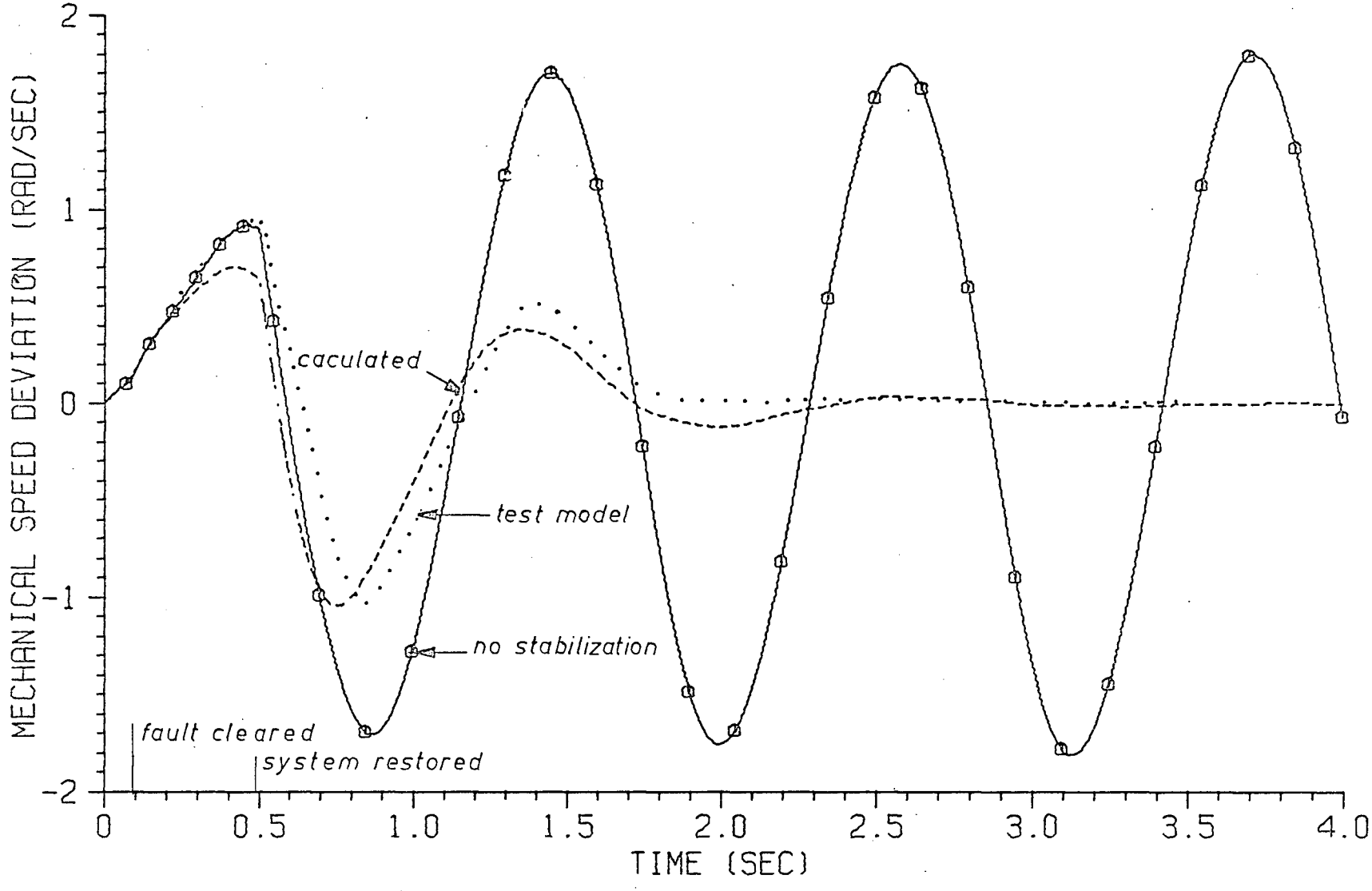

(a) Mechanical Speed Deviation

Fig. 5.3 Transient Responses with Accelerating Power Stabilization

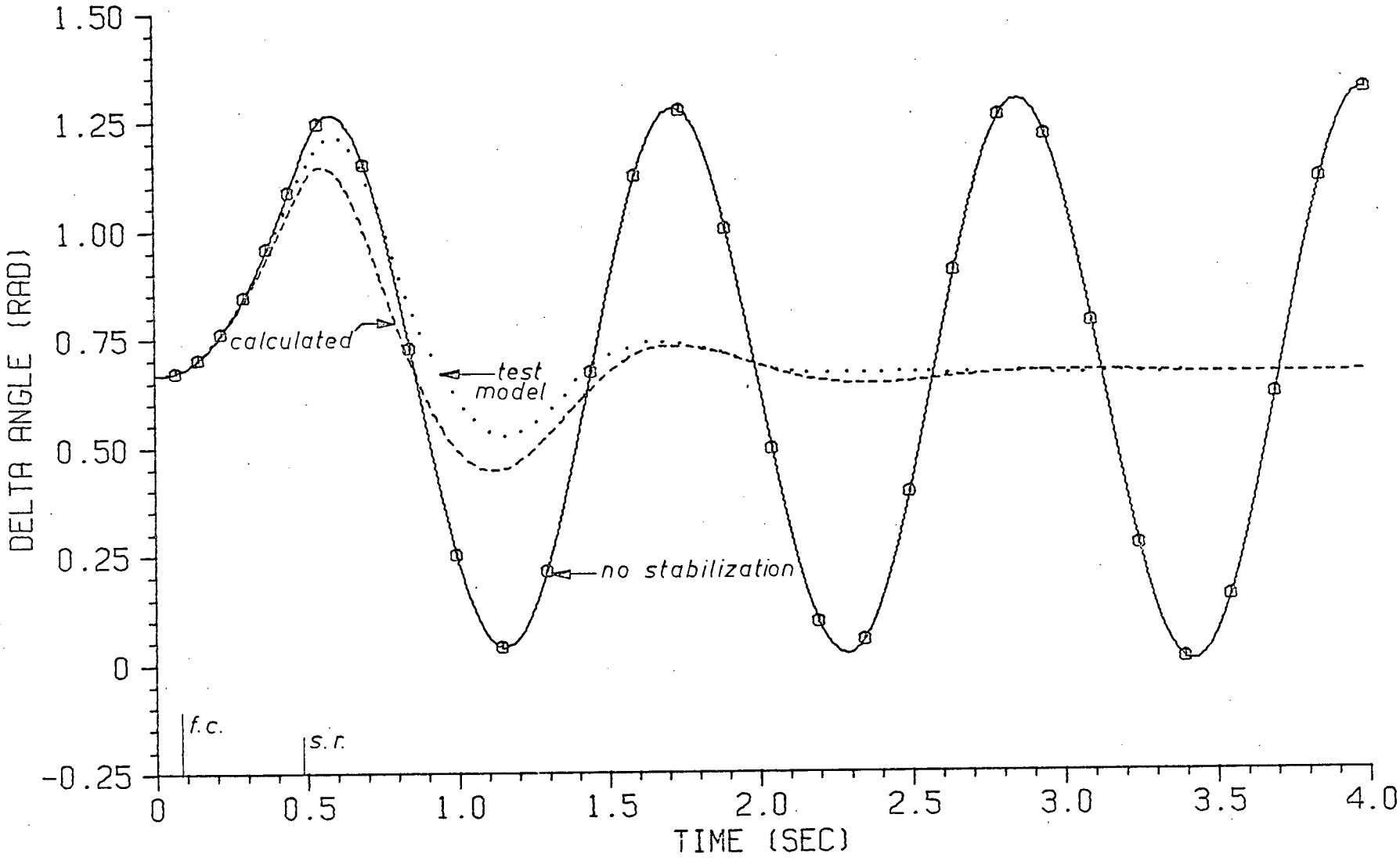

(b) Torque Angle

Fig. 5.3 Transient Responses with Accelerating Power Stabilization

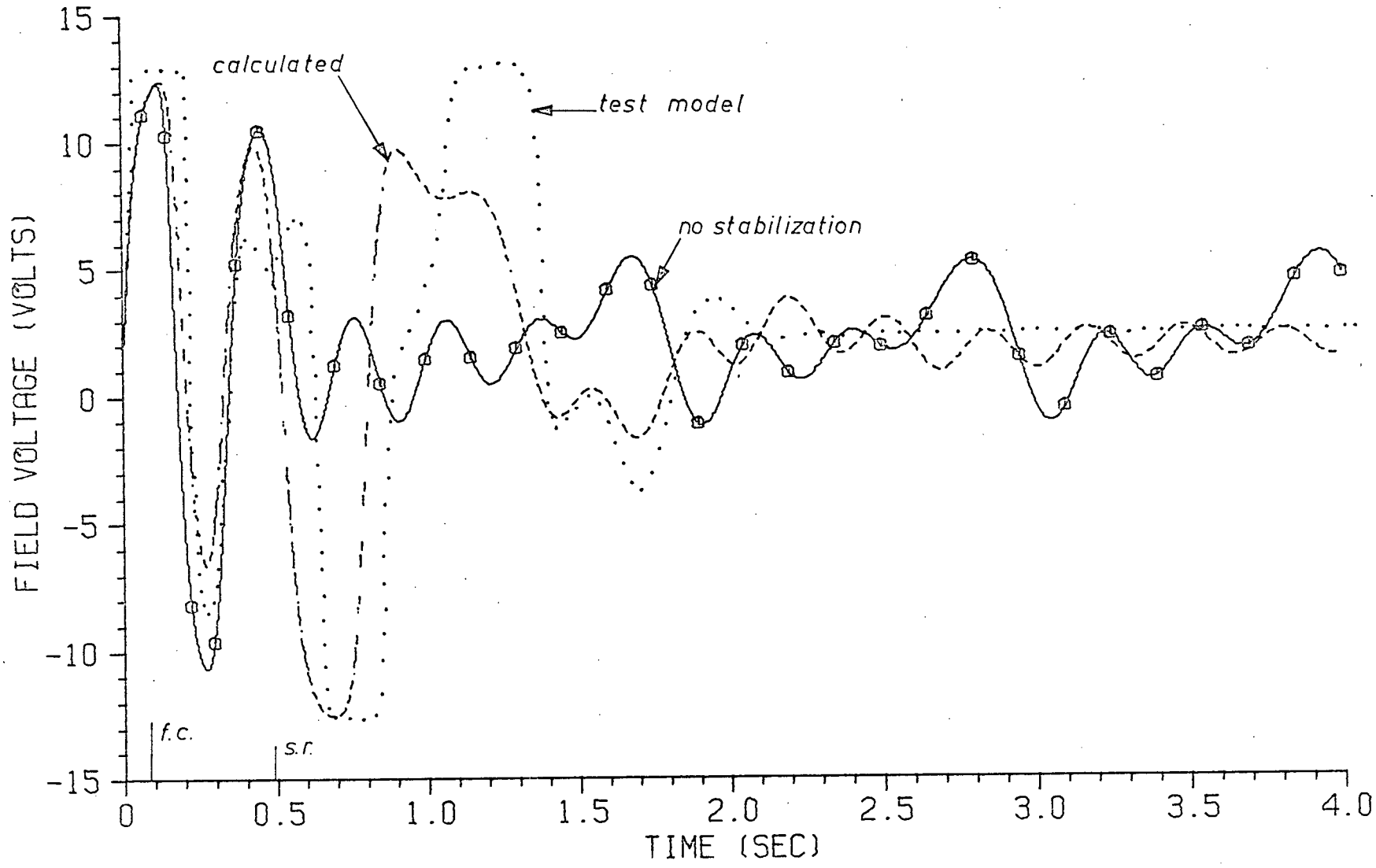

(c) Field Voltage

Fig. 5.3 Transient Responses with Accelerating Power Stabilization

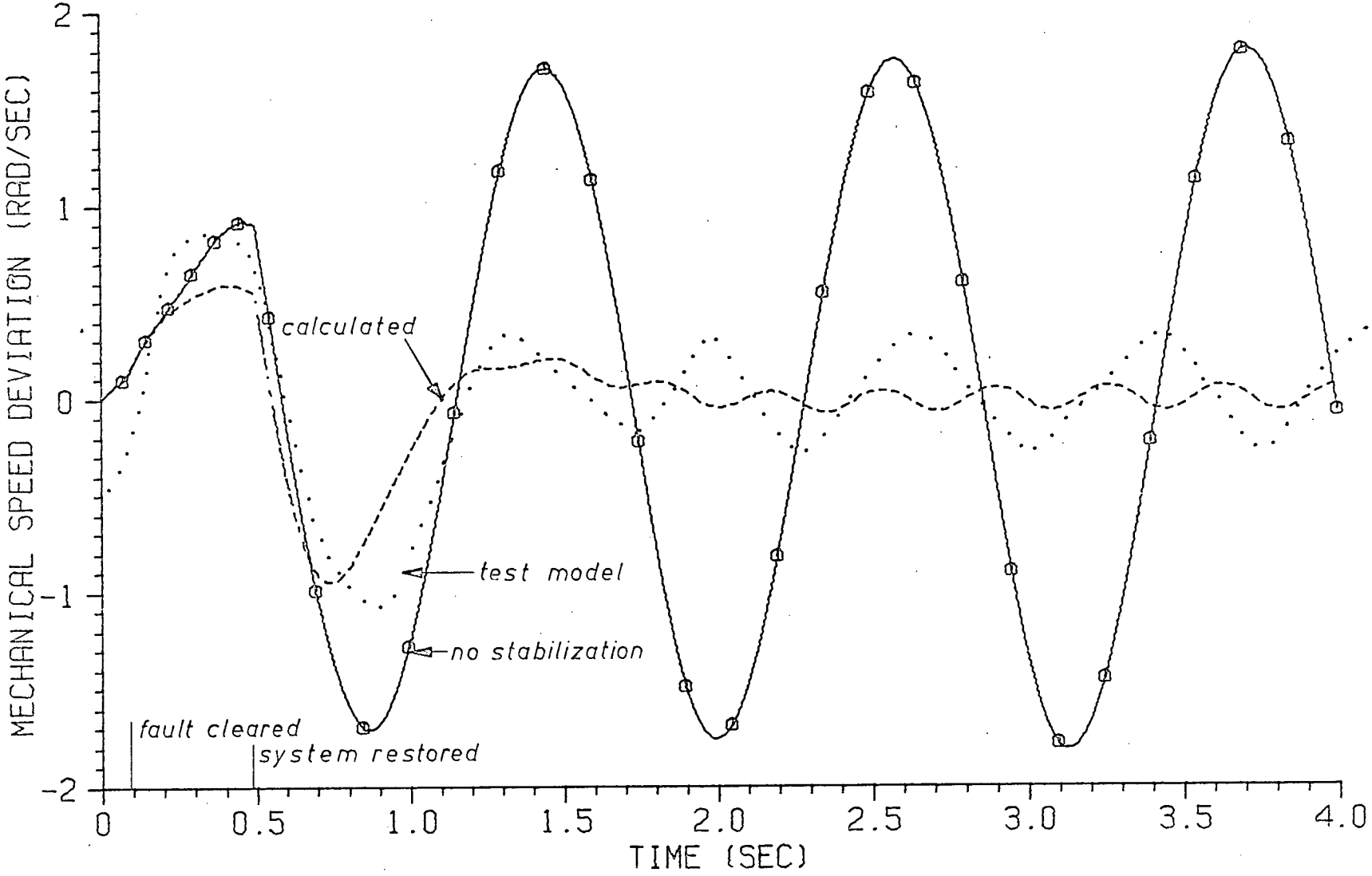

(a) Mechanical Speed Deviation

Fig. 5.4 Transient Responses with Speed Deviation Stabilization

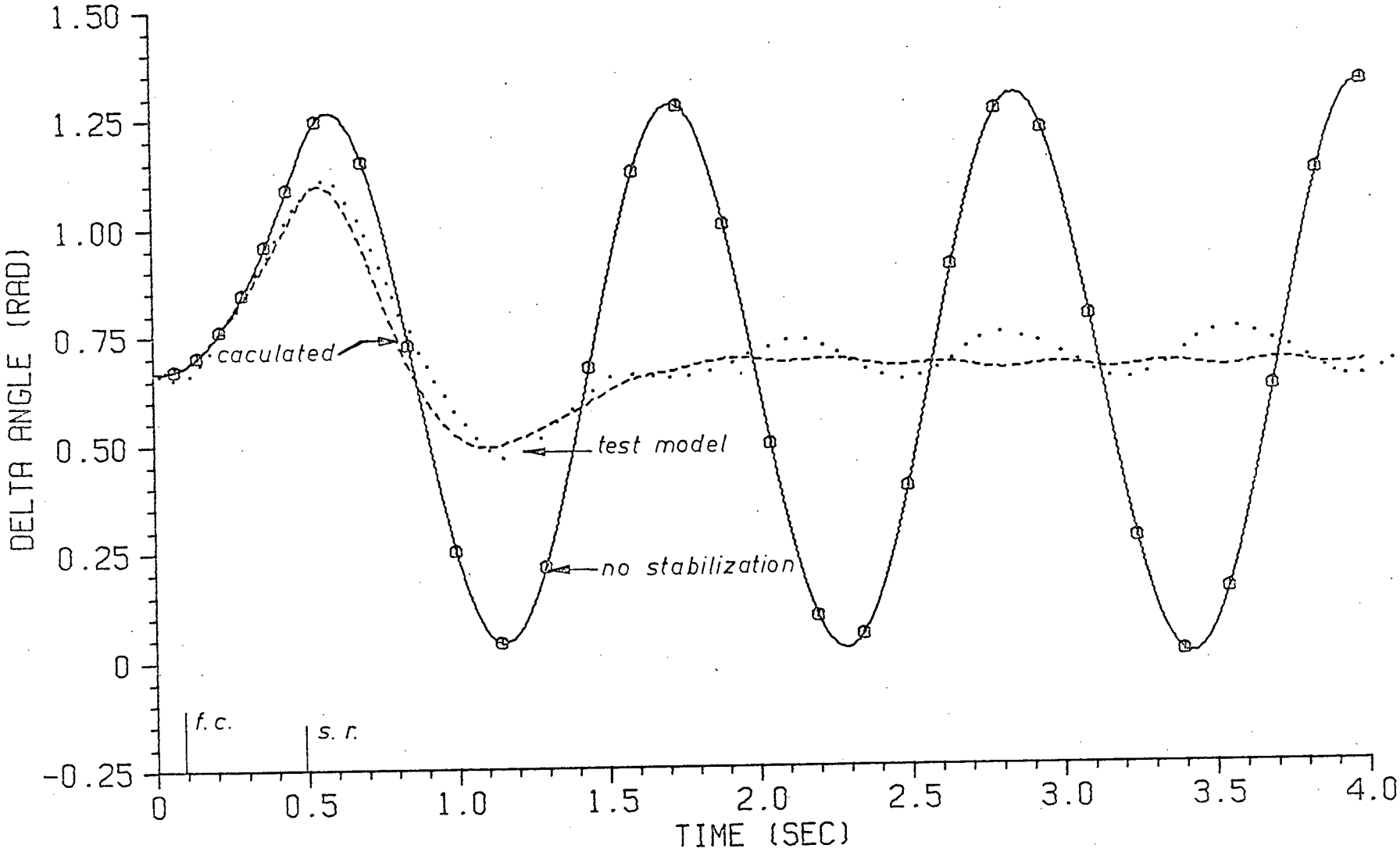

(b) Torque Angle

Fig. 5.4 Transient Responses with Speed Deviation Stabilization

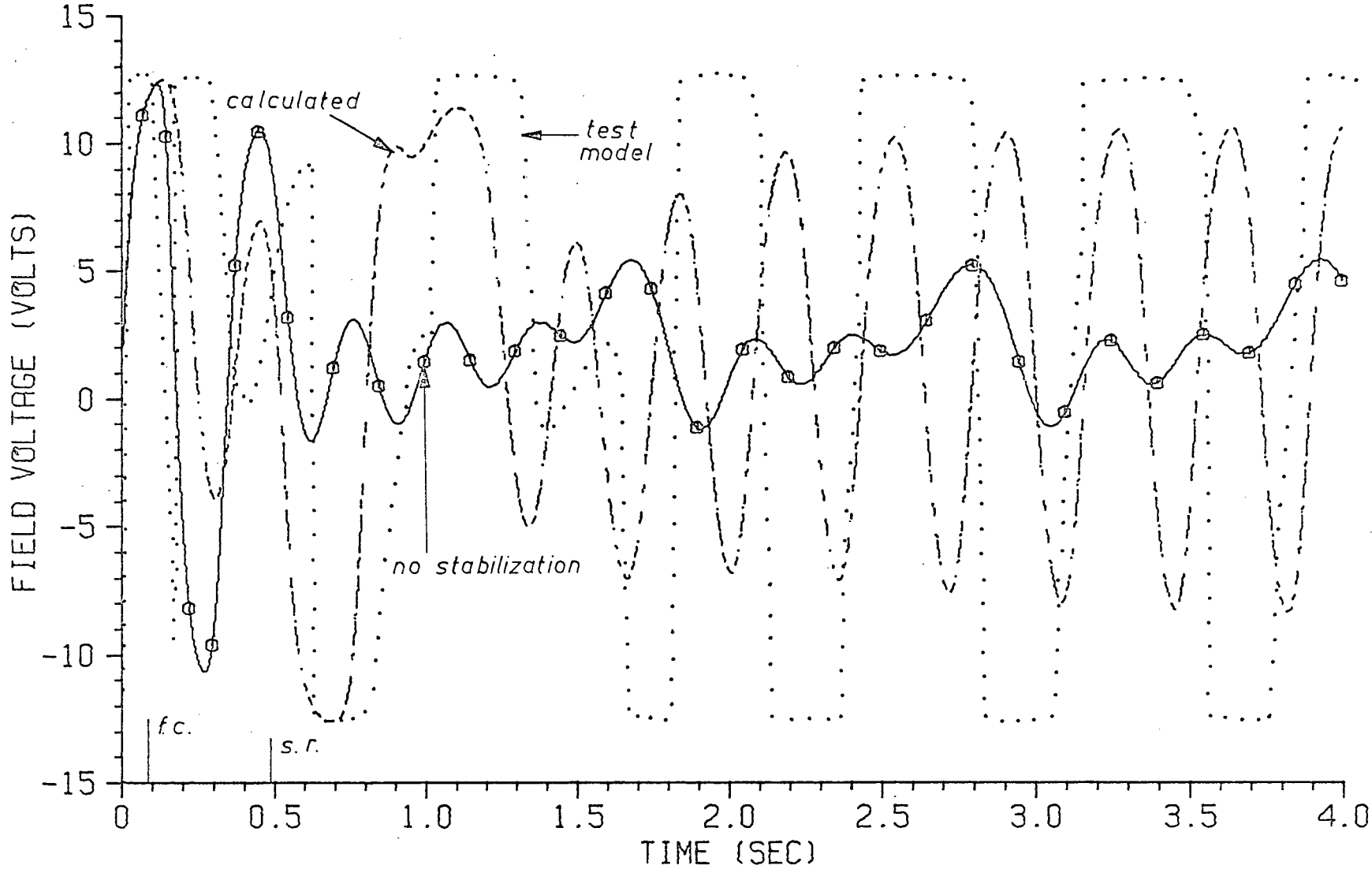

(c) Field Voltage

Fig. 5.4 Transient Responses with Speed Deviation Stabilization

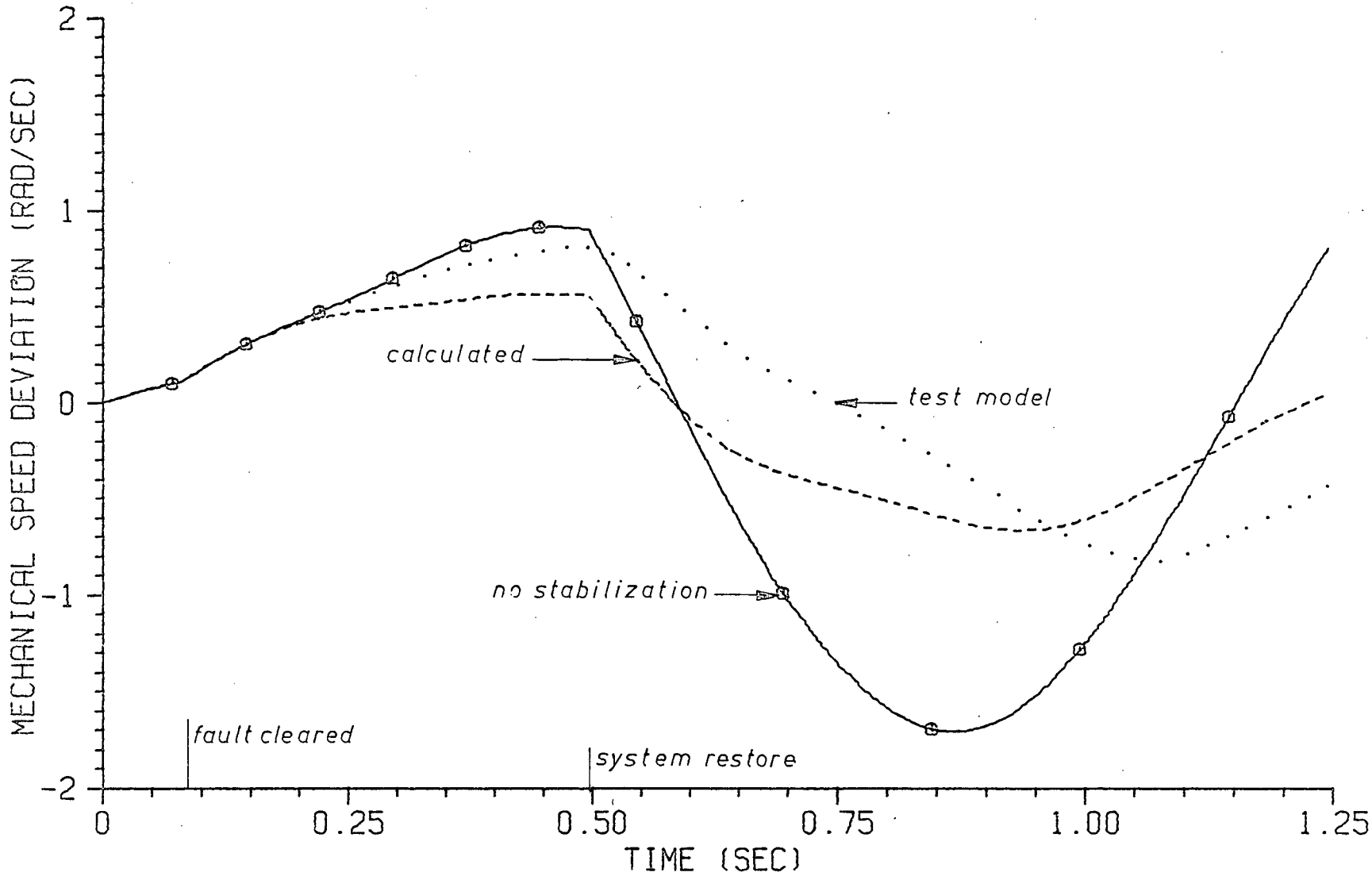

(a) Mechanical Speed Deviation

Fig. 5.5 Transient Responses with Optimal Control Stabilization

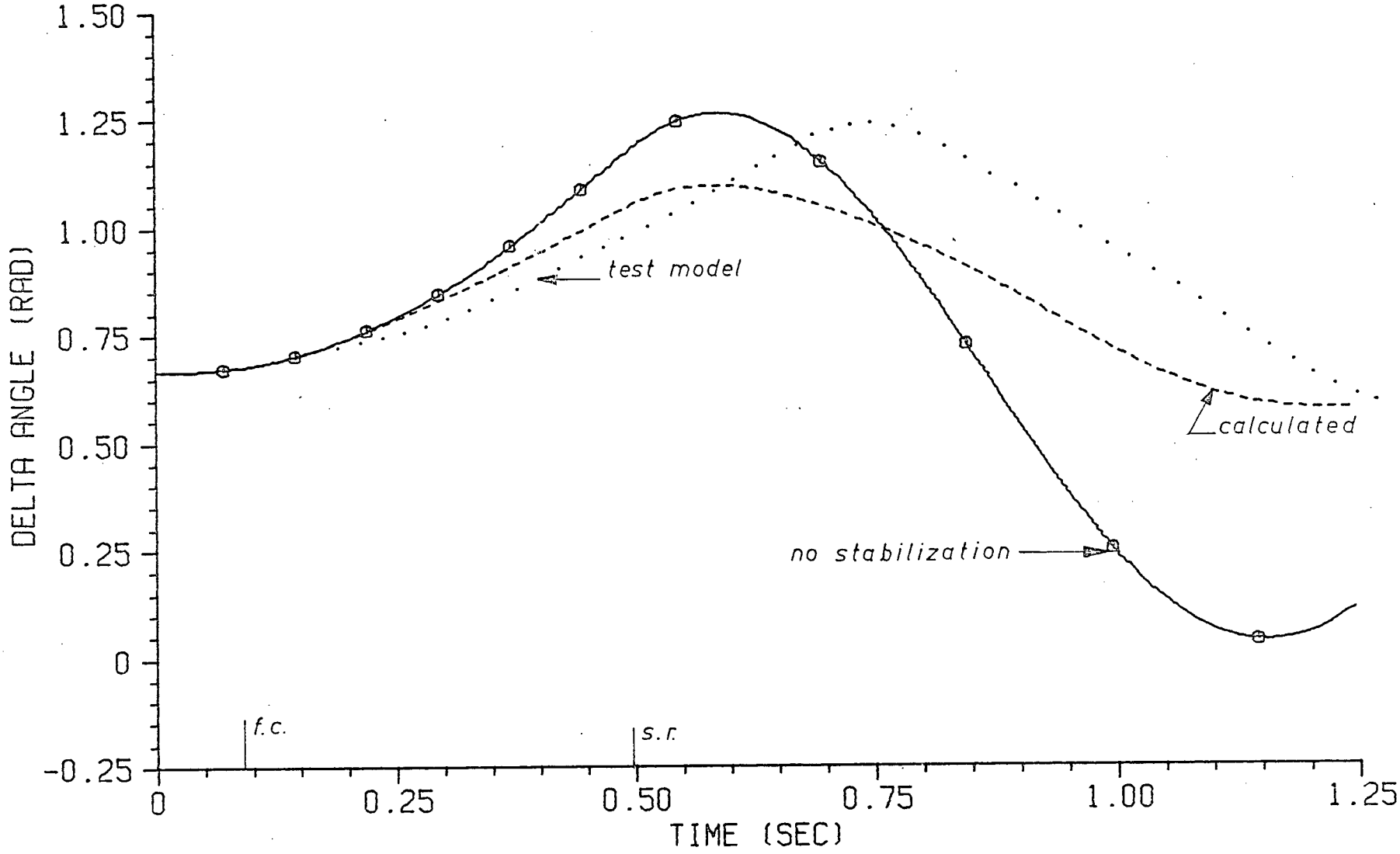

(b) Torque Angle

Fig. 5.5 Transient Responses with Optimal Control Stabilization

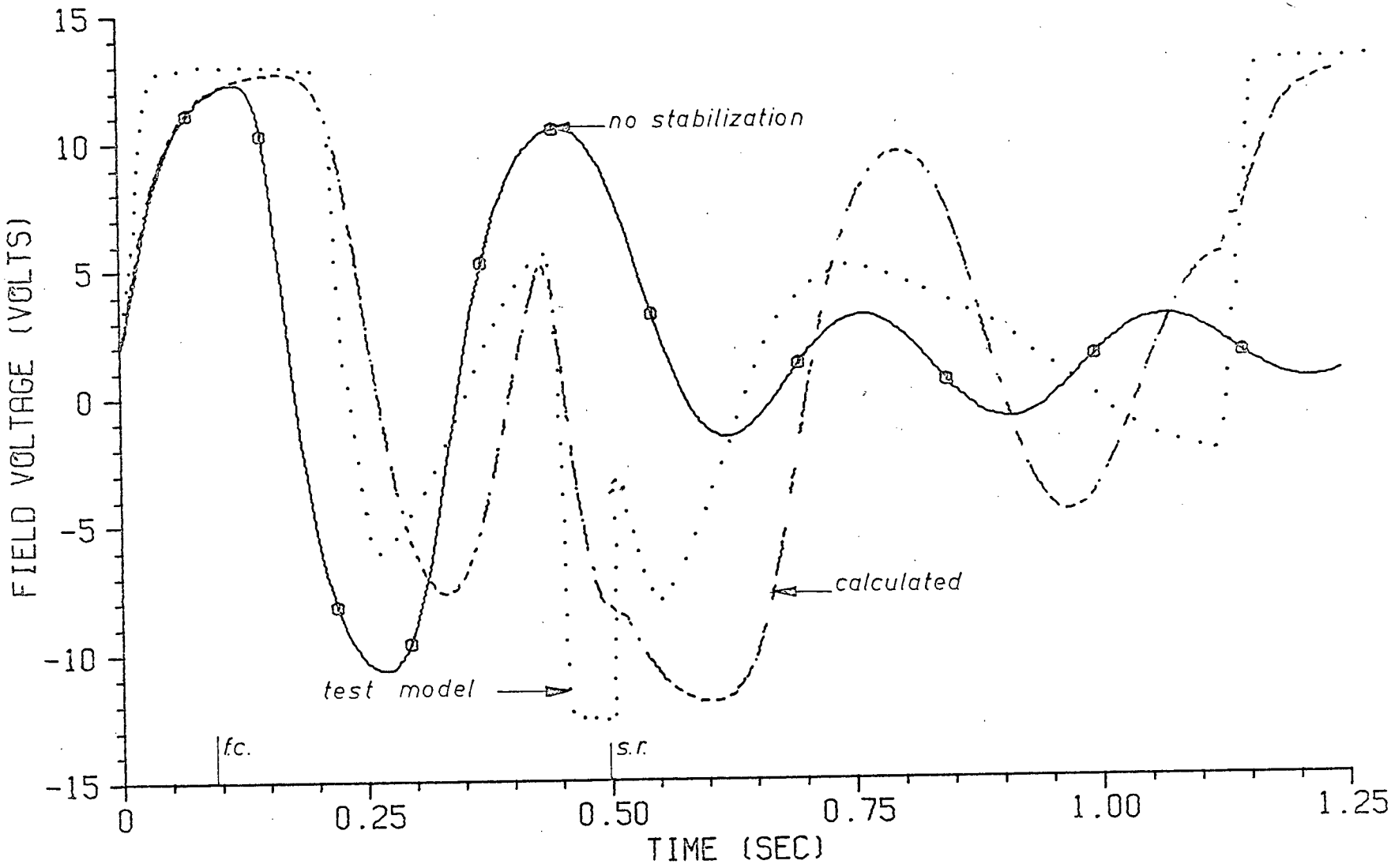

(c) Field Voltage

Fig. 5.5 Transient Responses with Optimal Control Stabilization

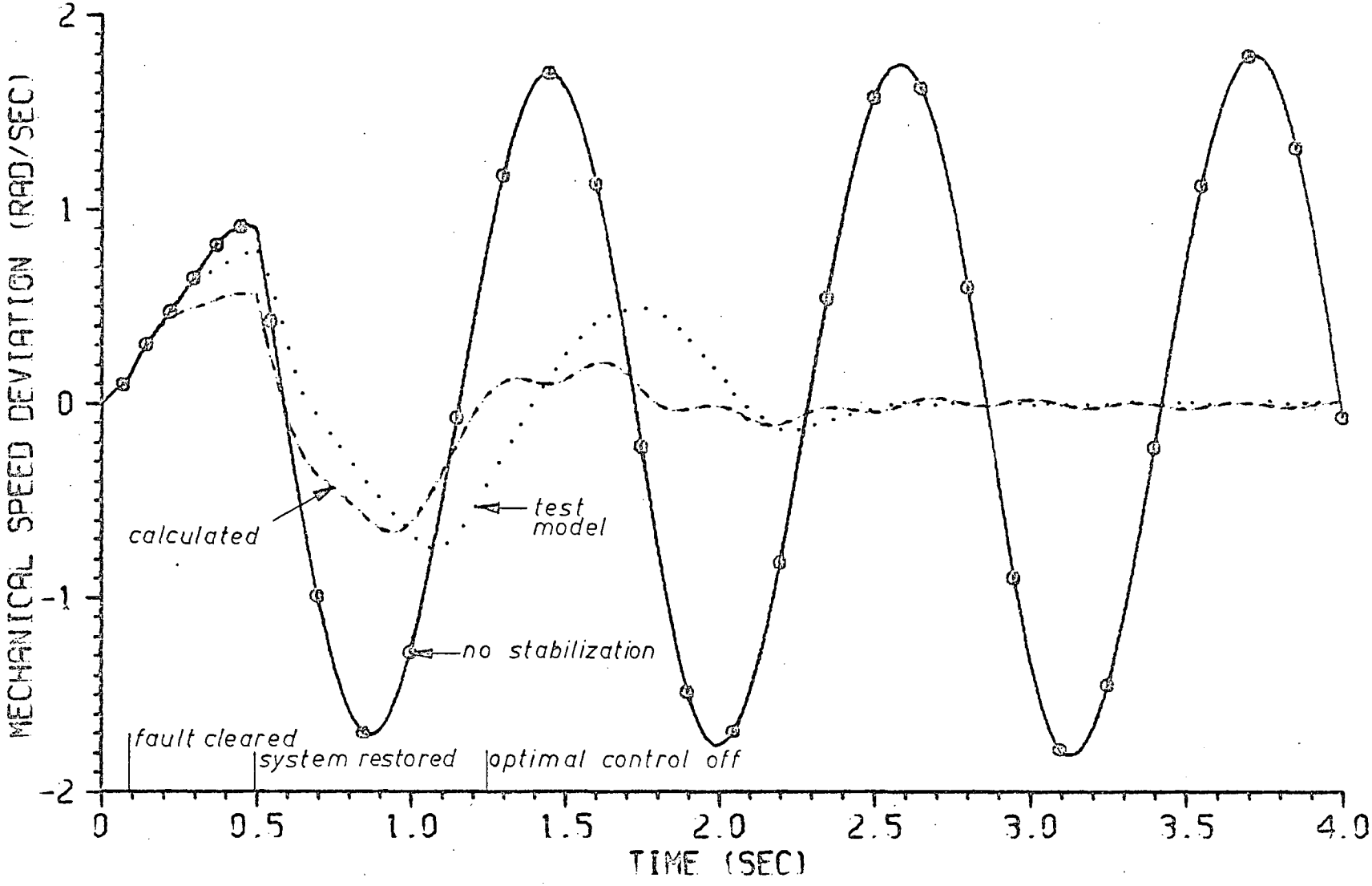

(a) Mechanical Speed Deviation

Fig. 5.6 Transient Responses with Composite Stabilization

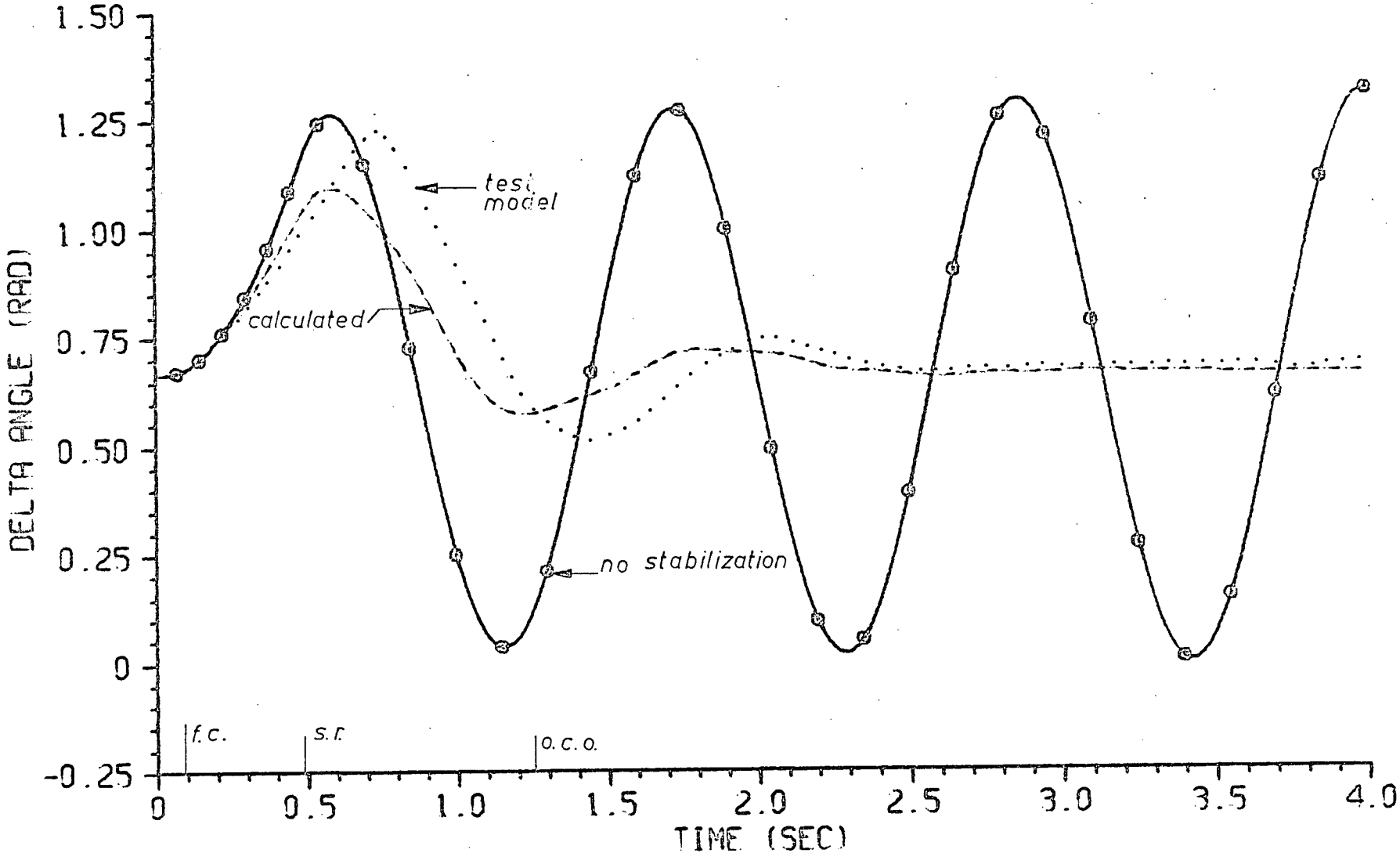

(b) Torque Angle

Fig. 5.6 Transient Responses with Composite Stabilization

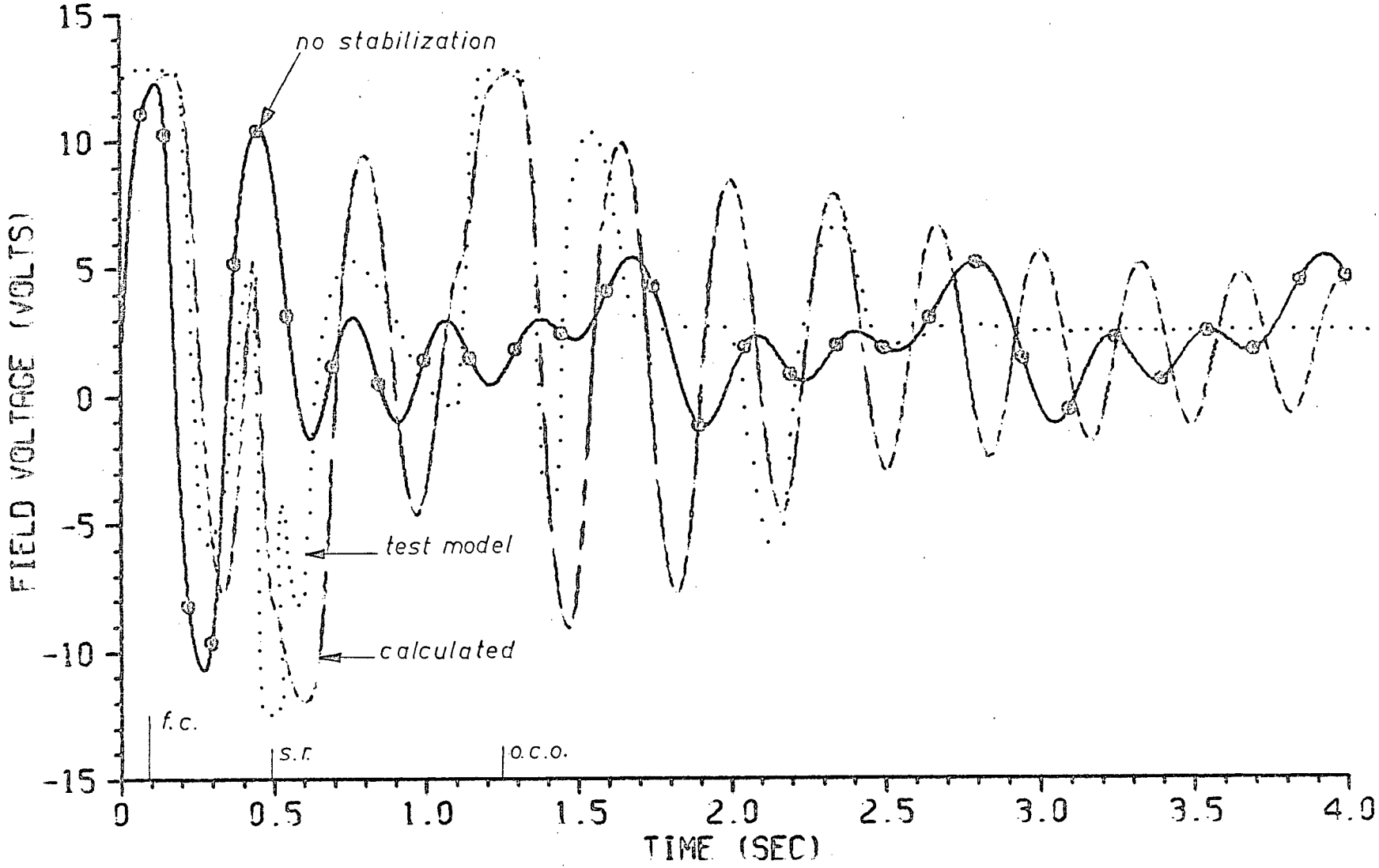

(c) Field Voltage

Fig. 5.6. Transient Responses with Composite Stabilization

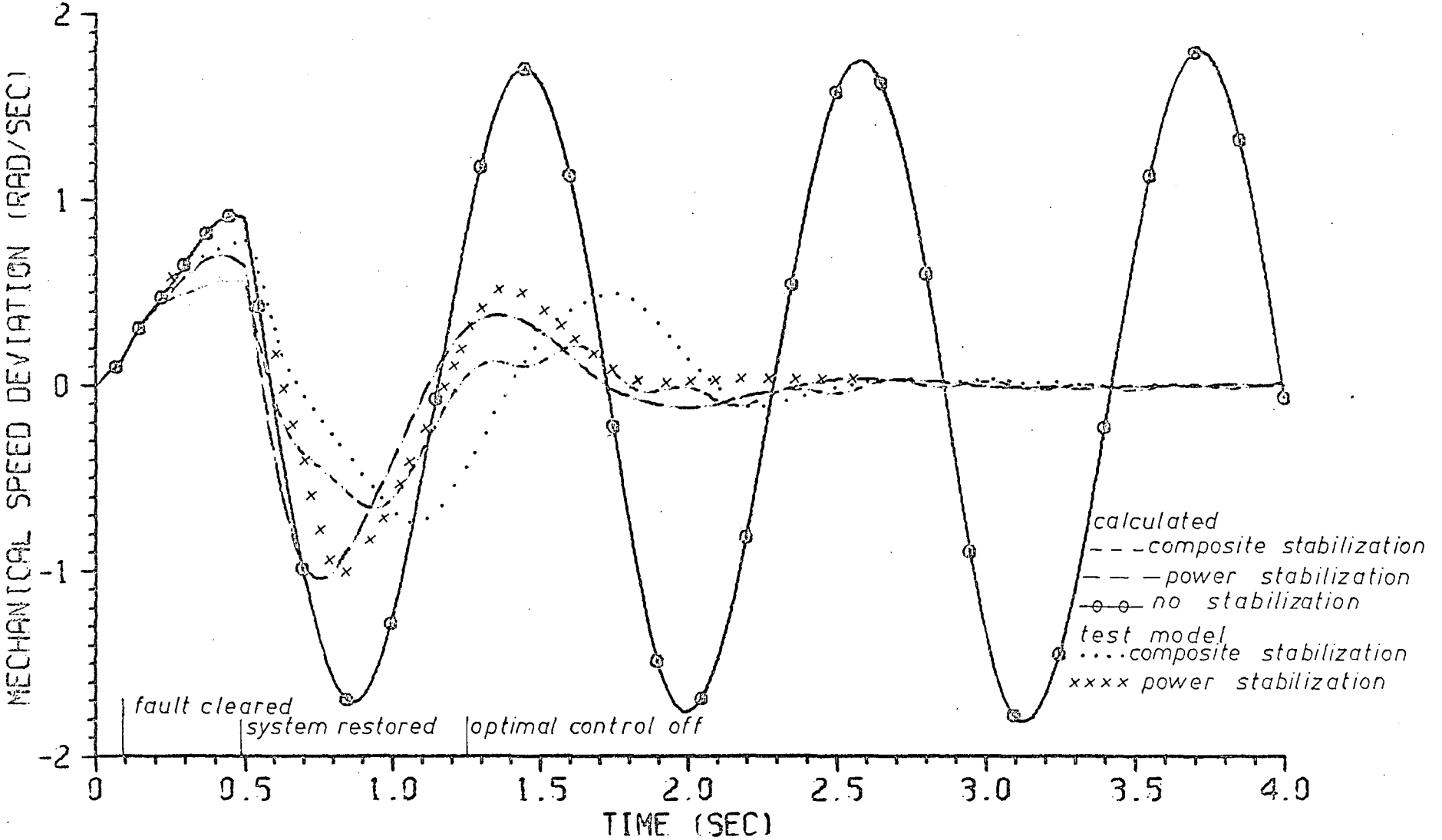

(a) Mechanical Speed Deviation

Fig. 5.7 Transient Responses with Accelerating Power Stabilization and Composite Stabilization

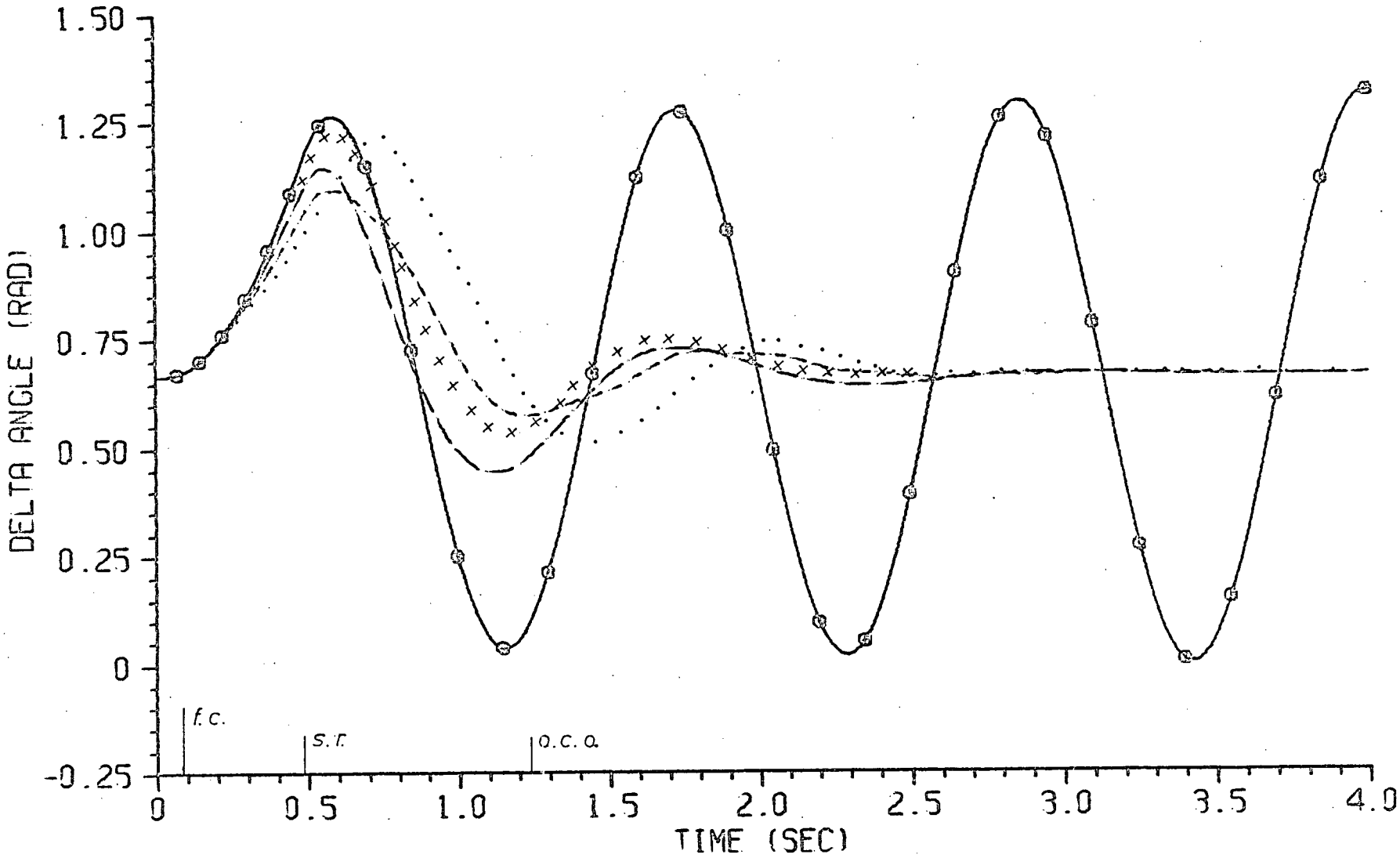

(b) Torque Angle

Fig. 5.7 Transient Responses with Accelerating Power Stabilization and Composite Stabilization

CONCLUSION

A new model for power system transient stability and control tests has been developed capable of representing any conventional one machine infinite bus system in detail. The model system has a synchronous machine with an adjustable field time constant, a solid state regulator-exciter system and an adapted dc motor prime mover with typical speed governor characteristics. The model can be used to investigate power system dynamics over a wide range of operating conditions.

A general fifth order state variable model for a synchronous machine has been derived from Park's equations. It has been shown that parameters in this state variable model can be determined directly from experimental machine tests. This is an improvement over existing models which are based on parameters not directly measurable.

Three variations on this general model have been shown to be useful in predicting the dynamic behaviour of a synchronous machine and interconnected systems. From the comparison of computation and model test results, it has been found that the first order synchronous machine ($p\psi_F$) and the second order dynamics ($p\delta, p\omega_m$) are sufficient for most studies except subtransient and switching phenomenon which has not been included in this study.

A parameter sensitivity study has been carried out. It has been found that x_q, T'_{do} and J are the most sensitive parameters but not r_a, x_d, T_E and the governor hydraulic operator parameters.

The usefulness of the model has been demonstrated with the study of the stabilizing signal. A "bang-bang" type nonlinear optimal control signal for a fault-fault cleared-system restored power system

has been treated as a two-point-boundary-value problem in this thesis. A gradient method has been applied to obtain the switching times of the control. The control signal thus obtained has been implemented on the test model. The model test results have been shown to agree favourably with those obtained from computation. Thus, it has proven that the test model provides a convenient means to check the design.

The test model has also been used to test conventional speed and accelerating power stabilizing signals. The experimental results have compared favourably with computed values. It has been demonstrated experimentally that the nonlinear optimal control provides better system damping than conventional signals. The principal contribution of the thesis is the development of a compatible test model and higher order state variable synchronous machine models for power system dynamic studies.

For future studies it is felt that

1) the mathematical model could be improved, if necessary, to include subtransient and switching phenomenon,

2) comparison of alternative schemes of prime mover simulation should be made,

3) the prototype test model should be developed to include a universal transmission system since the present one is of special purpose,

4) and the model developed could be multiplied for multi-machine studies.

APPENDIX 3A

Park's Equations in the State Variable Form

Equation (3.3) is expanded to obtain

$$\psi_d = \left(\frac{R}{\omega_{eo}(1+T'_{do}p)} + \frac{S}{\omega_{eo}(1+T'_{do}p)}\right) v_F - \left(\frac{1+T_c p}{\omega_{eo}(1+T'_{do}p)} + \frac{T_D p}{\omega_{eo}(1+T''_{do}p)}\right) x_d i_d \qquad (3A.1)$$

where $v_F = \frac{x_{ad}}{R'_f} v_{fd}$

$$R = \frac{T'_{do} - T_{D1}}{T'_{do} - T''_{do}}$$

$$S = \frac{T''_{do} - T_{D1}}{T''_{do} - T'_{do}}$$

$$T_c = \frac{T'_{do}(T''_d + T'_d - T''_{do}) - T'_d T''_d}{T'_{do} - T''_{do}}$$

$$T_D = \frac{-T''_{do}(T''_d + T'_d - T''_{do}) + T'_d T''_d}{T'_{do} - T''_{do}}$$

Terms in (3A.1) are combined to obtain

$$\psi_d = \frac{1}{\omega_{eo}}\left(\frac{Rv_F - (1+T_c p) x_d i_d}{1 + T'_{do} p} + x_d i_d\right) - \frac{x_d i_d}{\omega_{eo}} + \frac{1}{\omega_{eo}}\left(\frac{Sv_F - T_D p x_d i_d}{1 + T''_{do} p}\right) \qquad (3A.2)$$

which can be written

$$\Psi_d = \frac{-x_d i_d}{\omega_{eo}} + \frac{v_{FR}}{\omega_{eo}} + \frac{v_{DR}}{\omega_{eo}} \tag{3A.3}$$

where $$v_{FR} = \frac{Rv_F + (T'_{do} - T_c)\, x_d\, pi_d}{1 + T'_{do}\, p} \tag{3A.4}$$

and $$v_{DR} = \frac{Sv_F - T_D\, px_d i_d}{1 + T''_{do}\, p} \tag{3A.5}$$

From (3A.4) one has

$$v_F = \frac{1}{R}\left(v_{FR} + p\left(T'_{do}\, v_{FR} - x_d\,(T'_{do} - T_c) i_d\right)\right) \tag{3A.6}$$

and when compared with

$$Rv_F = v_{FR} + p\Psi_F \tag{3A.7}$$

the results yield

$$\Psi_F = T'_{do}\, v_{FR} - x_d\,(T'_{do} - T_c)\, i_d \tag{3A.8}$$

From (3A.5) one has

$$0 = v_{DR} - Sv_F + p\,(T''_{do}\, v_{DR} + T_D x_d i_d) \tag{3A.9}$$

and when compared with

$$0 = v'_{DR} + p\Psi_D \tag{3A.10}$$

the results yield

$$\Psi_D = T''_{do}\, v_{DR} + T_D x_d i_d \tag{3A.11}$$

and

$$v'_{DR} = v_{DR} - Sv_F$$

Equations (3A.3), (3A.8) and (3A.11) can be written in matrix form

$$\begin{bmatrix} \psi_F \\ \psi_d \\ \psi_D \end{bmatrix} = \begin{bmatrix} T'_{do} & -x_d(T'_{do} - T_c) & 0 \\ \frac{1}{\omega_{eo}} & \frac{-x_d}{\omega_{eo}} & \frac{1}{\omega_{eo}} \\ 0 & x_d T_D & T''_{do} \end{bmatrix} \begin{bmatrix} v_{FR} \\ i_d \\ v_{DR} \end{bmatrix} \qquad (3A.12)$$

Since the determinant is equal to $-\frac{x''_d\ T''_{do}\ T'_{do}}{\omega_{eo}}$, the solutions v_{FR}, i_d and v_{DR} are

$$\begin{bmatrix} v_{FR} \\ i_d \\ v_{DR} \end{bmatrix} = \begin{bmatrix} \frac{x_d(T''_{do} + T_D)}{x''_d\ T''_{do}\ T'_{do}} & \frac{-x_d(T'_{do}-T_c)\omega_{eo}}{x''_d\ T'_{do}} & \frac{x_d(T'_{do}-T_c)}{x''_d\ T''_{do}\ T'_{do}} \\ \frac{1}{x''_d\ T'_{do}} & \frac{-\omega_{eo}}{x''_d} & \frac{1}{x''_d\ T''_{do}} \\ \frac{-\ x_d T_D}{x''_d\ T''_{do}\ T'_{do}} & \frac{\omega_{eo}\ x_d\ T_D}{x''_d\ T''_{do}} & \frac{x_d T_c}{x''_d\ T''_{do}\ T'_{do}} \end{bmatrix} \begin{bmatrix} \psi_F \\ \psi_d \\ \psi_D \end{bmatrix} \qquad (3.10)$$

A similar approach can be used to obtain state equations in the q-axis. The flux linkages due to the armature winding and the damper winding are obtained by rewriting (3.4) as follows

$$\psi_q = -\frac{(1+T''_q p)\ x_q i_q}{(1+T''_{qo} p)\omega_{eo}} + \frac{x_q i_q}{\omega_{eo}} - \frac{x_q i_q}{\omega_{eo}} \qquad (3A.13)$$

When (3A.13) is compared with

$$\psi_q = \frac{v'_{QR}}{e_o} - \frac{x_q}{e_o} \; i_q \tag{3A.14}$$

the result yields

$$v'_{QR} = p \; \frac{x_q(T''_{qo} - T''_q) \; i_q}{1+T''_{qo} \; p} \tag{3A.15}$$

Equation (3A.15) can be further written

$$0 = v'_{QR} + p(T''_{qo} \; v'_{QR} - x_q(T''_{qo} - T''_q) i_q) \tag{3A.16}$$

and when it is compared to

$$0 = v'_{QR} + p\psi_Q \tag{3A.17}$$

the result yields

$$\varrho = T''_{qo} \; (v'_{QR} - (x_q - x''_q) \; i_q) \tag{3A.18}$$

Equations (3A.15) and (3A.18) can be written in matrix form

$$\begin{bmatrix} \psi_q \\ \psi_Q \end{bmatrix} = \begin{bmatrix} -\frac{x_q}{\omega_{eo}} & \frac{1}{\omega_{eo}} \\ -(x_q - x''_q) \; T''_{qo} & T''_{qo} \end{bmatrix} \begin{bmatrix} i_q \\ v'_{QR} \end{bmatrix} \tag{3A.19}$$

and the solutions of i_q and v'_{QR} are

$$\begin{bmatrix} i_q \\ v'_{QR} \end{bmatrix} = \begin{bmatrix} \frac{-\omega_{eo}}{x_q} & \frac{1}{x''_q T''_{qo}} \\ \frac{-\omega_{eo}(x_q - x''_q)}{x''_q} & \frac{x_q}{x''_q T''_{qo}} \end{bmatrix} \begin{bmatrix} \psi_q \\ \psi_Q \end{bmatrix} \tag{3.11}$$

Therefore Park's equations can be written in the state variable form as follows

$$p\psi_d = v_d + \omega_e \psi_q + r_a i_d \tag{3.5}$$

$$p\psi_q = v_q - \omega_e \psi_d + r_a i_q \tag{3.6}$$

$$p\psi_F = Rv_F - v_{FR} \tag{3.7}$$

$$p\psi_D = - v'_{DR} \tag{3.8}$$

$$p\psi_Q = - v'_{QR} \tag{3.9}$$

APPENDIX 3B

Determination of Effective Voltage Ratio R_f'/x_{ad}

The value of $\frac{R_f'}{x_{ad}}$ in (3.3) is in fact an effective voltage ratio of the synchronous machine and can be determined from a short circuit test and machine parameters. For a three phase steady state short circuit of the synchronous machine Park's equations become

$$\omega_{eo}\psi_q = -r_a i_d \tag{3B.1}$$

$$\omega_{eo}\psi_d = r_a i_q \tag{3B.2}$$

$$\omega_{eo}\psi_d = \frac{x_{ad}}{R_f'} v_{fd} - x_d i_d \tag{3B.3}$$

$$\omega_{eo}\psi_q = -x_q i_q \tag{3B.4}$$

Combining (3B.1) and (3B.3) yields

$$i_q = \frac{r_a}{x_q} i_d \tag{3B.5}$$

Substituting (3B.2) and (3B.5) into (3B.3) gives

$$i_d = \frac{x_q}{r_a^2 + x_d x_q} \frac{x_{ad}}{R_f'} v_{fd} \tag{3B.6}$$

Substituting i_d into (3B.5) yields

$$i_q = \frac{r_a}{r_a^2 + x_d x_q} \quad \frac{x_{ad}}{R_f'} \quad v_{fd} \tag{3B.7}$$

Thus the a-phase short circuit current equals

$$i = \sqrt{i_d^2 + i_q^2} = \frac{\sqrt{r_a^2 + x_q^2}}{r_a^2 + x_d\, x_q} \quad \frac{x_{ad}}{R_f'} \quad v_{fd} \tag{3B.8}$$

When (3B.8) is compared to the test results obtained from the steady state short circuit test, one has

$$\text{'slope'} = i \Big/ \left(\frac{v_{fd}}{R_f}\right) \tag{3B.9}$$

Thus

$$\frac{R_f'}{x_{ad}} = \frac{R_f \sqrt{r_a^2 + x_q^2}}{(r_a^2 + x_d\, x_q)\ \text{'slope'}} \tag{3.45}$$

REFERENCES

Chapter 1

1.1 R. Robert, "Micromachine and microreseaux: study of the problems of transient stability by the use of models similar electromechanically to existing machines and systems," C.I.G.R.E., vol. III, 1950.

1.2 V. A. Venikov, "Representation of electrical phenomena on physical models as applied to power system," C.I.G.R.E., vol. III, 1952.

1.3 B. Adkins, "Micromachine studies at Imperial College," Electrical Times, July 1960.

1.4 J. Roy, "Effects of synchronous machine parameters on dynamic and transient stability," Paper presented to C.E.A. Winnipeg Meeting, March 1967.

1.5 J. J. Dougherty and V. Caleca, "The EEI ac/dc transmission model," IEEE Transactions, vol. PAS-87, pp. 504-512, February 1968.

Chapter 2

2.1 "Test procedures for synchronous machines," IEEE publication No. 115, March 1965.

2.2 Y. N. Yu and G. E. Dawson, "Modeling a four electric machine system on analog using parameters directly determined from tests," IEEE Transactions, vol. PAS-87, pp. 632-641, March 1968.

2.3 R. G. Siddall, "A prime mover-governor test model for large power systems," U.B.C. MASc. Thesis, January 1968.

2.4 L. M. Hovey, "Optimum Adjustment of Governors in Hydro Generating Stations," Engineering Institute of Canada Journal, pp. 64-71, Nove. 1960.

2.5 J. A. Bond, "A solid state voltage regulator and exciter for a large power system test model," U.B.C. MASc. Thesis, July 1967.

Chapter 3

3.1 R. H. Park, "Two reaction theory of synchronous machines, generalized method of analysis," AIEE Transactions, vol. 48, pp. 716-730, July 1929.

3.2 K. Vongsuriya, "The application of Lyapunov function to power system stability analysis and control," U.B.C. PhD Thesis, February 1968.

3.3 R. Fletcher and M. J. D. Powell, "A rapidly convergent descent method for minimization," The Computer Journal, vol. 6, pp. 163-168, 1963.

3.4 Y. N. Yu and K. Vongsuriya, "Steady state stability limits of a regulated synchronous machine connected to an infinite system," IEEE Transactions, vol. PAS-85, pp. 759-767, July 1966.

Chapter 4

4.1 R. Tomovic, Sensitivity analysis of dynamic systems. New York: McGraw-Hill, 1963.

4.2 A. P. Sage, Optimum Systems Control, Englewood Cliffs, N.J.: Prentice Hall, 1968, Chapter 12.

Chapter 5

5.1 P. L. Dandeno et al., "Effect of high-speed rectifier excitation system on generator stability limits," IEEE Transactions, vol. PAS-87, pp. 190-201, January 1968.

5.2 R. H. Schier and A. L. Blythe, "Field tests of dynamic stability using a stabilizing signal and computer program verification," IEEE Transactions, vol. PAS-87, pp. 315-322, February 1968.

5.3 F. R. Schlief et al., "Control of rotating exciters for power system damping-pilot applications and experience," IEEE Transaction Paper 69 TP 155-PWR.

5.4 F. P. deMello and C. Concordia, "Concepts of synchronous machine stability as affected by excitation control," IEEE Transactions, vol. PAS-88, pp. 316-329, April 1969.

5.5 G. A. Jones, "Transient stability of a synchronous generator under conditions of bang-bang excitation scheduling," IEEEE Transactions, vol. PAS-84, pp. 114-121, February 1965.

5.6 A. P. Sage, Optimum systems control, Englewood Cliffs, N.J.: Prentice Hall, 1968.

5.7 C. H. Schley, Jr. and I. Lee, "Optimal Control computation by the Newton-Raphson method and the Riccati transformation," IEEE Transactions, vol. AC-12, pp. 139-144, April 1967.

5.8 M. J. Box, "A comparison of several current optimization methods, and the use of transformations in constrained problems," The Computer Journal, vol. 9, pp. 67, 1966.

5.9 J. W. Sutherland, "The synthesis of optimal controllers for a class of aerodynamical systems, and the numerical solution of nonlinear optimal control problems," U.B.C. PhD Thesis, May 1967.

5.10 Y. N. Yu and C. Siggers, "Stabilization and optimal control signals for a power system." Accepted as transaction paper for IEEE 1970 Summer Power Meeting.